Ca^{2+} dynamics in retinal horizontal cells of teleost fish: Ca^{2+}-based action potentials and tolerance to hypoxia

By Michael Country

Thesis submitted to the University of Ottawa
in partial fulfillment of the requirements for the
Ph. D. degree at the
Ottawa-Carleton Institute of Biology

Department of Biology
Faculty of Science
University of Ottawa

24 July, 2020

ACKNOWLEDGMENTS

To coffee. Let us never be apart.

To my family. Let us be apart for a little while longer.

To Michael Jonz, who is as motivated, inquisitive, diplomatic, kind, and cultured as Jean-Luc Picard. I guess that makes Vance your Riker, which makes sense since he looks better with the beard. Mike, I honestly can't imagine a supervisor who I'd rather have worked with, and I appreciate all your patience, advice, and hospitality. I'm sorry that my bad looks almost prevented us from getting seated that one time in St. John's. I only hope to one day have a lab as welcoming as yours, and to be a scientist and human as upstanding and well-rounded as you are.

To my labmates. Wen Pan, thank you for being supportive as we started together in the lab, and for our long talks. Ben Campbell, you not only took time out of your final months to set me up for success, but you gave me course-changing advice and were an excellent friend. To Peter Zachar, who went out of his way to help me prepare for my comprehensive exam and give me advice. To Maddy, Laura, and Nicole, whose friendship and coffee trips kept me motivated. To all undergrads and others in our lab, thank you for such a wonderful experience.

To this supportive department. Nearly every professor and technician in our department has given me formative advice. It's impossible to list you all, but: Jean-Michel Weber, for giving me a clear model of metabolism that will influence my future job talk. Katie Gilmour, I hope to one day model your level of integrity and public speaking. To Andrew Ochalski, my best friend in the department. Finally, to my committee members, for always keeping your doors open.

To Pat Cullen, the hoopiest frood.

ABSTRACT

Horizontal cells (HCs) are retinal interneurons which provide feedback to photoreceptors to produce visual contrast. They are depolarized by glutamate released from photoreceptors, leading to a constant influx of Ca^{2+} which would be fatal to most neurons. In addition, HCs present spontaneous Ca^{2+}-based action potentials, which are poorly understood and whose function is unknown. Given these unique Ca^{2+} dynamics, the present thesis sought to define action potentials (APs) and mechanisms of Ca^{2+} homeostasis in HCs. APs were observed in isolated goldfish HCs with electrophysiology, Ca^{2+} imaging, and voltage-sensitive dye imaging. Pharmacological inhibition of ion channels suggests APs required extracellular Ca^{2+} entry *via* L-type Ca^{2+} channels, followed by Ca^{2+}-induced Ca^{2+} release from ryanodine receptors. Next, we developed a novel system to classify all four HC subtypes *in vitro*, and validated it with immunocytochemistry for a subtype-specific biomarker. All subtypes presented APs, although frequency and duration varied by subtype. APs were also found in HCs of tissue slices prepared from whole retina, where similar trends were found between subtype, frequency, and duration. This highlights subtype-specific differences in Ca^{2+} dynamics. Lastly, $[Ca^{2+}]_i$ was monitored throughout hypoxia in HCs of the hypoxia-tolerant goldfish and the hypoxia-sensitive rainbow trout. In Ca^{2+} imaging experiments, hypoxia destabilized $[Ca^{2+}]_i$ in HCs of trout; but in goldfish, HCs were resistant to the effects of hypoxia. However, when mitochondrial ATP-dependent K^+ (mK_{ATP}) channels were inhibited, goldfish HCs lost the ability to maintain $[Ca^{2+}]_i$ homeostasis during hypoxia. By contrast, in trout HCs, opening of mK_{ATP} stabilized $[Ca^{2+}]_i$ during hypoxia. Furthermore, in goldfish, hypoxia protected against increases in $[Ca^{2+}]_i$ caused by inhibiting glycolysis, showing that hypoxia is not just tolerated, but is actively protective in goldfish HCs. The present thesis includes the first comprehensive description of spontaneous Ca^{2+}-based APs

in HCs, and introduces the first cellular model of intrinsic hypoxic neuroprotection in the vertebrate retina.

RÉSUMÉ

Les cellules horizontales (HC) sont des interneurones de la rétine qui fournissent de rétroaction aux photorécepteurs pour produire du contraste visuel. Elles sont dépolarisées par le glutamate des photorécepteurs pendant l'obscurité, et ensuite elles subissent un afflux constant de Ca^{2+} qui serait fatal pour la plupart des neurones. De plus, les HCs des poissons présentent des potentiels d'action (APs) spontanés à base de Ca^{2+} dont la fonction est inconnue. Compte tenu de ces dynamiques uniques de Ca^{2+}, cette thèse cherchait à clarifier les APs et l'homéostasie du Ca^{2+} dans les HCs du poisson rouge. Des APs ont été observés dans des HCs isolées, avec l'électrophysiologie et deux sondes fluorescentes (une, sensible pour Ca^{2+} ; l'autre, pour le potentiel de la membrane cellulaire). L'inhibition pharmacologique des canaux ioniques suggère que les APs nécessitent l'entrée de Ca^{2+} *via* les canaux « L-type », suivie d'une libération de Ca^{2+} issue du réticulum endoplasmique *via* les récepteurs ryanodine. Ensuite, nous avons développé un nouveau système pour classer les quatre sous-types de HCs, et nous l'avons validé avec l'immunocytochimie utilisant un biomarqueur spécifique pour un sous-type de HC. Tous les sous-types présentaient des APs, mais la fréquence et la durée variaient selon le sous-type. Des APs ont également été trouvés dans des tranches de la rétine, avec ces mêmes tendances entre le sous-type, la fréquence et la durée. Ces données suggèrent que les sous-types de HC ont des différences physiologiques importantes. Ensuite, nous avons mesuré la concentration de Ca^{2+} intracellulaire ($[Ca^{2+}]_i$) pendant des traitements de l'hypoxie dans une espèce tolérante de l'hypoxie (le poisson rouge) et une espèce sensible à l'hypoxie (la truite arc-en-ciel). Dans les

expériences avec la sonde Fura-2, l'hypoxie a augmenté la $[Ca^{2+}]_i$ dans les HCs de la truite, mais pas de la poisson rouge. Les HCs de la poisson rouge n'ont pas maintenu $[Ca^{2+}]_i$ dans l'hypoxie lorsque les canaux de K^+ mitochondriaux dépendant de l'ATP (mK_{ATP}) étaient inhibés. Dans les HCs de la truite, l'ouverture du mK_{ATP} a stabilisé la $[Ca^{2+}]_i$ dans l'hypoxie. De plus, l'hypoxie a protégée contre les augmentations de $[Ca^{2+}]_i$ causées par l'inhibition de la glycolyse, montrant que l'hypoxie n'est pas seulement tolérée, mais qu'elle protège les HCs des poissons rouges. Cette thèse comprend les premières expériences à clarifier directement le mystère des APs spontanés à base de Ca^{2+}, et introduit le premier modèle cellulaire de neuroprotection intrinsèque contre l'hypoxie, chez la rétine des vertébrés.

TABLE OF CONTENTS

LIST OF FIGURES

LIST OF TABLES

LIST OF ABBREVIATIONS AND UNITS

ABBREVIATIONS

$[Ca^{2+}]_i$	Intracellular concentration of calcium ions
$[Ca^{2+}]_o$	Extracellular concentration of calcium ions
$[Na^{+}]$	Sodium concentration
℃	Degrees Celsius
β	Ca^{2+} buffering capacity
µl	Microliter
µM	Micromolar
µm	Micron
2-APB	2-aminoethyldiphenyl borate
2-DG	2-deoxyglucose
5-HD	5-hydroxydecanoate
AMPA	α-amino-3-hydroxy-5-methyl-4-isoxazolepropionic acid
AMPAR	α-amino-3-hydroxy-5-methyl-4-isoxazolepropionic acid receptor
AP	Action potential
ATP	Adenosine triphosphate
AUC	Area under the curve
BC	Bipolar cell
Ca^{2+}_e	Extracellular Ca^{2+}
CCD	Charge coupled device
CDI	Ca^{2+}-dependent inactivation

cGMP	Cyclic guanosine monophosphate
CICR	Ca^{2+}-induced Ca^{2+} release
Cx	Connexin
DMSO	Dimethyl sulfoxide
ECS	Extracellular solution
EGTA	Ethylene glycol-bis(β-aminoethyl ether)-N,N,N′,N′-tetraacetic acid
F_{340}/F_{380}	Ratio of fluorescence from 340 nm excitation over 380 nm excitation
FITC	Fluorescein isothiocyanate
Fura-2-AM	Fura-2-acetoxymethyl ester
GABA	Gamma aminobutyric acid
GABAR	Gamma aminobutyric acid receptor
GAD	Glutamate decarboxylase
GΩ	Gigaohm
h	Hour
HC	Horizontal cell
HEPES	4-(2-hydroxyethyl)-1-piperazineethanesulfonic acid
HVA	High voltage-activated
iGluR	Ionotropic glutamate receptor
I_H	Hyperpolarization-activated current
INL	Inner nuclear layer
IP_3	Inositol 1,4,5-trisphosphate
IP_3R	Inositol 1,4,5-trisphosphate receptor
IPC	Ischemic preconditioning

IPL	Inner plexiform layer
IQR	Interquartile range
IR	Immunoreactivity
JST-3	Joro spider toxin-3
KAR	Kainate receptor
K_{ATP}	Adenosine triphosphate-dependent potassium channel
K_{Ca}	Calcium-dependent potassium channel
kDa	Kilodaltons
kHz	kilohertz
l	Liter
MgATP	Magnesium adenosine triphosphate
mGluRs	Metabotropic glutamate receptors
min	Minutes
mKATP	Mitochondrial adenosine triphosphate-dependent potassium channel
ml	Milliliter
mM	Millimolar
mm	Millimeter
mPTP	Mitochondrial permeability transition pore
ms	Millisecond
mV	Millivolt
MΩ	Megaohm
NCX	Sodium-calcium exchanger
nM	Nanomolar

nm	Nanometer
NMDA	*N*-methyl-D-aspartate
NMDAR	*N*-methyl-D-aspartate receptor
O_2	Oxygen
ONL	Outer nuclear layer
OS	Photoreceptor outer segments
PBS	Phosphate buffered solution
PKC	Protein kinase C
PMCA	Plasma membrane Ca^{2+}-ATPase
PO_2	Partial pressure of oxygen
PR	Photoreceptors
$r_{d/s}$	Ratio of dendritic field area *versus* soma area
RNA	Ribonucleic acid
ROS	Reactive oxygen species
RyR	Ryanodine receptor
s	Second
S.D.	Standard deviation
SERCA	Sarcoplasmic/endoplasmic reticulum Ca^{2+} ATPase
SNARE	Soluble *N*-ethylmaleimide sensitive factor attachment protein receptor
SOC	Store-operated channel
TTP	Time to peak
v/v	Volume by volume
VGCC	Voltage-gated Ca^{2+} channel

V_L	Liquid junction potential
V_m	Membrane potential
V_p	Pipette potential
w/v	Weight by volume

1 General introduction

This chapter includes material from the following article:

Country, M. W., and Jonz, M. G. 2017. Calcium dynamics and regulation in horizontal cells of the vertebrate retina: lessons from teleosts. *J Neurophysiol*. 177, 523-536.

1.1 Introduction

Horizontal cells (HCs) are inhibitory neurons that provide the first layer of neural processing in the vertebrate retina. They receive glutamatergic input from pre-synaptic photoreceptors (PRs), and return inhibitory feedback to produce visual contrast and edge detection (Baylor et al. 1971; Thoreson and Mangel 2012). HCs share a long history as model central neurons and have been studied for over a century (Ramón y Cajal 1909). Teleost HCs in particular are especially large, lending themselves well to physiological experiments, and were the first cells of the retina from which intracellular recordings were obtained (Dowling 1987; Svaetichin 1953). Their graded responses to light demonstrated, for the first time, that neurons could encode and relay information without using action potentials (APs). Today, the membrane properties and ionic currents of teleost HCs are well characterized (DeVries and Schwartz 1992; Dixon et al. 1996; Jonz and Barnes 2007; McMahon and Brown 1994; Shingai and Christensen 1986; Tachibana 1983; 1981), yet their Ca^{2+} dynamics are only beginning to be clarified. In neurons, Ca^{2+} plays a central role in vesicular neurotransmitter release (Wadel et al. 2007), synaptic plasticity (Zucker 1999), gene transcription (Lyons and West 2011), and second messenger pathways (Clapham 2007). In addition, high levels of cytosolic Ca^{2+} are toxic to neurons (Choi 1992; Lipton 1999), and therefore, Ca^{2+} sequestration and efflux mechanisms must be present to maintain cell viability. Therefore, understanding the dynamics and effects of Ca^{2+} in a given neuron, is often crucial to understanding its function.

This thesis examined the Ca^{2+} dynamics of HCs of the common goldfish (*Carassius auratus*). It is divided into five chapters, including an introductory chapter, three autonomous research chapters, and a general discussion chapter. This chapter aims to introduce relevant information, which is not covered in detail in the introductions of the research chapters, beginning with an

overview of Ca^{2+} homeostasis in HCs of fish. This introductory chapter will also provide background information on hypoxia and hypoxia tolerance, which is relevant to Chapter 4. Finally, the specific objectives for each research chapter will be provided.

1.2 Ca^{2+} pathways in teleost HCs

This section will review the Ca^{2+}-permeable pathways in teleost HCs. For reference, the Ca^{2+}-permeable channels in fish HCs are summarized in Table 1.1, and a working model of Ca^{2+}-permeable pathways and their regulation in teleost HCs is presented in Fig. 1.1.

1.2.1 Ca^{2+} influx

In the vertebrate outer retina, PRs are tonically depolarized in the dark by a Na^{+}-dominant "dark current" (Stryer 1991; Yau 1994). As a result, glutamate is constantly released onto HCs and bipolar cells (BCs) (Dowling and Ripps 1973; Miller and Schwartz 1983). PRs, HCs, and off BCs are constantly depolarized to approximately –30 to –20 mV in the dark (Dowling 1987). For HCs, this triggers prolonged Ca^{2+} influx through both ionotropic glutamate receptors (iGluRs) and voltage-gated Ca^{2+} channels (VGCCs; Linn and Christensen 1992; Tachibana 1983; 1985).

iGluR subtypes have different biophysical properties and physiological functions – including Ca^{2+} permeability. N-methyl-D-aspartate receptors (NMDARs) are permeable to Ca^{2+}, while both α-amino-3-hydroxy-5-methyl-4-isoxazolepropionic acid receptors (AMPARs) and kainate receptors (KARs) can be either Ca^{2+}-permeable or Ca^{2+}-impermeable. Notably, AMPARs lacking GluR2 subunits are Ca^{2+}-permeable. Ca^{2+} permeability for AMPARs containing GluR2 subunits depends on editing at a single amino acid site (Hollmann and Heinemann 1994; Peng et al. 2006). Similarly, the Ca^{2+} permeability of KARs depends on RNA editing for at least some subunits (Köhler et al. 1993).

Table 1.1. Ca^{2+}-permeable ion channels, pumps, and exchangers found in teleost HCs.

Ion channel, pump, or exchanger	Species	Common Name	Subtype†	Reference
Ionotropic glutamate receptors				
NMDARs	*Carassius auratus*	Goldfish*	H1	(Jiang et al. 2008; Shen et al. 2006; Wang et al. 2008)
	Ictalurus punctatus	Catfish	Cone	(Linn and Christensen 1992; O'Dell and Christensen 1986; O'Dell and Christensen 1989)
	Perca fluviatus	European perch	Cone	(Schmidt 1997)
	Roccus americana	White perch	Cone	(Schmidt 1997)
Ca^{2+}-permeable AMPARs	*Carassius auratus*	Goldfish*	Cone	(Huang and Liang 2005)
			H1	(Huang et al. 2006; Sun et al. 2010)
	Not provided	Carp	Cone	(Okada et al. 1999)
Voltage-gated Ca^{2+} channels				
L-type	*Carassius auratus*	Goldfish	–	(Jonz and Barnes 2007; Tachibana 1983; 1981)
	Cyprinus carpio	Carp	–	(Hayashida and Yagi 2002; Murakami and Takahashi 1987)
	Roccus americana	White perch	All	(Lasater 1986)
	Ictalurus punctatus	Channel catfish	Cone	(Dixon et al. 1993; Linn and Gafka 2001; Shingai and Christensen 1986; 1983; Takahashi et al. 1993)
P/L-type	*Roccus chrysops*	White bass	All	(Sullivan and Lasater 1992)
			Cone	(Pfeiffer-Linn and Lasater 1996)
T-type	*Roccus chrysops*	White bass	All	(Sullivan and Lasater 1992)

Store- and extrusion-related channels				
Ryanodine receptors	*Carassius auratus*	Goldfish*	–	(Huang et al. 2006; Huang et al. 2004)
			H1	(Lv et al. 2014)
	Ictalurus punctatus	Channel catfish	Cone	(Linn and Gafka 2001; Linn and Christensen 1992)
			–	(Micci and Christensen 1998)
	Moroni chrysops	White bass	H2	(Solessio and Lasater 2002)
Inositol triphosphate receptors	*Ictalurus punctatus*	Channel catfish	–	(Micci and Christensen 1996)
	Ictalurus punctatus	Channel catfish	Cone	(Linn and Gafka 2001)
Store-operated channels	*Carassius auratus*	Goldfish*	H1	(Lv et al. 2014)
Na^+/Ca^{2+}-exchanger	*Carassius auratus*	Goldfish	–	(Hayashida et al. 1998; Yasui 1987)
	Cyprinus carpio	Carp	–	(Yasui 1987)
	Ictalurus punctatus	Channel catfish	–	(Micci and Christensen 1998)
Plasma membrane Ca^{2+} pump	*Carassius auratus*	Goldfish	–	(Hayashida et al. 1998; Kreitzer et al. 2012)
	Ictalurus punctatus	Channel catfish	–	(Jacoby et al. 2012; Kreitzer et al. 2007; Micci and Christensen 1998)
Gap junctions and hemichannels				
Cx26‡	*Carassius carassius*	Carp	–	(Janssen-Bienhold et al. 2001)
	Danio rerio	Zebrafish	–	(Kamermans et al. 2001)
Cx35/36‡	*Carassius auratus*	Goldfish*	H1, H2	(Liu et al. 2009)
Cx43‡	*Carassius carassius*	Carp	–	(Dermietzel et al. 2000; Janssen-Bienhold et al. 1998)
Cx52.6‡	*Danio rerio*	Zebrafish	–	(Shields et al. 2007; Sun et al. 2012; Zoidl et al. 2004)

Cx55.5‡	*Danio rerio*	Zebrafish	–	(Dermietzel et al. 2000; Klaassen et al. 2011; Shields et al. 2007; Sun et al. 2012)
Pannexin-1	*Danio rerio*	Zebrafish	–	(Prochnow et al. 2009a; Prochnow et al. 2009b)
Uncharacterized	*Carassius auratus*	Goldfish	–	(Jonz and Barnes 2007)
			H1	(Schmitz and Wolburg 1991)
			Cone	(Shen et al. 2003)
	Cyprinus carpio	Carp	All	(Kaneko and Stuart 1984; Teranishi et al. 1983; Yamada and Ishikawa 1965)
	Danio rerio	Zebrafish	–	(McMahon 1994; McMahon and Brown 1994)
	Devario danio	Giant danio	H1	(McMahon and Mattson 1996)
	Ictalurus punctatus	Channel catfish	Cone	(DeVries and Schwartz 1989; DeVries and Schwartz 1992; Dixon et al. 1996; Sakuranaga and Naka 1985)
	Roccus americana	White perch	All	(Lasater and Dowling 1985)
	Roccus chrysops	White bass	Cone	(Lasater 1987)
	Roccus chrysops x roccus saxitalis	Hybrid striped bass	–	(Sun et al. 2009; Zhang and McMahon 2000)

* In these papers, the authors referred to *Carassius auratus* as carp instead of goldfish.
† In this column, "All" means that the ion channel, pump, or exchanger was found on all subtypes. "–" depicts papers in which no mention was made of subtypes.
‡ Cx, connexin.

Figure 1.1. Ca^{2+} pathways and their regulation in teleost horizontal cells.

(1) In darkness, glutamate (red circles) is released from photoreceptors, and binds onto HC glutamate receptors, allowing Ca^{2+} influx through Ca^{2+}-permeable AMPARs and NMDARs and leading to depolarization of the plasma membrane. (2) Depolarization also opens VGCCs, including L-type and (at least in bass) T-type VGCCs. (3) Glutamate receptors acidify the cytosol, downregulating L-type VGCCs. In contrast, group I and/or III mGluRs may upregulate VGCCs (see text). (4) Additionally, glutamate triggers CICR from RyRs, further downregulating L-type VGCCs. (5) The SERCA pump then refills Ca^{2+} stores, along with (6) SOCs and/or NCXs functioning in reverse. (7) IP3Rs have been found in catfish but do not contribute to CICR. (8) Gap junctions and hemichannels might allow Ca^{2+} flow between coupled cells or with the extracellular environment in some conditions. (9) Ca^{2+} influx from AMPARs, NMDARs, and VGCCs is extruded by the NCX and, possibly to a lesser extent, the PMCA. (10) Cytosolic Ca^{2+} is strongly buffered by Ca^{2+} binding proteins. Abbreviations: AMPAR, α-amino-3-hydroxy-5-methyl-4-isoxazolepropionic acid receptor; NMDAR, N-methyl-D-aspartate receptor; VGCC, voltage-gated Ca^{2+} channel; mGluR, metabotropic glutamate receptor; CICR, Ca^{2+}-induced Ca^{2+} release; RyR, ryanodine receptor; SERCA, sarcoplasmic/endoplasmic reticulum Ca^{2+} ATPase; SOC, store-operated channel; NCX, Na^{+}/Ca^{2+} exchanger; IP3R, inositol triphosphate receptor, PMCA, plasma membrane Ca^{2+}-ATPase.

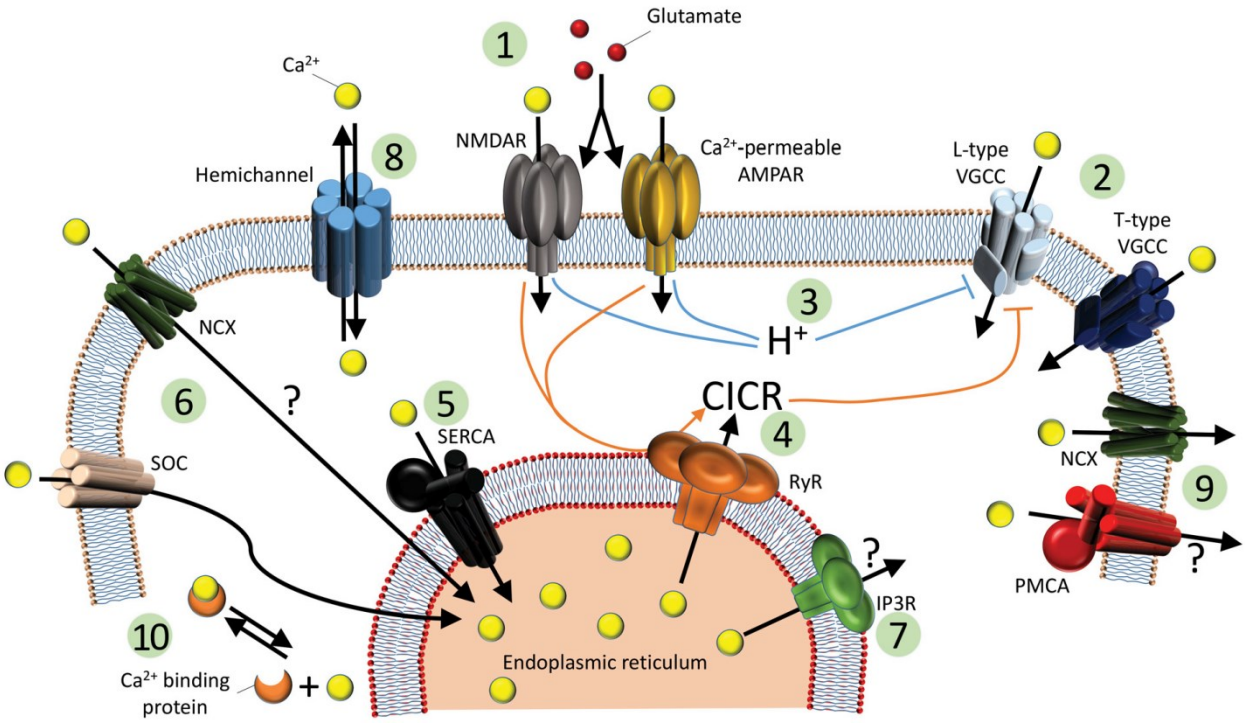
Glutamate
1
Ca2+
NMDAR
Ca2+-permeable
AMPAR
L-type
VGCC
2
Hemichannel
8
T-type
VGCC
NCX
3
H+
6
?
5
CICR
SERCA
4
SOC
RyR
NCX
9
?
?
PMCA
IP3R
7
10
Endoplasmic reticulum
Ca2+ binding
protein
+

Figure 1.1

Teleost HCs respond to a variety of iGluR agonists, including glutamate, kainate, quisqualate, AMPA, and NMDA (Huang et al. 2006; Ishida et al. 1984; Lasater and Dowling 1982; Linn and Christensen 1992; O'Dell and Christensen 1986; Okada et al. 1999; Schmidt 1997). However, evidence is strongest for AMPARs and weaker for KARs and NMDARs. Using modulators which preferentially potentiate KARs or AMPARs, Shen et al. (1999) found evidence only for AMPA-preferring receptors in carp HCs. Early investigators were unable to find NMDARs in fish HCs, in a variety of species (Lasater and Dowling 1982; Lasater et al. 1984; Okada et al. 1999), and some even found a *hyper*polarizing response to NMDA – and only at high concentrations (Ariel et al. 1984; Ariel et al. 1986; Rowe and Ruddock 1982). However, other studies found NMDA elicits a depolarizing response in HCs of the catfish (*Ictalurus punctatus*) (Linn and Christensen 1992; O'Dell and Christensen 1986), Crucian carp (*Carassius carassius*) (Jiang et al. 2008; Shen et al. 2006) and goldfish (Wang et al. 2008). Perhaps these later studies found greater success because they included co-application of glycine (a necessary NMDAR co-agonist; Van Dongen 2008) with NMDA or removal of extracellular Mg^{2+} (a voltage-dependent NMDAR blocker).

NMDARs may exist only on cone HCs. In most species, teleost HC subtypes are designated H1, H2, H3 and H4, in order of increasing dendritic field size, decreasing somatic size, and increasing distance from the outer retinal layers (Stell and Lightfoot 1975). These subtypes synapse with PRs selectively: H1, H2 and H3 synapse with cones, while H4 synapses with rods. All aforementioned studies that found NMDARs in HCs focused solely on cone HCs (predominantly H1), with one exception: a study on Crucian carp looked at both rod and cone HCs, but failed to find NMDARs in H4 (Shen et al. 2006).

Interestingly, Huang and Liang (2005) proposed that Ca^{2+}-permeable and Ca^{2+}-impermeable AMPARs coexist on HCs. When they co-applied AMPA with the selective Ca^{2+}-permeable AMPAR blocker, joro spider toxin-3 (JST-3), they found a decrease in $[Ca^{2+}]_i$ transients; in a similar manner, the selective Ca^{2+} impermeable AMPAR antagonist, pentobarbital (Yamakura et al. 1995), reduced AMPA-elicited responses. As further evidence for a Ca^{2+}-permeable AMPAR, AMPA applied *in situ* elicits a rise in $[Ca^{2+}]_i$, even when co-applied with Co^{2+} to block VGCCs (Okada et al. 1999). This increase in $[Ca^{2+}]_i$ is not due to Na^+-Ca^{2+} exchange because it persists even as extracellular Na^+ is replaced with N-methyl-D-glucamine (Okada et al. 1999). Therefore, Ca^{2+}-permeable AMPARs likely represent a major source of steady Ca^{2+} influx into HCs. Indeed, Sun et al. (2010) recently found that Ca^{2+}-permeable AMPARs account for 75% of all iGluR currents.

Although the relative contribution of NMDARs and AMPARs to the $[Ca^{2+}]_i$ response has not been clearly established, both may contribute to Ca^{2+} influx in the dark in teleosts where NMDARs are present.

HC responses to glutamate are especially well-characterized in Ca^{2+} imaging experiments, in which changes in $[Ca^{2+}]_i$ are quantified over time. Initially, glutamate induces a large, transient peak in $[Ca^{2+}]_i$. $[Ca^{2+}]_i$ is then lowered to a sustained, elevated baseline for as long as glutamate is applied (Hayashida and Yagi 2002). The transient peak is blocked by ryanodine and is likely due to Ca^{2+}-induced Ca^{2+} release (CICR) through ryanodine-sensitive stores (Huang et al. 2004).

Several studies suggest that the sustained $[Ca^{2+}]_i$ component is due to activation of more than one Ca^{2+}-permeable pathway (Hayashida and Yagi 2002; Hayashida et al. 1998; Linn and Christensen 1992). Part of this sustained response is due to L-type VGCCs, because the selective L-type VGCC blocker, nifedipine, reduces Ca^{2+} responses to glutamate (Hayashida et al. 1998)

or AMPA (Huang and Liang 2005). In concurrent voltage-clamp and Ca^{2+}-imaging experiments, glutamate only subtly increased sustained $[Ca^{2+}]_i$ after a voltage-step to –5 mV (Hayashida and Yagi 2002), suggesting that once VGCCs are open by depolarization, iGluRs do not greatly increase $[Ca^{2+}]_i$. The other part of the sustained Ca^{2+} response to glutamate is through iGluRs themselves: blocking VGCC conductance with the L-type blocker, nimodipine, does not abolish responses to kainate in catfish HCs (Linn and Christensen 1992). Furthermore, under voltage-clamp at potentials high enough to ensure VGCCs are deactivated, iGluR agonists such as NMDA, glutamate, quisqualate, and kainate increase $[Ca^{2+}]_i$ to a new, elevated baseline (Hayashida et al. 1998; Linn and Gafka 2001; Linn and Christensen 1992). Collectively this suggests that once glutamate from PRs opens iGluRs, HCs depolarize to open VGCCs. Many reports found that L-type VGCCs contribute nearly 50% of the Ca^{2+} current elicited by glutamate application *in situ* (Hayashida and Yagi 2002; Hayashida et al. 1998; Huang and Liang 2005) and, therefore, they represent a major source of Ca^{2+} influx in teleost HCs.

L-type VGCCs in HCs have been well studied with electrophysiological techniques in a number of species, including goldfish (Tachibana 1983), channel catfish (Shingai and Christensen 1986; 1983), white perch (Lasater 1986), and white bass (*Roccus chrysops*) (Sullivan and Lasater 1992). These studies reported an inward conductance that activated in a range between –45 to –30 mV, and peaked between 0 and 25 mV.

It should be mentioned here that unlike typical VGCCs which undergo strong Ca^{2+}-dependent inactivation, such inactivation is weaker in HCs (Tachibana 1983). Instead, there is evidence that VGCCs are down-regulated by low intracellular pH, which can be induced by extracellular acidification (Jonz and Barnes 2007) or by intracellular acidification caused by glutamate application (Dixon et al. 1993; Takahashi et al. 1993). In addition, VGCCs are down-

regulated by CICR (Linn and Gafka 2001). The available evidence suggests that CICR can raise $[Ca^{2+}]_i$ enough for substantial VGCC inactivation, but currents through VGCCs cannot.

HCs of a given type are electrically coupled to each other by gap junctions, forming a syncytium throughout the inner nuclear layer (Kaneko and Stuart 1984; Sakuranaga and Naka 1985). These channels are permeable to ions and molecules up to ~1 kDa (Contreras et al. 2004), and allow for Ca^{2+} diffusion between cells (D'Andrea and Vittur 1996; Höfer et al. 2001; Nielsen et al. 2012; Saez et al. 1989). Functionally, electrical coupling through gap junctions provides HCs with a large receptive field size (Kaneko and Stuart 1984), whereas uncoupling decreases this receptive field size and reduces center-surround antagonism (Shen et al. 2003).

Additionally, both pannexin-1- and ZfCx26-based hemichannels have been found in zebrafish HC dendrites, where they have been theorized to assist in feedback to cones (Kamermans et al. 2001; Prochnow et al. 2009b). Many retinal connexin and pannexin transcripts have recently been cloned (Zoidl et al. 2008), suggesting that more may be found in HCs in the near future.

1.2.2 Ca^{2+} extrusion mechanisms

Because high levels of cytosolic Ca^{2+} are toxic to neurons (Choi 1992; Lipton 1999), sustained Ca^{2+} influx through iGluRs and VGCCs must be balanced by sequestration and efflux mechanisms to maintain cell viability. Although cytosolic buffering mechanisms and sequestration into intracellular Ca^{2+} stores are known in HCs (see below), these stores must be finite and would be replete with Ca^{2+} over time. Therefore, Ca^{2+} must be extruded across the plasma membrane to limit $[Ca^{2+}]_i$. Two major Ca^{2+} extrusion mechanisms have been shown to exist in teleost HCs: a plasma membrane Ca^{2+}-ATPase (PMCA), and a Na^+/Ca^{2+} exchanger (NCX) (Kreitzer et al. 2007; Micci and Christensen 1998; Yasui 1987).

To demonstrate Na^+/Ca^{2+} exchange, Hayashida et al. (1998) applied glutamate for over an hour so as to ensure that Ca^{2+} uptake and efflux reached equilibrium – both across the plasma membrane and in/out of intracellular Ca^{2+} stores. Changes in this new $[Ca^{2+}]_i$ would have therefore reflected a change in Ca^{2+} homeostasis. When extracellular Na^+ was removed, or when Li^+ (which cannot functionally replace Na^+ in NCX activity) was applied, $[Ca^{2+}]_i$ increased, suggesting the presence of NCX activity. Similarly, Na^+/Ca^{2+} exchange was also inhibited by high $[Ca^{2+}]_o$, which reduced the driving force for Ca^{2+} and made NCX exchange energetically unfavourable.

The first report of PMCAs in teleost HCs came from Micci and Christensen (1998), who found that the non-specific P-type ATPase inhibitor, vanadate, greatly increased $[Ca^{2+}]_i$ in freshly-dissociated cells. Vanadate can also inhibit Na^+/K^+-ATPases, which would increase intracellular $[Na^+]$ and therefore the driving force for NCX activity. Yet $[Ca^{2+}]_i$ only slightly increased when oubain, a selective Na^+/K^+-ATPase inhibitor, was applied (Micci and Christensen, 1998). Vanadate, however, has been shown to inhibit refilling of certain intracellular Ca^{2+} stores (Watson et al. 2003), so a vanadate-elicited increase in $[Ca^{2+}]_i$ may be caused by either sarco/endoplasmic reticulum Ca^{2+}-ATPase (SERCA) or PMCA antagonism.

Further evidence for PMCAs on HCs comes from studies of proton efflux in skate, catfish, and goldfish. PMCAs exchange extracellular protons and intracellular Ca^{2+} at the cost of ATP, so that changes in extracellular pH may be related to PMCA activity (Di Leva et al. 2008). Using self-referencing proton electrodes, several studies found that depolarizing isolated HCs with glutamate, kainate, high K^+ solutions, or voltage-clamp increased extracellular pH (Jacoby et al. 2012; Kreitzer et al. 2007; Kreitzer et al. 2012; Molina et al. 2004). This extracellular alkalization was abolished with low Ca^{2+} solutions, Co^{2+}, and nifedipine, or with PMCA

antagonists such as carboxyeosin and lanthanum (Jacoby et al. 2012; Kreitzer et al. 2007; Kreitzer et al. 2012). Furthermore, concurrent recordings showed that extracellular pH and $[Ca^{2+}]_i$ varied synchronously, suggesting an exchange mechanism (Kreitzer et al. 2012). Collectively, these studies suggest that Ca^{2+} influx from VGCCs leads to Ca^{2+} extrusion, and simultaneous proton influx, through PMCAs. Along with immunohistochemical labeling in the outer plexiform layer and in dissociated cells of the skate (Molina et al. 2004), these findings strongly support PMCA activity in teleost and skate HCs.

It is unclear how physiologically important PMCAs are in HCs. In one report in goldfish and carp, orthovanadate was found to increase $[Ca^{2+}]_i$ only marginally in HCs during prolonged glutamate application, and had no effect in the absence of glutamate (Hayashida et al. 1998). This presents the possibility that the PMCA plays a minimal role in maintaining resting $[Ca^{2+}]_i$ in HCs, and that NCX dominates Ca^{2+} extrusion in these cells. This may be a strategy to reduce ATP expenditure. HCs are constantly taxed with Ca^{2+} influx and so PMCA activity would be energetically costly.

1.2.3 Ca^{2+} buffering

Very few studies have analyzed buffering in HCs; however, the limited information available suggests that teleost HCs have some of the highest buffering capacities known of any cell type. Ca^{2+} buffering (β) is often defined as the ratio of entering Ca^{2+} ions that bind to cytosolic buffers, compared to the Ca^{2+} ions that remain free in solution. As an example, β has been estimated to be 100 in rat gonadotrophs, so that for every 101 Ca^{2+} ions that enter the cytosol, only one Ca^{2+} ion would remain free (Tse et al. 1994). A review of neuronal Ca^{2+} buffering lists typical β values between 20–200, with nearly all values below 300 (Matthews and Dietrich 2015).

Surprisingly, the only study to examine Ca^{2+} buffering in teleost HCs measured β at 2,500 as a lower limit (Solessio and Lasater 2002). The authors also showed that this extraordinarily high buffering capacity slowed increases in $[Ca^{2+}]_i$. Although VGCC current reaches a maximal value within milliseconds, the resulting increases in $[Ca^{2+}]_i$ have time constants over 8 seconds. Functionally, this extraordinarily high Ca^{2+} buffering capacity may be neuroprotective by reducing free $[Ca^{2+}]_i$ during prolonged Ca^{2+} influx.

1.2.4 Ca^{2+} stores in HCs

Non-mitochondrial intracellular Ca^{2+} stores are often categorized by the involvement of either ryanodine receptors (RyRs) or inositol triphosphate receptors (IP_3Rs). Numerous Ca^{2+} imaging experiments provide strong support for RyRs in HCs, which mediate CICR in these neurons (Huang et al. 2004; Linn and Gafka 2001; Lv et al. 2014; Solessio and Lasater 2002). In contrast, there are only two reports that suggest IP_3Rs exist in teleost HCs (both in catfish) – specifically, an immunohistochemical report (Micci and Christensen 1996), and Ca^{2+} imaging experiments which showed a slow increase in $[Ca^{2+}]_i$ with IP_3 application (Linn and Gafka 2001). However, IP_3Rs do not elicit CICR in these cells (Linn and Gafka 2001); furthermore, CICR does not occur when ryanodine or dantrolene are used to block RyRs *in vitro* (Lv et al. 2014; Micci and Christensen 1998). The role of IP_3Rs in these cells is largely unexplored, and it is unknown if they exist in HCs of other teleosts.

In catfish, Ca^{2+} stores were shown to be sensitive to caffeine, a RyR agonist that elicited CICR and presumably depleted Ca^{2+} from stores (Micci and Christensen 1998). If it was applied twice within a short period of time, the second caffeine pulse induced a smaller CICR transient, which was comparably smaller than the first caffeine pulse. The authors interpreted this to mean that stores were refilling with Ca^{2+} during the interim, and estimated that refilling of stores

occurred after 2 minutes. Refilling was shown to be dependent on extracellular Ca^{2+}, even in the presence of nifedipine to block Ca^{2+} influx through VGCCs. Interestingly, while extrusion mechanisms are blocked, HC Ca^{2+} stores can accumulate enough Ca^{2+} to double CICR amplitudes (Micci and Christensen 1998). This suggests that stores are not replete with Ca^{2+}, but have an unexpectedly large capacity to accommodate additional Ca^{2+}. Because HCs can be depolarized for hours at a time and undergo constant Ca^{2+} influx, large-capacity stores might buffer against otherwise excitotoxic increases in $[Ca^{2+}]_i$.

Micci and Christensen (1998) proposed that the NCX operates in reverse to refill stores. By inhibiting NCX activity with Li^+, they found that subsequent caffeine application could not elicit CICR. This has been observed in bovine smooth muscle, where NCX may operate in reverse to refill RyR-sensitive stores (Hirota et al. 2007); however, confirmation of this in teleost HCs awaits the use of selective NCX inhibitors. Alternatively, it is possible that store-operated channels (SOCs) refill stores. In goldfish, it was shown that a SOC inhibitor (2-aminoethoxydiphenyl borate, or 2-APB) prevented stores from refilling (Lv et al. 2014). Further research will need to clarify whether both mechanisms exist in both species, and what their relative contributions are to refilling.

Functionally, CICR is known to occur immediately after glutamate application in HCs, followed by a sustained Ca^{2+} influx from VGCCs and iGluRs. Linn and Gafka (2001) found that Ca^{2+} from CICR is able to down-regulate VGCCs. This down-regulation was not seen when CICR was blocked (with ryanodine) or when stores were depleted (with caffeine). Conceivably, this would serve to decrease the sustained Ca^{2+} influx through VGCCs during glutamate application, preventing excitotoxic increases in $[Ca^{2+}]_i$.

1.3 Ca^{2+} action potentials (APs) in HCs

In teleosts (i.e. goldfish, carp, and catfish) and skates, isolated HCs are known to produce APs (Johnston and Lam 1981; Lasater et al. 1984; Murakami and Takahashi 1987; Tachibana 1981). There has been brief mention of similar regenerative membrane activity in HCs of white perch (Lasater 1986) and white bass (Sullivan and Lasater 1992). The physiological significance of APs in HCs is currently unknown.

Despite their all-or-nothing activity, these APs are quite unique. They persist in the absence of Na^+ (Shingai and Christensen 1983) and are not abolished by Na^+ channel blockers, such as tetrodotoxin (Tachibana 1981); although in some fish, Na^+ currents contribute to the rising phase of the AP (Malchow et al. 1990; Shingai and Christensen 1986; 1983). Instead, APs in HCs are primarily Ca^{2+}-dependent. They are amplified with high $[Ca^{2+}]_o$ and diminished with low $[Ca^{2+}]_o$ (Tachibana 1981); blocked by Co^{2+}, Mn^{2+}, and Ni^{2+} (Johnston and Lam 1981); and enhanced and prolonged by VGCC-permeant ions, such as Ba^{2+} and Sr^{2+} (Tachibana 1981). The APs are also slow, lasting on the order of seconds to minutes (Dixon et al. 1993; Tachibana 1981).

APs have been described in fish HCs in a number of preparations, including the intact retina (Murakami and Takahashi 1987), cultured cells (Lasater et al. 1984; Tachibana 1981), and freshly dissociated cells (Shingai and Christensen 1983). Although all investigators could induce APs with depolarizing current pulses (e.g. Dixon et al. 1993; Lam and Ayoub 1983; Shingai and Christensen 1983), some reports found them to occur spontaneously, especially with Ba^{2+} or K^+ channel blocker application (Murakami and Takahashi 1987; Tachibana 1981). Furthermore, both Lasater et al. (1984) and Ishida et al. (1984) initiated AP activity with glutamate application.

APs may not be specific to fish. Ueda et al. (1992) found that A-type HCs of the cat showed spiking activity, while B-type cells did not. The authors demonstrated that APs were generated by VGCC current, and that A-type HCs have a greater VGCC current density than B-type cells. In a turtle (*Pseudemys scripta elegans*) eyecup preparation, HCs showed spike-like depolarizations during the light-to-dark transition; furthermore, these spikes require extracellular Ca^{2+} and are suppressed by Co^{2+} (Akopian et al. 1991). In a similar eyecup preparation, *Xenopus* HCs were found to depolarize during the light-to-dark transition. This effect was enhanced by Ba^{2+} and Sr^{2+} and blocked by nifedipine (Akopian et al. 1997). This suggests that VGCCs may serve to quickly repolarize HCs to their dark membrane potential at light offset.

1.4 $[Ca^{2+}]_i$ and feedback

In the outer retina, HCs provide inhibitory feedback to photoreceptors (PRs), modulating synaptic gain and mediating a center-surround antagonism that allows for edge detection (Baylor et al. 1971; Thoreson and Mangel 2012). Although there is no consensus as to how this feedback occurs, three mechanisms have been proposed in vertebrates: hemichannels at HC dendrites may alter PR membrane potential by an ephaptic mechanism (Byzov and Shura-Bura 1986; Fahrenfort et al. 2009; Gardner et al. 2015; Kamermans et al. 2001); HCs may release protons or regulate cleft acidity (Vroman et al. 2014; Warren et al. 2016) to reduce the conductance of PR VGCCs and shift their activation to more depolarized voltages (Barnes 2003; Hirasawa and Kaneko 2003; Vessey et al. 2005), and/or; HCs may release less GABA onto PRs during light stimulation (GABA disinhibition) (Hirano et al. 2005; Hirano et al. 2016; Liu et al. 2013; Wu and Dowling 1980), by vesicular release in mammals and largely through an unconventional transporter mechanism in non-mammalian vertebrates (Schwartz 2002).

Ca^{2+} signaling in HCs would likely affect all three mechanisms. HC hemichannels are regulated by extracellular Ca^{2+} concentrations ($[Ca^{2+}]_o$) (DeVries and Schwartz 1992; Jonz and Barnes 2007). There is also evidence that intracellular Ca^{2+} concentration ($[Ca^{2+}]_i$) affects extracellular pH, and may therefore affect pH at the HC-PR synapse (Kreitzer et al. 2012). In rats, HC VGCCs have been shown to be necessary for vesicular GABA release, and for feedback, in a pH-dependent fashion (Liu et al. 2013), and GABA release from HCs in fish is probably partially Ca^{2+}-dependent (Ayoub and Lam 1985; Lasater and Lam 1984). In light of this evidence, a model for Ca^{2+} dynamics in HCs will be instrumental in understanding HC to PR feedback, and neural processing in the outer retina in general.

Both GABA and the enzyme that synthesizes it (glutamic acid dehydrogenase, or GAD) have been found in HCs from both fish and mammals (Brandon 1985; Guo et al. 2010; Lam et al. 1980; Mosinger and Yazulla 1987; Mosinger et al. 1986), suggesting that at least some HCs are GABAergic. However, in fish, only one HC subtype (H1) accumulates and releases GABA (Ayoub and Lam 1987; Lam et al. 1980; Marc et al. 1978) which has, in part, led to the suggestion that GABA may not mediate feedback from fish HCs, but may instead modulate it (Endeman et al. 2012; Schwartz 2002).

Mechanisms of GABA release likely differ between mammalian and non-mammalian species. In mammals, there is growing support for a Ca^{2+}-dependent, vesicular release of GABA from HCs (Cueva et al. 2002; Haverkamp et al. 2000; Lee and Brecha 2010; Liu et al. 2013; Thoreson and Mangel 2012), as occurs elsewhere in the nervous system (Wadel et al. 2007). Several essential components for vesicular GABA release have been localized to HCs (Cueva et al. 2002; Guo et al. 2010; Lee and Brecha 2010), including SNARE proteins and synaptotagmin-2, a Ca^{2+} sensor for exocytosis (Lee and Brecha 2010). In retinal slices from rat, HC VGCCs

open during depolarization, allowing $[Ca^{2+}]_i$ to rise, which triggers vesicular GABA release (Liu et al. 2013).

In HCs of teleost and other non-mammalian species, only a small number of studies have found evidence for Ca^{2+}-dependent release (Ayoub and Lam 1985; Lasater and Lam 1984). Instead, GABA release may occur through Ca^{2+}-independent plasmalemmal GABA transporters operating in reverse (reviewed in Schwartz 2002). Both mechanisms (Ca^{2+}-independent transporter and Ca^{2+}-dependent vesicular release) might dominate in certain illumination conditions. Ayoub and Lam (1985) proposed a model in which mild depolarization would trigger Ca^{2+}-dependent GABA release, whereas strong depolarization would rapidly exhaust the supply of GABA-containing vesicles while triggering transporter-dependent GABA release. Translated into light responses, this model suggests that GABA transport dominates in the dark, whereas Ca^{2+}-dependent vesicular release dominates in dim lighting. There is no evidence for plasmalemmal GABA transporters in mammals (Feigenspan and Weiler 2004).

For mammals and other vertebrates alike, it is unclear whether PRs are the primary targets for GABA, since feedback has not been blocked by GABA antagonists in goldfish (Verweij et al. 1996), monkey (Verweij et al. 2003), or turtle (Thoreson and Burkhardt 1990). In the rat, a unifying mechanism for inhibitory feedback to PRs has been proposed in which GABA may modulate pH and/or ephaptic feedback (Liu et al. 2013). In this model, Ca^{2+}-dependent GABA release would activate ionotropic GABARs on the HCs themselves. As GABARs are permeable to both Cl^- and HCO_3^-, they could modulate cleft pH and shunt current into HCs (Liu et al. 2013). As further support, targeted deletion of HC vesicular GABA transporters in mouse abolished inhibitory feedback to PRs (Hirano et al. 2016). Therefore, at least in rodents, Ca^{2+}-dependent GABA release from HCs is important for negative feedback to PRs.

1.5 Hypoxia tolerance in neurons of the brain and retina

Neurons spend over 50% of their ATP budget on Na^+/K^+-ATPase pumps, which maintain transmembrane ion gradients and support resting membrane potential (Ames 1992; Erecińska and Silver 1994). During periods of reduced O_2 supply (hypoxia) or blood flow (ischemia), a reduction in available ATP starves Na^+/K^+-ATPases and limits their activity. The resulting depolarization activates VGCCs, leading to increased $[Ca^{2+}]_i$ (Bickler 1992; Bickler and Buck 1998; Bickler and Kelleher 1992; Szydlowska and Tymianski 2010). Depolarization also leads to decreased glutamate uptake; excess extracellular glutamate then activates iGluRs and further increases $[Ca^{2+}]_i$ (Bradford et al. 1987; Choi and Rothman 1990; Milton et al. 2002; Szydlowska and Tymianski 2010). Ultimately this increase in $[Ca^{2+}]_i$ triggers multiple deleterious and fatal pathways, including overstimulation of catabolic, Ca^{2+}-dependent enzymes; increased production of reactive oxygen species (ROS) by mitochondria; cytoskeletal breakdown; and apoptosis (Arundine et al. 2004; Choi 1992; Shibata et al. 2002; Szydlowska and Tymianski 2010). Collectively, these events are termed excitotoxicity or excitotoxic cell death.

Some ectotherms have evolved to withstand long periods of hypoxia, and may therefore hold insights into how $[Ca^{2+}]_i$ can be maintained despite low O_2 supply. Anoxia tolerant turtles such as the red-eared slider (*Chrysemys picta*) are considered the champions of hypoxia tolerance because they overwinter in hypoxic ponds by suppressing their electrical activity to a mere "pilot light" level (Jackson 2002; Lutz and Nilsson 2004; Overgaard et al. 2007). At the neuronal level, this is seen as a downregulation of ion channels including NMDARs, AMPARs, Na^+ channels, and K^+ channels (Bickler et al. 2000; Buck and Bickler 1998; Dukoff et al. 2014; Pamenter et al. 2008a; Perez-Pinzon et al. 1992; Rodgers-Garlick et al. 2013). By reducing membrane permeability, this strategy of "channel arrest" lowers the ATP requirement for Na^+/K^+

ATPase pumps, while maintaining neuronal membrane potential (Buck and Hochachka 1993; Hochachka 1986). Furthermore, downregulation of Ca^{2+} permeable channels, such as NMDARs, limits Ca^{2+} entry to avoid excitotoxicity (Bickler and Buck 1998).

The anoxia-tolerant turtle is often contrasted with the hypoxia-tolerant fish of the genus *Carassius*: the Crucian carp (*C. carassius*) and the common goldfish (*C. auratus*) (Bickler and Buck 2007; Lutz and Nilsson 1997; Nilsson and Lutz 2004). Crucian carp can overwinter in hypoxic, ice-covered ponds (Holopainen and Pitkänen 1985) like turtles, but they do not suppress their electrical activity as strongly. Instead they maintain locomotor and neural activity throughout hypoxia, albeit at reduced levels (Lutz and Nilsson 1997; Nilsson 2001; Nilsson et al. 1993b). Likewise, goldfish also survive days of anoxia at ~4ºC and hours at room temperature (Walker and Johansen 1977; Wilkie et al. 2008). In these species (and in contrast to the turtle), glycolysis is upregulated to fuel the brain and maintain ion homeostasis throughout hypoxia (Johansson and Nilsson 1995; Lutz and Nilsson 1997; Nilsson 2001; Nilsson et al. 1993a). To sustain high rates of glycolysis without the toxic and acidic buildup of lactate, *Carassius* muscle tissue converts lactate to ethanol, which is soluble enough to diffuse out at the gills (Nilsson 2001; Shoubridge and Hochachka 1980). Early reports suggested that the *Carassius* brain does not undergo channel arrest like the turtle (Hylland et al. 1997; Johansson and Nilsson 1995), although a later report suggests NMDARs are downregulated in goldfish neurons of the telencephalon (Wilkie et al. 2008). This highlights the need for more experiments to clarify the cellular mechanisms of hypoxia tolerance in *Carassius*, which likely differ from those of the turtle.

The retina is part of the central nervous system, and has a metabolism higher than that of the brain (Ames 1992; Country 2017). The retina is sensitive to hypoxia in mammals and most

ectotherms (Country 2017; Osborne et al. 2004; Szabadfi et al. 2010). In the red-eared slider turtle (Stenslokken et al. 2008) and the Crucian carp (Johansson et al. 1997), electroretinogram activity is reduced during hypoxia, but recovers completely upon reperfusion, suggesting that retinal function is restored. In contrast, hypoxia quickly and irreversibly deteriorates electroretinogram responses of the hypoxia-sensitive rainbow trout (*Oncorhynchus mykiss*) (Hoffert and Ubels 1979; Ubels 1979). Furthermore, the goldfish retina undergoes little apoptosis after hypoxic insult, partly due to protection by metabotropic glutamate receptors (Beraudi et al. 2007). The cellular mechanisms of hypoxia tolerance are completely unexplored in the ectotherm retina.

1.6 Mitochondria are central to hypoxia tolerance

Mitochondria are central to both hypoxic cell death, and to hypoxia tolerance (Pamenter 2014). In hypoxia-sensitive species, decreases in O_2 supply limit the pumping of protons across the inner mitochondrial membrane. The subsequent depolarization and matrix alkalinization increases ROS production and opens the high-conductance mitochondrial megachannel, the mitochondrial permeability transition pore (mPTP) (Dirnagl and Meisel 2008; Zorov et al. 2000; Zorov et al. 2014). Cytochrome c and Ca^{2+} release from the mPTP can lead to catabolism and apoptosis (Halestrap 2009), while ROS can lead to oxidative damage (Zorov et al. 2014). Furthermore, complex V (ATP synthase) can operate in reverse in hypoxia, rapidly consuming the limited supply of ATP and exacerbating excitotoxicity (Wei-LaPierre and Dirksen 2019).

However, as the site of oxidative phosphorylation, mitochondria are well positioned to sense when O_2 supply is low. Most pathways of hypoxia tolerance therefore involve mitochondria (Pamenter 2014). In turtle neurons, mitochondrial K^+ ATP-dependent (mK_{ATP})

channels open early in the response to hypoxia, where they trigger neuroprotective pathways (Pamenter et al. 2008b). Once open, K^+ influx through mK_{ATP} channels slightly depolarizes mitochondria, opening the mitochondrial permeability transition pore (mPTP) to a low-conductance state (Hawrysh and Buck 2013). Even though $[Ca^{2+}]_i$ must be kept minimal to prevent excitotoxicity (Bickler and Buck 1998), paradoxically, mitochondria release a small amount of Ca^{2+} through the mPTP as part of the neuroprotective pathway (Dukoff et al. 2014; Hawrysh and Buck 2013). This slight increase in Ca^{2+} then activates second messengers such as protein kinase C (PKC) (Rodgers-Garlick et al. 2013) and protein phosphatases (Shin et al. 2005) to downregulate ion channels (Bickler et al. 2000; Pamenter et al. 2008a; Pamenter et al. 2008b; Perez-Pinzon et al. 1992; Rodgers-Garlick et al. 2013). mK_{ATP} channels are also protective in goldfish cardiomyocytes during hypoxia (Chen et al. 2005), suggesting goldfish may also benefit from a similar pathway. However, mK_{ATP} or mK_{ATP} neuroprotection have yet to be shown in the goldfish brain or retina.

In many mammals, short, sublethal treatments of ischemia protect the heart, brain, and retina from future ischemic insult (Heurteaux et al. 1995; Liu et al. 1998; Murry et al. 1990; Roth et al. 1998). This ischemic preconditioning (IPC) is mediated by protective pathways which route through mitochondria, and shows similarities with the strategies of hypoxia-tolerant organisms (Dirnagl and Meisel 2008; Pamenter 2016). As in the hypoxia-tolerant turtle, mK_{ATP} opens in hypoxia, leading to mild uncoupling of mitochondria (O'Rourke 2004; Pamenter 2014). Yet unlike in turtle neurons, this mild uncoupling does not open the mPTP and lead to Ca^{2+} release in IPC. Instead, the mPTP is inhibited, preventing the catastrophic release of cytochrome c and Ca^{2+} seen in normoxia (Dirnagl and Meisel 2008; Halestrap and Richardson 2015). This

difference highlights the need for future experiments to compare the protective strategies among animals.

In the mammalian retina, both IPC and the mK_{ATP} agonist, diaxozide, protect the retina (Dreixler et al. 2008; Roth et al. 2006; Roth et al. 1998). mK_{ATP} leads to downstream activation of ROS and nitric oxide; instead of being damaging, these may activate protective second messengers including two Ca^{2+}-independent isoforms of PKC (PKC-δ and PKC-ε) (Dreixler et al. 2008; Roth et al. 2006). In hypoxia-tolerant retinas of turtles and goldfish, the role for mK_{ATP} in hypoxia tolerance is unknown.

1.7 Thesis objectives

The present thesis aimed to expand our understanding of Ca^{2+} dynamics in goldfish HCs. Spontaneous Ca^{2+}-based APs are shown with three techniques; they are shown in isolated cells and in retinal slices; and they are found in both goldfish and rainbow trout (*Oncorhynchus mykiss*). This work sets a strong foundation for future experiments, to test for a possible role for APs. The final chapter studies both APs and baseline $[Ca^{2+}]_i$ throughout hypoxia in HCs, to create the first cellular model of hypoxic neuroprotection in the ectotherm retina. The objectives of each research chapter are outlined below:

Chapter 2: The objective of this study was to clarify which ion channels are involved in the generation of spontaneous Ca^{2+}-based APs in goldfish HCs. We tested the hypothesis that extracellular Ca^{2+} was necessary through L-type Ca^{2+} channels, and that intracellular Ca^{2+} stores contributed to APs *via* RyR-mediated Ca^{2+} release.

Chapter 3: This study tested the hypothesis that APs would be generated in retinal slices. A novel classification method was created to distinguish HC subtypes *in vitro*, to test the hypothesis that all subtypes of HC present APs. Lastly, we tested the hypothesis that APs differ among subtypes (in frequency, duration, etc.).

Chapter 4: This final study tested the hypothesis that hypoxia would dysregulate $[Ca^{2+}]_i$ in HCs of the hypoxia-sensitive rainbow trout, but not in HCs of the hypoxia-tolerant goldfish. In follow-up experiments, this study tested the hypotheses that mK_{ATP} channels are necessary for protection in goldfish, and that they are sufficient for protection in trout.

2 Spontaneous action potentials in retinal horizontal cells of goldfish (*Carassius auratus*) are dependent upon L-type Ca^{2+} channels and ryanodine receptors

This chapter includes material from the following article:

Country, M. W., Campbell, F. N. B., and Jonz, M. G. 2019. Spontaneous action potentials in retinal horizontal cells of goldfish (*Carassius auratus*) are dependent upon L-type Ca^{2+} channels and ryanodine receptors. *J Neurophysiol*. 122, 2284-2293.

I performed all experiments presented in this chapter, except for those illustrated in Figs. 2.1, 2.2, 2.3B, and those corresponding to 10 out of 18 cells in Fig. 2.3A, which were performed by former graduate student, Benjamin Campbell. I wrote the majority of the published manuscript, and played a primary role in designing the research and interpreting the results.

2.1 Abstract

Horizontal cells (HCs) are interneurons of the outer retina that undergo graded changes in membrane potential during the light response and provide feedback to photoreceptors. We characterized spontaneous Ca^{2+}-based action potentials (APs) in isolated goldfish (*Carassius auratus*) HCs using electrophysiological and intracellular imaging techniques. Transient changes in intracellular Ca^{2+} concentration ($[Ca^{2+}]_i$) were observed with Fura-2, and were abolished by removal of extracellular Ca^{2+}, or by inhibition of Ca^{2+} channels by 50 μM Cd^{2+} or 100 μM nifedipine. Inhibition of Ca^{2+} release from stores, with 20 μM ryanodine or 50 μM dantrolene, abolished Ca^{2+} transients and increased baseline $[Ca^{2+}]_i$. This increased baseline was prevented by blocking L-type Ca^{2+} channels with nifedipine, suggesting that Ca^{2+}-induced Ca^{2+} release (CICR) from stores may be needed to inactivate membrane Ca^{2+} channels. 3 mM caffeine increased the frequency of Ca^{2+} transients, and the store-operated channel antagonist, 2-aminoethyldiphenylborinate (2-APB, 100 μM), counteracted this effect. Action potentials were detected with voltage-sensitive dye imaging (FluoVolt) and current-clamp electrophysiology. In current-clamp recordings, regenerative APs were abolished by removal of extracellular Ca^{2+}, or in the presence of 5 mM Co^{2+} or 100 μM nifedipine, and APs were amplified with 15 mM Ba^{2+}. Collectively, our data suggest that during APs, Ca^{2+} enters through L-type Ca^{2+} channels and that Ca^{2+} stores (gated by ryanodine receptors) contribute to the rise in $[Ca^{2+}]_i$. This work may lead to further understanding of the possible role APs have in vision, such as transitioning from light to darkness, or modulating feedback from HCs to photoreceptors.

2.2 Introduction

Horizontal cells (HCs) are second-order interneurons in the inner nuclear layer of the retina. They facilitate visual processing, including lateral feedback inhibition onto photoreceptors to mediate edge detection and colour opponency (Thoreson and Mangel 2012; Twig et al. 2003). HCs receive glutamatergic input from photoreceptors, and characteristically respond with graded changes in membrane potential (Baylor et al. 1971; Perlman et al. 2011).

Less frequently, action potentials (APs) have been reported in HCs of fish, including the catfish (*Ictalurus punctatus*) (Dixon et al. 1993; Johnston and Lam 1981; Shingai and Christensen 1986; 1983; Takahashi et al. 1993), goldfish (*Carassius auratus*) (Tachibana 1981), common carp (*Cyprinus carpio*) (Murakami and Takahashi 1987), and skate (*Raja* spp.) (Lasater et al. 1984). APs have been observed in isolated HCs and in the intact retina (Murakami and Takahashi 1987; Tachibana 1981). They are dependent on Ca^{2+} influx through membrane ion channels and persist in the absence of Na^{+} (Shingai and Christensen 1983; Tachibana 1981). In addition, Kreitzer et al. (2012) observed spontaneous increases in intracellular Ca^{2+} concentration ($[Ca^{2+}]_i$) with Fluo-4 imaging. Neither APs nor spontaneous Ca^{2+} events are well characterized in HCs, and their role in vision (if any) is unknown.

HCs provide inhibitory feedback to photoreceptors by release of protons into the synaptic cleft (Barnes 2003; Hirasawa and Kaneko 2003; Vessey et al. 2005; Warren et al. 2016), by an ephaptic mechanism involving hemichannels (Gardner et al. 2015; Kamermans et al. 2001), or by release of GABA (Hirano et al. 2005; Hirano et al. 2016; Liu et al. 2013). APs in HCs involve changes in $[Ca^{2+}]_i$ and membrane voltage (V_m) that would be likely to impact any of these mechanisms of feedback.

In the present study, we observed spontaneous changes in $[Ca^{2+}]_i$ and membrane potential in goldfish HCs. We designed experiments to quantitatively characterize these events, and to identify the source of Ca^{2+}. We compared the parameters of Ca^{2+} transients using Fura-2-based imaging with those of voltage-sensitive dye (FluoVolt) and current-clamp recordings. For the first time, we show that Ca^{2+}-based APs are driven by plasma membrane ion channels and intracellular stores, and that AP frequency and amplitude is modulated by membrane potential in HCs.

2.3 Methods

2.3.1 Ethical approval

Procedures for animal care and use were approved by the University of Ottawa Animal Care and Veterinary Services (protocol BL-1760), which was implemented in accordance with regulations of the Canadian Council on Animal Care. Adult common goldfish were obtained from a commercial supplier (AQUAlity Tropical Fish Supply Inc., Mississauga, ON, Canada) and were housed in the aquatic facilities at the University of Ottawa. Fish were maintained in 170 l tanks fitted with a flow-through system of fresh, aerated, and dechloraminated water at a constant temperature of 18°C. Tank photoperiod was kept at a constant cycle of 12 h light:12 h dark. Goldfish were dark adapted for approximately 1 h, euthanized by rapid decapitation and pithed.

2.3.2 Isolated cell preparation

Horizontal cell isolation closely followed that of Jonz and Barnes (2007). Unless otherwise stated, all reagents and chemicals were sourced from Sigma-Aldrich (Oakville, ON, Canada). Eyes were removed and placed in cold Ca^{2+}-free Ringer's solution (Table 1). The

sclera and lens were dissected and the whole retina removed from the eye cup and placed in hyaluronidase (100 U ml^{-1}, Cat. No. H-3506) in L-15 solution for 20 min at room temperature. L-15 solution was composed of 70% L-15 (Leibovitz's medium) and 30% Ca^{2+}-free Ringer's. Retinas were washed 3 times for 3 min each in fresh L-15 solution and then placed in L-15 solution containing 7 U ml^{-1} papain (Cat. No. 3126, Worthington Biochemical Corporation, Lakewood, NJ, USA) for 40 min. Papain was previously activated with 2.5 mM L-cysteine. Retinas were again rinsed 3 times in fresh L-15 solution. Small (~4 mm^2) sections of retina were removed and mechanically dissociated by repeated, gentle trituration in L-15 solution. The resulting cell suspension was plated onto uncoated plastic-bottomed dishes (Corning Inc. Bedford, MA, USA) and allowed to settle and adhere for approximately 20 min before use.

2.3.3 Relative $[Ca^{2+}]_i$ measurements

Relative changes in free $[Ca^{2+}]_i$ were assessed using microspectrofluorometric imaging with the membrane-permeable form of the Ca^{2+} indicator, Fura-2 (Fura-2-LeakRes-AM; Teflabs, Austin, TX, USA). Isolated cell preparations were protected from light and incubated in normal extracellular solution (see Table 1), containing 5 μM of Fura-2 and 0.1% v/v of a 10% w/v Pluronic F-127 solution, for 30 min at room temperature to facilitate dye loading. Cells were then washed 3 times in extracellular solution to remove remaining esterified products. Isolated HCs were identified from other isolated cell types by their distinguished large, flat bodies and thick dendrites (Tachibana 1983) under low intensity brightfield illumination with an upright, compound microscope (FN-1, Nikon, Tokyo, Japan). Fluorescence imaging was performed using a Lambda DG-5 wavelength changer (Sutter Instruments, Novato, CA, USA) and a Chroma 79001 filter set (340 nm and 380 nm bandpass filters for excitation, 510 nm bandpass for emission; Chroma Technology, Bellows Falls, VT, USA). Excitation and emission light was

passed through a Nikon 40× water-immersion objective lens (numerical aperture 0.8). Images were collected with a CCD camera (QImaging, Surrey, BC, Canada) by focusing on a region of interest that encompassed an HC soma. Excitation wavelength was iteratively changed between 340 and 380 nm, and emission intensity was recorded for both excitation wavelengths every 2 s using NIS Elements (Nikon) software. For some experiments, Northern Eclipse software (Empix Imaging Inc., Mississauga, ON, Canada) was used for data collection. Imaging data was logged in Excel (Microsoft Corp., Redmond, WA, USA).

2.3.4 Relative V_m measurements

Relative changes in V_m were monitored using a FluoVolt voltage-sensitive dye kit (ThermoFisher Scientific, Waltham, MA, USA). FluoVolt accurately measures relative changes in voltage (see also McPheeters et al. 2017), and product information states that a 25% change in fluorescence represents a change of up to 100 mV. 2 µl of FluoVolt dye and 20 µl of PowerLoad (a dye loading agent) were added to 2 ml of extracellular solution (Table 1). Cells were incubated for 30 min at room temperature, washed 3 times in extracellular solution, and imaged within 4 h. HCs were identified under low intensity brightfield illumination with a compound microscope (FN-1, Nikon). A Chroma 41012 filter set was used (480 nm bandpass filter for excitation; 510 nm long-pass for emission). Light passed through a Nikon 40× water-immersion objective lens. Exposure time was 100 ms. Recordings were taken once every second with NIS Elements software (Nikon).

2.3.5 Electrophysiology

Patch-clamp recordings were taken using the whole-cell configuration. Capillary glass (PG52151-4, Sarasota, FL, USA) was pulled on a vertical micropipette puller (PC-10, Narishige International Inc., East Meadow, NY, USA) to make patch electrodes with tip resistances of 5–8

MΩ. Electrodes were filled with intracellular solution consisting of (in mM): 10 NaCl, 120 KCl, 2 $CaCl_2$, 2 MgATP, 5 EGTA, and 10 HEPES, and adjusted to pH 7.4 with KOH. Only cells for which >1 GΩ membrane seals were achieved were used. Preliminary experiments in current-clamp mode indicated that resting V_m was often unstable at I=0, precluding further analysis. In order to establish stable recordings of V_m, we first held each cell briefly at a command potential in voltage-clamp mode and recorded the holding current (I_H). Cells were then switched to current clamp and the value of I_H was injected. This effectively reduced rapid shifts in V_m. All protocols were implemented with pClamp 7 software, an Axopatch 1D amplifier (Axon Instruments), and a Digidata 1440A (Axon Instruments, Sunnyvale, CA, USA). Signals were filtered at 5 kHz. All recordings of V_m are corrected for liquid junction potential (V_L), which was subtracted from the pipette potential (V_p) using the formula: $V_m = V_p - V_L$.

2.3.6 Experimental procedures and solutions

For all experiments, a perfusion chamber (Warner Instruments Inc., Hamden, CT, USA) was inserted into 35 mm culture dishes (Corning), within which cells were plated and maintained. The chamber was continuously perfused at approximately 2 ml min^{-1} by gravity-fed recording solutions at room temperature. Recording solution was removed from the chamber at the same rate using a peristaltic pump (Fisher Scientific Canada, Ottawa, ON, Canada). The involvement of Ca^{2+} channels in the generation of spontaneous events was tested by perfusing the chamber with either Ca^{2+}-free solution, containing 1 mM EGTA, solutions containing divalent cations (Ba^{2+}, Cd^{2+}, or Co^{2+}), or solutions containing the L-type Ca^{2+} channel blocker, nifedipine (100 μM; Table 1). The role of internal Ca^{2+} stores was tested with ryanodine (20 μM), dantrolene (50 μM), or caffeine (3 mM). A role for store-operated channels (SOC) was tested with 2-aminoethyldiphenylborinate (2-APB; 100 μM).

2.3.7 Analysis

Raw traces from imaging experiments are presented as units of the ratio of fluorescence emission intensity after excitation at 340 nm and 380 nm (F_{340}/F_{380}). These values are proportional to $[Ca^{2+}]_i$. Parameters chosen to describe each spontaneous event included event frequency, duration, amplitude, area under the curve (AUC), and time to peak (TTP) from baseline level. Baseline $[Ca^{2+}]_i$ levels were also analyzed. Ca^{2+} events were analysed using a peak analysis algorithm in OriginPro 2016 (OriginLab Corp. Northampton, MA, USA). Frequency was measured as the number of events per sampling period (5 min) of observation. Duration was measured as the time between the start and end of each event using a local maximum function compared to baseline. Amplitude was measured as the difference between peak F_{340}/F_{380} and baseline before the event, as determined by the Origin peak analysis gadget using a second derivative algorithm for determining baseline values. AUC ($F_{340}/F_{380}\cdot s$) was calculated as the integral of amplitude over time of each event. This value approximates Ca^{2+} influx into the cytosol. TTP was the time between the start of the event and peak amplitude. Baseline F_{340}/F_{380} measurements were determined as the average of the last 30 s of the algorithm-determined baseline for each period. For amplitude, AUC and baseline measurements, values were scaled to the largest magnitude event for each experiment (Lv *et al.,* 2014) due to variability between cells.

All statistical tests for Ca^{2+} imaging were performed in Prism 8 (GraphPad Software Inc., San Diego, CA, USA). The one-tailed Wilcoxon matched-pairs signed rank test was used for ryanodine and dantrolene experiments. Mann-Whitney tests were used for experiments in which dantrolene was co-applied with 2-APB or nifedipine. Friedman's and Dunn's Multiple Comparison tests were used for caffeine and 2-APB experiments.

Current-clamp recordings were analysed using peak analysis algorithms in OriginPro 2016. Duration, amplitude, and AUC were calculated as indicated for Ca^{2+} imaging traces. Frequency of voltage events was reported as the number of events per final 5 min of each treatment. For experiments in Fig. 2.6, baseline values were established with OriginPro baseline and peak analysis tools, to take an average of membrane potentials within 5-min sampling periods, excluding the duration of spontaneous events. Prism 8 was used for linear regressions. In Fig. 2.6C, three outliers were excluded from analysis, based on techniques in Motulsky and Brown (2006) . In Fig. 2.7, outliers were omitted for presentation only, including one duration value (303 s) and three AUC values (5130.97, 5700.94 and 21633.6 mV·s). Datasets for Fig. 2.8 were analyzed in Prism 8 software with a one-way ANOVA, with Bonferroni's post-test (α = 0.05).

2.4 Results

2.4.1 Characterization of spontaneous changes in $[Ca^{2+}]_i$

In the present study, spontaneous $[Ca^{2+}]_i$ events were defined as large, transient increases in whole cell $[Ca^{2+}]_i$ that occurred without stimulation in a glutamate-free solution, and that recovered to baseline $[Ca^{2+}]_i$ levels (Fig. 2.1A, B). Spontaneous Ca^{2+} activity of this type was recorded in 157 of 177 cells (89%).

In the retina, HCs receive glutamatergic input from photoreceptors. The $[Ca^{2+}]_i$ response of isolated HCs to glutamate application was characterised by an initial increase in $[Ca^{2+}]_i$ to a peak amplitude, a decay to an elevated plateau phase that persisted for as long as glutamate was applied, and recovery to baseline levels after glutamate washout (Fig. 2.1C). This response could be repeated multiple times in the same cell. Removal of Ca^{2+}_e eliminated glutamate-

elicited increases in $[Ca^{2+}]_i$ (Fig. 2.1D). Spontaneous $[Ca^{2+}]_i$ events were not observed during glutamate application.

To assess the characteristics of spontaneous $[Ca^{2+}]_i$ events, data from event frequency, duration, amplitude, AUC, and TTP were pooled from 279 spontaneous events. Frequency distributions of these data are presented in Fig. 2.2. Spontaneous events were of low frequency and long duration. Within a 5-min sampling period a median of 7.0 events with an interquartile range (IQR) of 6.0 was calculated (Fig. 2.2A). Spontaneous events lasted for a median duration of 18.0 s (IQR 10.0 s; Fig. 2.2B). The amplitude (Fig. 2.2C) and AUC (Fig. 2.2D) were obtained from relative changes in the Fura-2 emission ratio (F_{340}/F_{380}) and is proportional to $[Ca^{2+}]_i$. The median amplitude was 0.67 (units of F_{340}/F_{380}; IQR 0.30) and the AUC was 0.21 (units of F_{340}/F_{380}·s; IQR 0.17). The TTP of each event was 6.0 s (IQR 2.0 s).

2.4.2 Spontaneous $[Ca^{2+}]_i$ events required extracellular Ca^{2+}

Figure 2.3A shows that removal of Ca^{2+}_e resulted in elimination of spontaneous $[Ca^{2+}]_i$ activity, and could be achieved with full recovery upon re-application of normal extracellular solution (n = 18). Re-application of Ca^{2+}_e resulted in an initial persistent elevation of $[Ca^{2+}]_i$ (see *arrows*, Fig. 2.3A) that eventually recovered to pre-application baseline levels along with the return of spontaneous activity. L-type Ca^{2+} channels are the major type of voltage-gated Ca^{2+} channels in goldfish HCs (Country and Jonz 2017; Huang and Liang 2005; Tachibana 1983). Blockade of Ca^{2+} influx through these channels was therefore performed using Cd^{2+} (50 µM), or nifedipine (100 µM) in the presence of 2.5 mM Ca^{2+}_e. Extracellular Cd^{2+} reversibly eliminated spontaneous activity (Fig. 2.3B; n = 5). Nifedipine (100 µM) also eliminated spontaneous activity, which did not recover upon removal of nifedipine solution (Fig. 2.3C; n = 5). These

data suggest that the influx of Ca^{2+}_e via L-type channels is required for generation of spontaneous Ca^{2+} activity.

2.4.3 Ca^{2+} stores are implicated in spontaneous $[Ca^{2+}]_i$ events

Goldfish HCs are known to have both ryanodine receptors (RyRs) and SOCs (Lv et al. 2014). To test for the role of RyRs in spontaneous activity, ryanodine or dantrolene (two specific RyR antagonists) were applied in Ca^{2+} imaging experiments. 20 μM ryanodine abolished spontaneous activity and increased baseline (n = 8, Fig. 2.4A). Similarly, 50 μM dantrolene abolished activity and increased post-treatment baseline (n = 7, Fig. 2.4B). We tested for the source of this increased Ca^{2+} baseline, by co-applying 50 μM dantrolene with 100 μM 2-APB (a SOC antagonist) or with 100 μM nifedipine. Baseline Ca^{2+} increased with dantrolene and 2-APB (n = 13, $P < 0.05$; Fig. 2.4C), but there was no significant increase with dantrolene and nifedipine, compared to controls (n = 9; Fig. 2.4D).

At 3 mM, the RyR agonist, caffeine, significantly increased the frequency of spontaneous $[Ca^{2+}]_i$ events (n = 10, $P < 0.001$; Fig. 2.4E, F). In contrast, caffeine's effects on frequency were negated in the presence of 100 μM 2-APB (n = 10). In fact, co-application of caffeine and 2-APB reduced frequency to zero in several cells. In contrast, APs persisted in the presence of 2-APB alone, even after 20 minutes (n=3). Caffeine also hastened spontaneous events: median duration was reduced from 29.3 s to 18.7s (n = 10, $P < 0.01$), and TTP was reduced from 12.3 s to 7.8 s (n = 10, $P < 0.05$). AUC was reduced from 0.47 to 0.19 (units of F_{340}/F_{380}·s; n = 10, $P <$ 0.05), but amplitude was not significantly reduced.

2.4.4 Characterization of spontaneous changes in V_m

We tested whether isolated HCs showed spontaneous depolarizations with FluoVolt, a voltage-sensitive dye. FluoVolt permitted observation of spontaneous activity in cells with an intact cytosol and membrane, as in Fura-2 experiments. HCs displayed spontaneous increases in fluorescence, consistent with membrane depolarization ($n = 6$; Fig. 2.5). During each depolarizing event there was a sharp rise to peak fluorescence, followed by a slow decline, and then a steep return to baseline. Mean change in V_m was 10.2 ± 0.6%, and events lasted 8 to 20 s.

In current-clamp experiments, spontaneous changes in V_m, similar to those in FluoVolt experiments, were observed. Most often, however, current injection was required to stabilize and record regenerative changes in V_m. Regenerative APs were observed in 48 out of 57 cells (84.2%). These events decayed slowly for several seconds and returned sharply to baseline (Fig. 2.6A,B). Both the frequency and amplitude of APs measured under current clamp were voltage dependent. HCs with more negative values of baseline V_m had fewer spontaneous events compared with cells with a more depolarized baseline ($n = 54$, $r^2 = 0.11$, $P < 0.05$; Fig. 2.6C). Events reached higher amplitudes in cells at relatively hyperpolarized V_m ($n = 49$, $r^2 = 0.45$, $P < 0.01$, Fig. 2.6D), likely due to a greater driving force.

Frequency, duration, amplitude, AUC, and TTP were pooled from 264 spontaneous events. Frequency distributions of these data are presented in Fig. 2.7. Spontaneous events were of low frequency and long duration. Within a 5-min sampling period, a median of 3.0 (IQR 4.0) events were recorded (Fig. 2.7A). Spontaneous events lasted for a duration of 11.5 s (IQR 13.9 s; Fig. 2.7B). Median amplitude was 61.9 mV (IQR 26.6 mV; Fig. 2.7C) and median AUC was 442.8 mV·s (IQR 704.8 mV·s; Fig. 2.7D). The median TTP was 1.8 s (IQR 1.7 s; Fig. 2.7E).

2.4.5 Action potentials required extracellular Ca^{2+}

To test for Ca^{2+} channel activity, Ba^{2+} was applied during current-clamp experiments. In L-type and other high voltage-activated (HVA) Ca^{2+} channels, Ba^{2+} increases current as it is more permeant through HVA channels than Ca^{2+} (Budde et al. 2002). Compared to Ca^{2+}, 15 mM Ba^{2+} increased AUC 3.8-fold and increased duration 3.0-fold ($n = 6$, $P < 0.05$; Fig. 2.8A). In separate experiments, 5 mM Co^{2+} (a non-specific Ca^{2+} channel blocker) or 100 μM nifedipine were applied to test for L-type channel involvement. Both drugs irreversibly abolished activity in all cells ($n = 5$; Fig. 2.8B,C). In experiments in which Ca^{2+} was removed, spontaneous activity was abolished irreversibly, or returned with a much smaller amplitude (Fig. 2.8D).

Figure 2.1: Fura-2 measurement of spontaneous changes in $[Ca^{2+}]_i$ in isolated horizontal cells.

A, Sequence of pseudocolour fluorescence images (1–5) indicates a spontaneous change in $[Ca^{2+}]_i$ during superfusion of a horizontal cell (HC) with normal extracellular solution, as determined by the Fura-2 emission ratio. Blue/violet indicates a lower $[Ca^{2+}]_i$; red/white indicates higher $[Ca^{2+}]_i$. Each frame is separated by 5 s; peak $[Ca^{2+}]_i$ was captured in frame 3. Scale bar = 25 μm. *B*, A representative trace illustrating transient $[Ca^{2+}]_i$ changes indicated by Fura-2 fluorescence in HCs during superfusion with normal extracellular solution. *C*, Representative trace shows a typical response of an HC to brief 100 μM glutamate application. An initial transient increase in $[Ca^{2+}]_i$ decays to an elevated $[Ca^{2+}]_i$ that persists for the duration of glutamate application ($n = 41$). *D*, Superfusion of Ca^{2+}-free solution during glutamate application eliminated increased $[Ca^{2+}]_i$ ($n = 6$). A spontaneous Ca^{2+} transient (*arrow*) was recorded before glutamate application. The scale bars indicate the Fura-2 fluorescence emission ratio (F_{340}/F_{380}) and time in seconds.

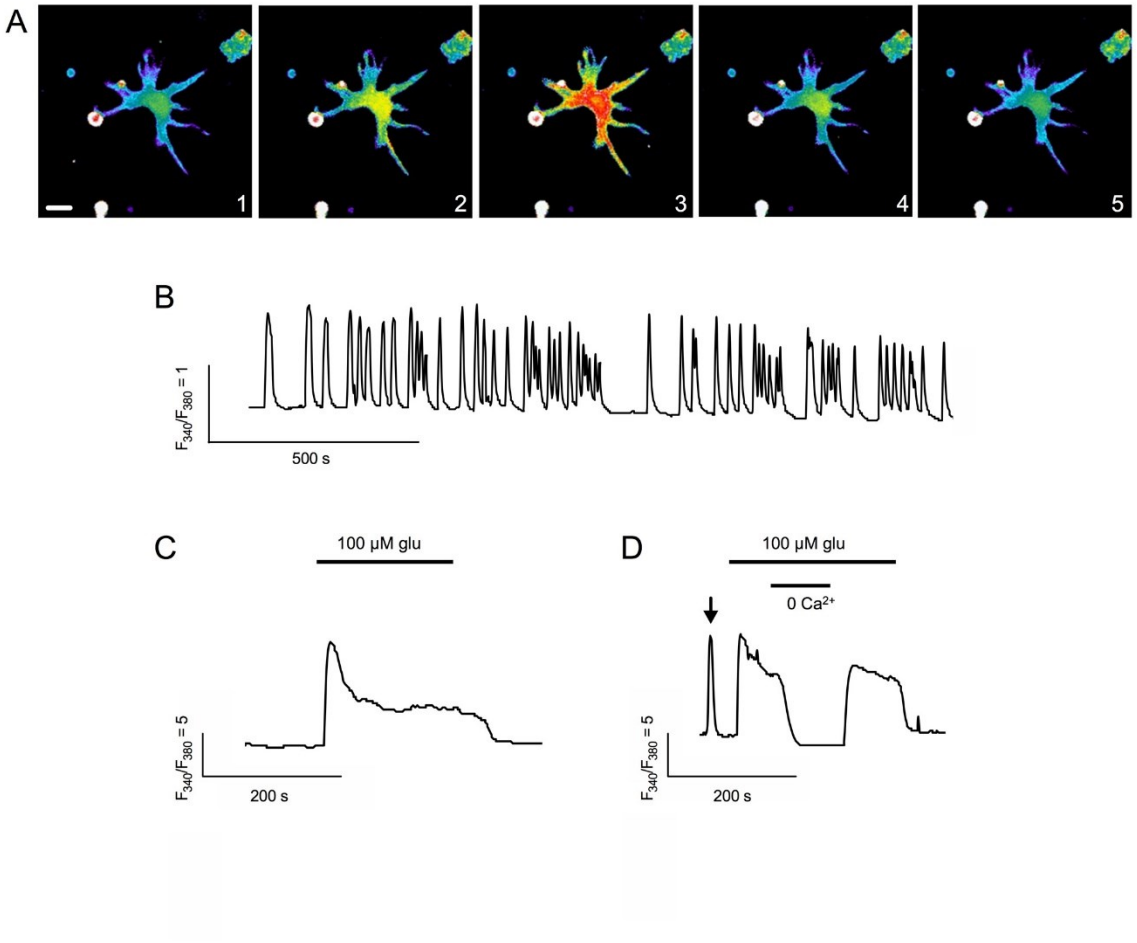
A
1
2
3
4
5
B
F340/F380 = 1
500 s
C
100 µM glu
F340/F380 = 5
200 s
D
100 µM glu
0 Ca2+
F340/F380 = 5
200 s

Figure 2.1

Figure 2.2: Frequency distributions of spontaneous Ca^{2+} event parameters in isolated horizontal cells.

279 spontaneous $[Ca^{2+}]_i$ events were measured in 5 cells and the frequency distribution for the following parameters were plotted: (*A*) the frequency of spontaneous events within a 5 min sampling period, (*B*) the duration of spontaneous events, (*C*) the amplitude of spontaneous events in units of the Fura-2 fluorescence emission ratio (F_{340}/F_{380}), (*D*) the area under the curve of spontaneous events (units of $F_{340}/F_{380}\ s^{-1}$), and (*E*) the time of rise from baseline to peak amplitude (s).

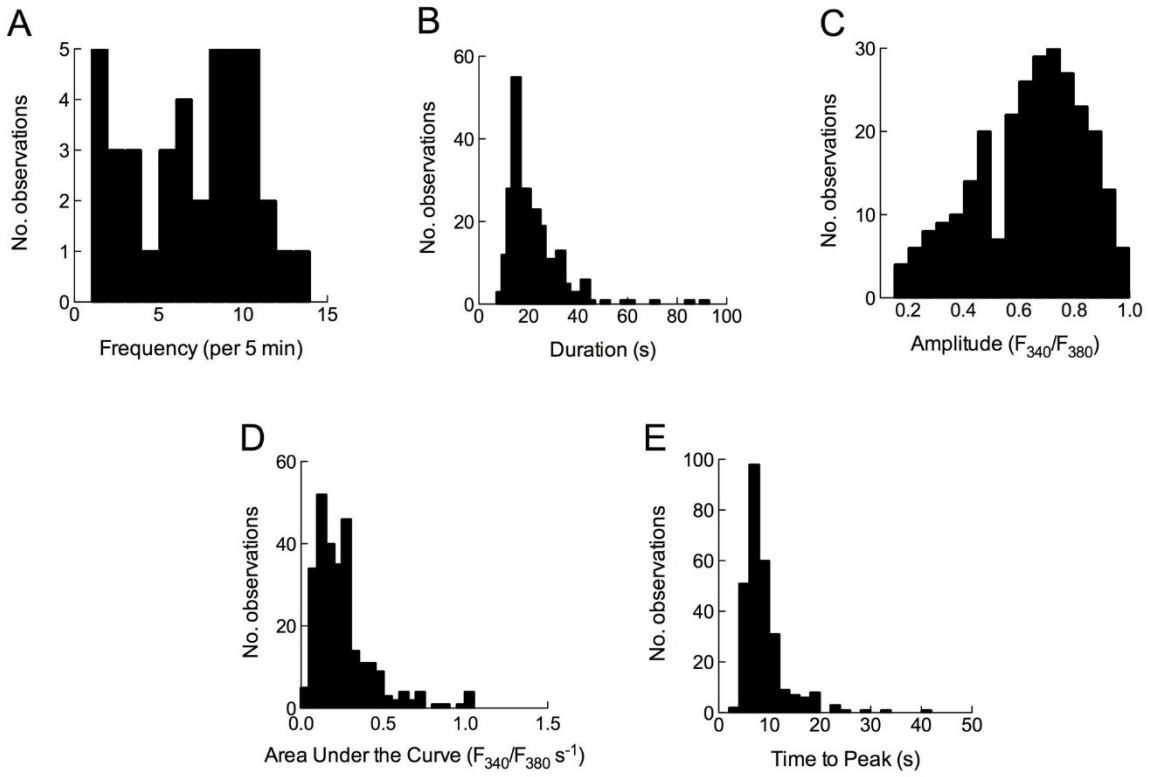
A
No. observations
Frequency (per 5 min)
B
No. observations
Duration (s)
C
No. observations
Amplitude (F_{340}/F_{380})
D
No. observations
Area Under the Curve (F_{340}/F_{380} s^{-1})
E
No. observations
Time to Peak (s)

Figure 2.2

Figure 2.3: Spontaneous activity required influx of Ca^{2+}.

A, Removal of extracellular Ca^{2+} (bar) reversibly eliminated spontaneous events (*n* = 18). Note the persistent elevation of $[Ca^{2+}]_i$ upon replacement of extracellular Ca^{2+} in the superfusate (*arrows*). *B*, 50 μM Cd^{2+} (bar) reversibly eliminated spontaneous events (*n* = 5). *C*, 100 μM nifedipine (bar) eliminated spontaneous events with no recovery (*n* = 5). The scale bars indicate the Fura-2 fluorescence emission ratio (F_{340}/F_{380}) and time in seconds.

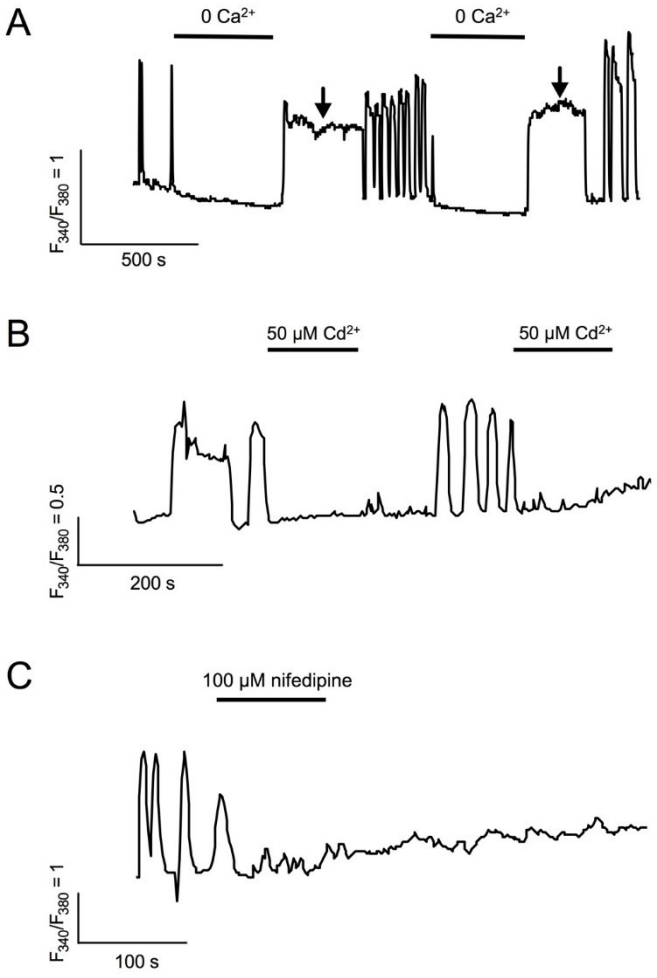
A
0 Ca2+
0 Ca2+
F340/F380 = 1
500 s
B
50 µM Cd2+
50 µM Cd2+
F340/F380 = 0.5
200 s
C
100 µM nifedipine
F340/F380 = 1
100 s

Figure 2.3

Figure 2.4: Intracellular Ca^{2+} stores contribute to spontaneous activity.

Both (*A*) ryanodine (20 μM; $n = 8$) and (*B*) dantrolene (50 μM; $n = 7$) irreversibly abolished spontaneous activity and increased baseline $[Ca^{2+}]_i$. *C,* $[Ca^{2+}]_i$ baseline increased in response to co-application of dantrolene and 2-APB (100 μM). *D,* Co-application of dantrolene and nifedipine (100 μM) prevented the dantrolene-induced increase in $[Ca^{2+}]_i$ baseline. *E*, Caffeine (3 mM; $n = 10$; black bar) increased the frequency of spontaneous activity. Co-application with 100 μM 2-APB (grey bar) prevented this increase. *F,* Summary of the effect of caffeine on frequency. The asterisk indicates significance ($P < 0.05$) compared to pre-application values. The scale bars indicate the Fura-2 fluorescence emission ratio (F_{340}/F_{380}) and time in seconds. Mean ± S.D. is presented.

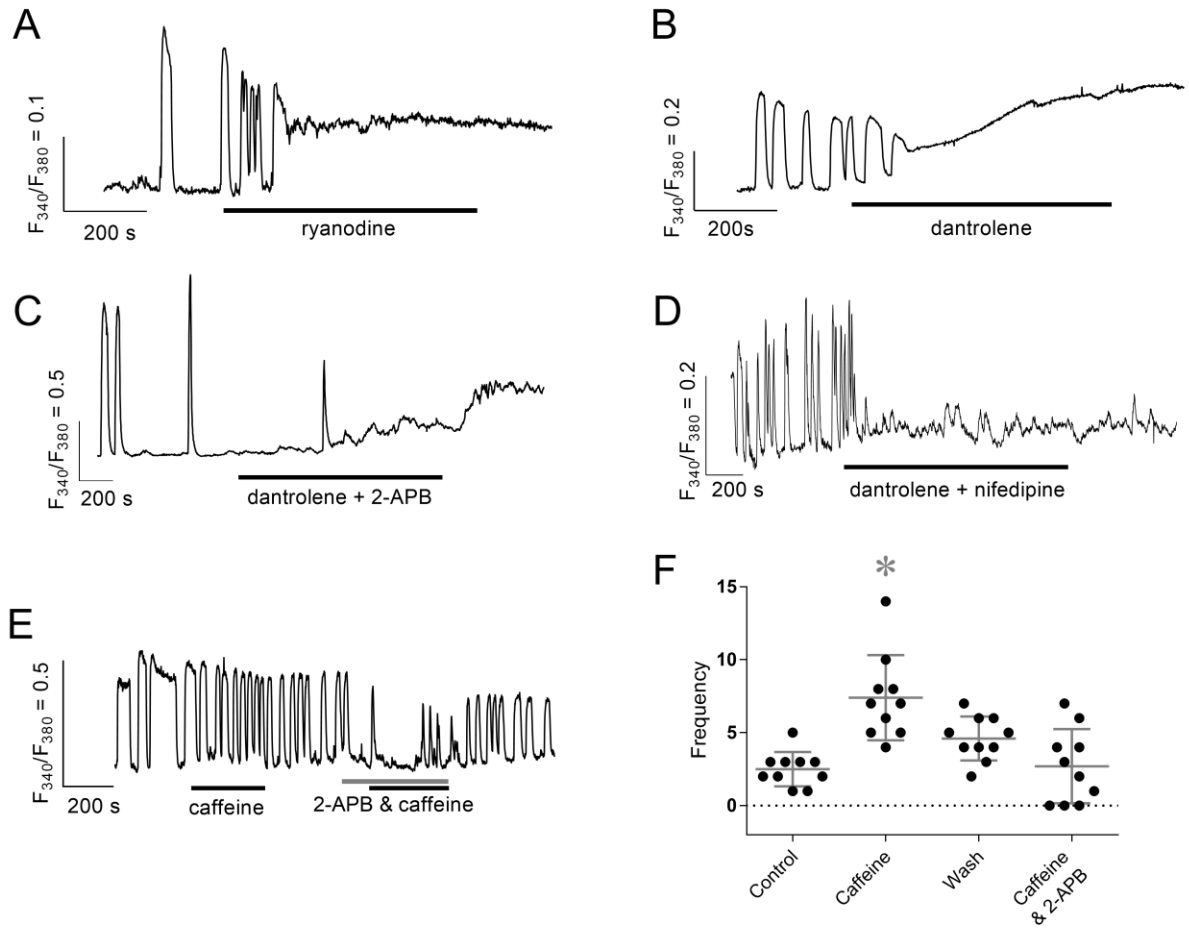
A
F340/F380 = 0.1
200 s
ryanodine
B
F340/F380 = 0.2
200s
dantrolene
C
F340/F380 = 0.5
200 s
dantrolene + 2-APB
D
F340/F380 = 0.2
200 s
dantrolene + nifedipine
E
F340/F380 = 0.5
200 s
caffeine
2-APB & caffeine
F
Frequency
15
10
5
0
*
Control
Caffeine
Wash
Caffeine & 2-APB

Figure 2.4

Figure 2.5: FluoVolt voltage-sensitive dye imaging in goldfish horizontal cells.
Relative changes in membrane potential were tracked over time (n = 6). Increases in fluorescence represent depolarizing events. The scale bars indicate the fluorescence normalized to the first 10 s of recording (F/F_0) and time in seconds; a 5% change in fluorescence corresponds to a change of up to 20 mV (see Methods).

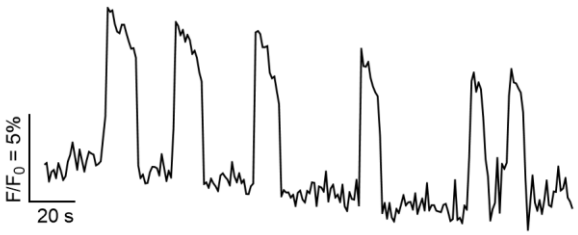

Figure 2.5

Figure 2.6: Spontaneous depolarizations of goldfish horizontal cells in current clamp.

A, B, In whole-cell current-clamp recordings, large depolarizations in membrane potential (V_m) are shown in cells from resting V_m of –82 mV and –67 mV. *C*, The number of events per 5-minute sampling period was greater in more depolarized cells ($n = 54$, $r^2 = 0.11$, $P = 0.0158$). Line of best fit ± 95% confidence interval is shown. *D,* The amplitude of spontaneous depolarizations was greater in hyperpolarized cells ($n = 49$, $r^2 = 0.45$, $P < 0.0001$). The scale bars indicate the membrane potential (in mV) and time in seconds. Line of best fit ± 95% confidence interval is shown.

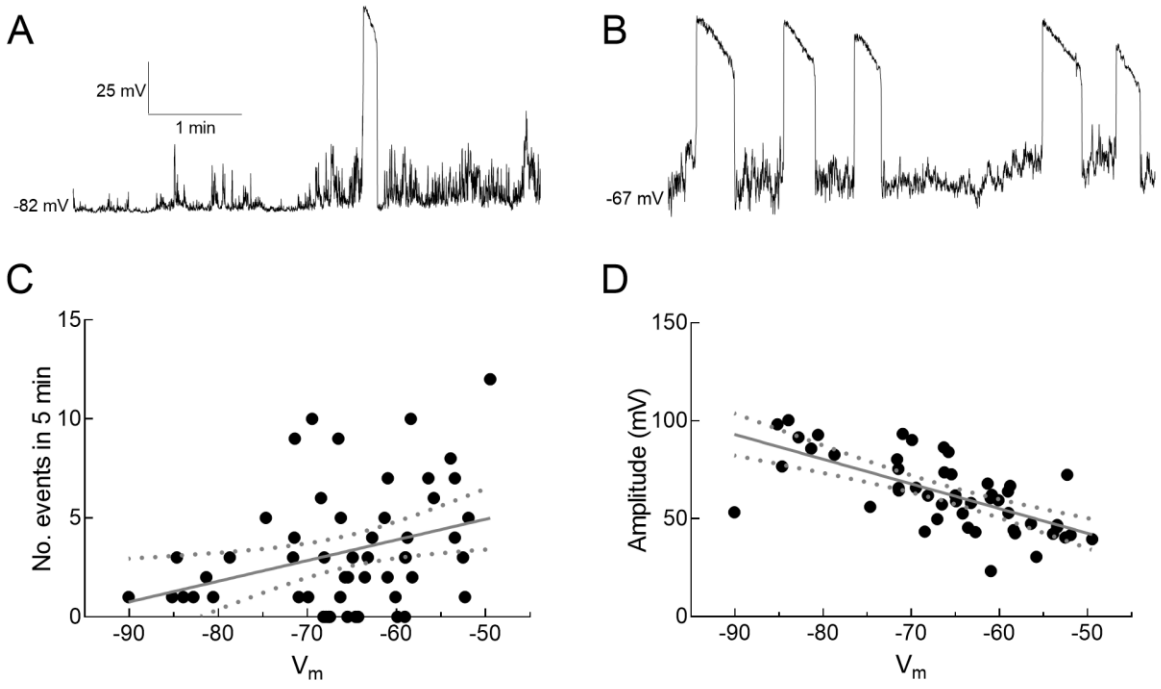
A
25 mV
1 min
-82 mV
B
-67 mV
C
No. events in 5 min
15
10
5
0
-90
-80
-70
-60
-50
Vm
D
Amplitude (mV)
150
100
50
0
-90
-80
-70
-60
-50
Vm

Figure 2.6

Figure 2.7: Frequency distributions of spontaneous depolarization parameters in isolated horizontal cells.

264 spontaneous depolarizations were measured in 57 cells and the frequency distribution for the following parameters were plotted: (*A)* frequency of spontaneous events within a 5-min sampling period, (*B*) duration, (*C*) amplitude, (*D*) area under the curve, and (*E*) the time of rise from baseline to peak amplitude (s).

Figure 2.7

Figure 2.8: Spontaneous depolarizations in current clamp were Ca^{2+} dependent.

A, Addition of 15 mM Ba^{2+} increased the amplitude, duration, and area under the curve of spontaneous events (*n* = 6). These effects were reversible upon washout. *B*, 100 μM nifedipine irreversibly abolished spontaneous events (*n* = 5). *C*, Addition of 5 mM Co^{2+} also irreversibly abolished spontaneous events (*n* = 5). *D*, In 6 cells, Ca^{2+}-free solutions abolished spontaneous activity. The scale bars indicate the membrane potential (in mV) and time in seconds.

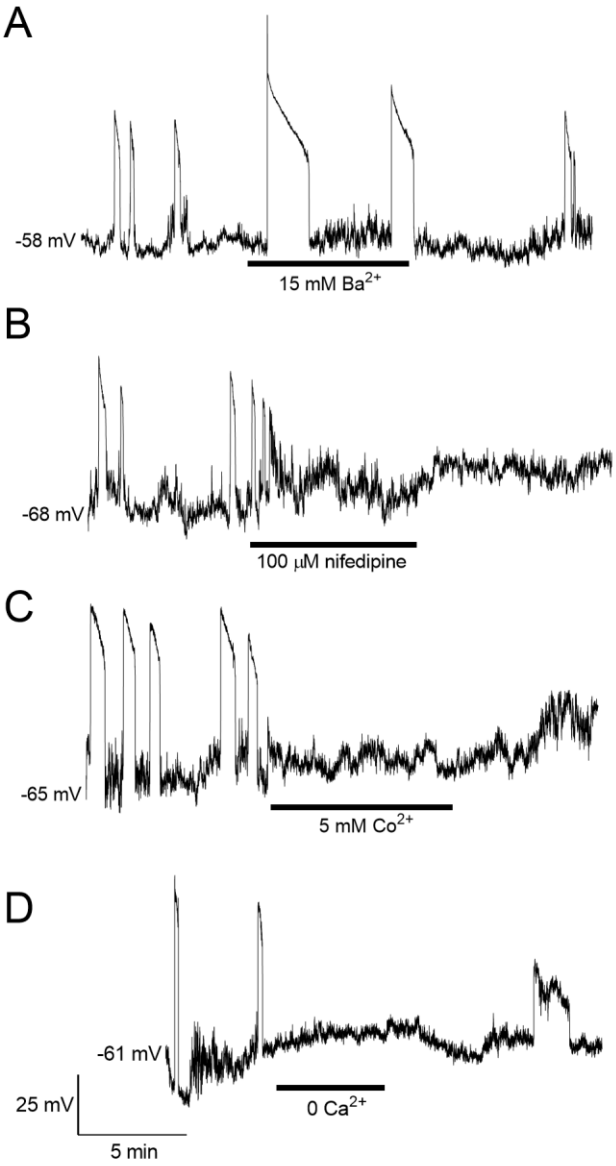
A
-58 mV
15 mM Ba2+
B
-68 mV
100 μM nifedipine
C
-65 mV
5 mM Co2+
D
-61 mV
0 Ca2+
25 mV
5 min

Figure 2.8

Table 2.1. Composition of Ringer's and extracellular recording solutions.

In all solutions, pH was adjusted to 7.8 with NaOH.

Reagent	Ca^{2+}-free Ringer's	Extracellular Recording Solutions (mM)					
		Control solution	Ca^{2+}-free	Cd^{2+}	OGD/0 glucose	Ba^{2+}	Co^{2+}
NaCl	120	120	120	120	120	97.5	112.5
KCl	2.6	5	5	5	5	5	5
$CaCl_2$	-	2.5	-	2.5	2.5	2.5	2.5
$MgCl_2$	-	2	3.5	2	2	2	2
Glucose	10	10	10	10	-	10	10
Sucrose	-	-	-	-	10	-	-
HEPES	10	10	10	10	10	10	10
NaH_2PO_4	0.5	-	-	-	-	-	-
EGTA	-	-	1	-	-	-	-
$CdCl_2$	-	-	-	0.05	-	-	-
$BaCl_2$	-	-	-	-	-	15	-
$CoCl_2$	-	-	-	-	-	-	5

2.5 Discussion

This study has demonstrated the spontaneous generation of APs in isolated retinal horizontal cells (HCs) of the goldfish by imaging changes in $[Ca^{2+}]_i$ and V_m, and by using electrophysiological techniques. We have shown that APs were dependent upon Ca^{2+} and were driven by activity of plasma membrane Ca^{2+} channels and intracellular RyRs. We have demonstrated that AP activity in HCs is maintained by prolonged membrane currents and is modulated by changes in membrane potential.

In most previous reports, APs recorded from HCs were not spontaneous but were instead elicited with a depolarizing stimulus (e.g. Johnston and Lam 1981; Shingai and Christensen 1986), or were potentiated with K^+ channel blockers and Ba^{2+} solutions (Murakami and Takahashi 1987). Tachibana (1981) was able to elicit APs with depolarizing current injections, but also found that ~50% of cells exhibited spontaneous APs, which he attributed to natural fluctuations in resting V_m. Additionally, spontaneous Ca^{2+} transients have been observed in isolated goldfish HCs (Kreitzer et al. 2012).

In all three techniques used in the present study (Ca^{2+} imaging, whole-cell current-clamp recording, and FluoVolt imaging), spontaneous events possessed similar characteristics. These included a steep rise in $[Ca^{2+}]_i$ (or depolarization of V_m), a slow decay period, and a steep return to baseline. However, Ca^{2+} transients were slower than changes in V_m (duration: 18.0 s *vs.* 11.5 s), took longer to reach their peak (TTP: 6.0 s *vs.* 1.8 s), and were more frequent (7.0 *vs.* 3.0 per 5-min sampling period). One possible explanation is that, during the recovery phase of APs, V_m returns to resting levels before $[Ca^{2+}]_i$. The slower characteristics of Ca^{2+} transients, compared to changes in V_m, may also be attributed to the effects of Fura-2 during imaging. Fura-2 is a Ca^{2+}

buffer, so it is expected to reduce free $[Ca^{2+}]_i$ and delay Ca^{2+}-dependent inactivation (CDI) of voltage-gated Ca^{2+} channels (Budde et al. 2002; Tachibana 1983; Tse et al. 1994).

2.5.1 Ca^{2+} dynamics during action potentials

Previous reports, in which APs were elicited by depolarization, found that APs depended on extracellular Ca^{2+}. Removing extracellular Ca^{2+} or blocking HVA Ca^{2+} channels with divalent ions (e.g. Cd^{2+} or Co^{2+}) abolished APs, while HVA channel-permeant ions (e.g. Ba^{2+}, Sr^{2+}) or high extracellular $[Ca^{2+}]$ amplified APs (Johnston and Lam 1981; Shingai and Christensen 1986; Tachibana 1981; Takahashi et al. 1993). Just as these depolarization-induced events were dependent on Ca^{2+}, we found that spontaneous Ca^{2+} transients and changes in V_m were abolished in the presence of divalent voltage-gated Ca^{2+} channel (VGCC) blockers and nifedipine, and were amplified and prolonged in the presence of Ba^{2+}. Our work links spontaneous and induced APs, and extends previous results by confirming that L-type channels are responsible for Ca^{2+} influx.

Ca^{2+} stores in goldfish HCs are gated by RyRs (Huang et al. 2004; Lv et al. 2014) and are refilled, at least in part, by SOCs (Lv et al. 2014). RyRs mediate Ca^{2+}-induced Ca^{2+} release (CICR) in HCs by releasing Ca^{2+} from the endoplasmic reticulum after cytosolic $[Ca^{2+}]$ increases (Country and Jonz 2017). In the present study, RyR blockade abolished spontaneous events, followed by an irreversible increase of baseline $[Ca^{2+}]_i$. This rise in $[Ca^{2+}]_i$ was likely due to L-type Ca^{2+} currents since co-applying nifedipine with dantrolene prevented the increase in baseline $[Ca^{2+}]_i$. In contrast, inhibiting SOCs with 2-APB in the presence of dantrolene did not prevent the rise in $[Ca^{2+}]_i$.

This $[Ca^{2+}]_i$ increase during RyR blockade might be explained by the relationship between VGCCs and CICR, as follows. During APs, Ca^{2+} enters *via* L-type Ca^{2+} channels and triggers CICR through RyR-gated stores. Then, CICR inhibits L-type channels through CDI (Linn and Gafka 2001). But during ryanodine or dantrolene blockade, CICR would not occur, and L-type channels would not be inhibited, letting baseline $[Ca^{2+}]_i$ rise.

Caffeine (a RyR agonist) reversibly increased the frequency of spontaneous events, and also reduced event duration and TTP. Because caffeine and elevations in $[Ca^{2+}]_i$ increase the probability that RyRs will open (Masumiya et al. 2001), CICR may occur faster in the presence of caffeine, increasing $[Ca^{2+}]_i$ enough to inactivate L-type channels through CDI (Budde et al. 2002; Linn and Gafka 2001) and rapidly returning $[Ca^{2+}]_i$ to baseline levels. A previous report found that 2-APB, a SOC inhibitor, prevents Ca^{2+} stores from refilling and prevents caffeine-induced CICR (Lv et al. 2014). If Ca^{2+} stores are depleted, SOCs in the plasma membrane can open, allowing Ca^{2+} entry to refill stores (Hogan and Rao 2007). In the present study, removing and reapplying Ca^{2+}_e led to a prolonged elevation of $[Ca^{2+}]_i$ (Fig. 2.3A, *arrows*). In separate experiments, when caffeine was co-applied with 2-APB, the frequency of Ca^{2+} transients was not affected. These experiments are consistent with findings from Lv et al. (2014), which suggest that SOCs are present in goldfish HCs, and confirm that Ca^{2+} stores contribute to spontaneous Ca^{2+} transients. Stored Ca^{2+} may be important for generating APs in HCs because of the limited availability of Ca^{2+} in the synaptic cleft. The volume of the invaginating synaptic cleft has been calculated to be miniscule (3×10^{-18} l) (Raviola and Gilula 1975; Vessey et al. 2005), so that an extracellular $[Ca^{2+}]$ of 2 mM would give ~3,600 ions of free Ca^{2+}. Ca^{2+} influx during an AP could therefore greatly decrease extracellular $[Ca^{2+}]$. A similar argument has been made for the importance of Ca^{2+} stores and CICR in maintaining tonic glutamate release from photoreceptor

terminals (Rabl and Thoreson 2002; Suryanarayanan and Slaughter 2006). In addition, CICR synchronizes Ca^{2+} oscillations among cardiomyocytes (Dougoud et al. 2016; Plummer et al. 2011). This raises the possibility that, in the retina, CICR may also synchronize spontaneous Ca^{2+} activity throughout HC syncytia by triggering Ca^{2+} flux into nearby cells through gap junctions.

2.5.2 What is the role of action potentials in horizontal cells?

HCs receive glutamatergic input from photoreceptors, which depolarizes HCs and triggers Ca^{2+} influx (Country and Jonz 2017; Thoreson and Mangel 2012). We observed spontaneous events *in vitro* in the absence of glutamate. Tachibana (1981) suggested that APs were the result of natural fluctuations in resting V_m. He proposed that V_m would fluctuate into the activation range of VGCCs, opening them and triggering an AP. In the current study, we found that cells with a more depolarized resting V_m had a higher frequency of APs, and that all cells observed had a resting V_m (–90 to –50 mV) that was more negative than the activation threshold for HC L-type channels (–45 to –30 mV; Country and Jonz 2017; Shingai and Christensen 1983; Sullivan and Lasater 1992; Tachibana 1983). By extension of Tachibana's model, our findings show that subthreshold resting V_m in HCs may, indeed, fluctuate until it reaches the L-type activation threshold, increasing the probability that L-type channels will open and initiate an AP. We observed fluctuations in resting V_m of up to 30 mV in current-clamp and voltage-sensitive dye experiments, and these fluctuations would put V_m well within range of L-type channel activation. Although our experiments were performed *in vitro*, our data suggest that, in the intact retina, light-dependent changes in glutamate release from photoreceptor terminals will modulate HC V_m, and these changes will accordingly control AP frequency. Furthermore, since glutamate seems to suppress or occlude spontaneous APs, this suggest that

APs may be more prevalent (though at lower frequency) in the retina during light stimulation, when glutamate release from photoreceptors is reduced and V_m in HCs is hyperpolarized.

In the intact retina, HCs are hyperpolarized by light (approx. –60 mV), and are depolarized in darkness (approx. –25 mV; Sun et al. 2017; Yang et al. 1988). APs may be important in the light-to-dark transition by rapidly shifting V_m to the more depolarized potential. This may be the case in the turtle. In sharp electrode recordings of HCs in red-eared turtle (*Pseudemys scripta elegans*) eyecups, off-responses (i.e. the response to removing a light stimulus) included regenerative changes in V_m, similar to an AP (Akopian et al. 1991). Applying Co^{2+} or removing extracellular Ca^{2+} abolished regenerative off-responses, and it took longer for HCs to resettle to a depolarized baseline. However, to our knowledge, this has not yet been tested in fish.

Understanding Ca^{2+}-based APs may offer novel insights into HC physiology, including their role in processing visual stimuli. HCs provide inhibitory feedback to photoreceptors (Baylor et al. 1971; Thoreson and Mangel 2012) via one of three mechanisms: 1) during light stimulation, HCs may reduce GABA release onto photoreceptors (GABA disinhibition) (Hirano et al. 2016; Liu et al. 2013; Wu and Dowling 1980); 2) hemichannels at HC dendrites may affect photoreceptor membrane potential *via* an ephaptic mechanism (Byzov and Shura-Bura 1986; Kamermans et al. 2001); and/or 3) HCs may affect pH or proton buffering (Barnes 2003; Vroman et al. 2014; Warren et al. 2016) in the synaptic cleft that may, in turn, affect the conductance and activation of photoreceptor voltage-gated Ca^{2+} channels (Barnes 2003; Hirasawa and Kaneko 2003; Vessey et al. 2005). Generation of Ca^{2+}-based APs might affect any of these mechanisms. For example, GABA release is partially Ca^{2+}-dependent in non-mammalian species (Ayoub and Lam 1985; Cunningham and Neal 1985; Lasater and Lam 1984;

Thoreson and Mangel 2012). In addition, during APs, Ca^{2+} influx would likely diminish extracellular [Ca^{2+}]. Low extracellular [Ca^{2+}], in turn, is known to increase hemichannel open probability (DeVries and Schwartz 1992; Jonz and Barnes 2007) and increase gap junctional coupling among HCs (McMahon and Mattson 1996). In isolated HCs, spontaneous Ca^{2+} transients cause extracellular acidification (Kreitzer et al. 2007; Kreitzer et al. 2012), so that Ca^{2+} APs may lead to photoreceptor inhibition.

2.6 Conclusion

We have characterized spontaneous, Ca^{2+}-based APs in isolated HCs of the goldfish retina. We propose a model in which V_m fluctuations are large enough to open L-type voltage-gated Ca^{2+} channels, which further depolarize the cell. The resulting Ca^{2+} influx triggers CICR through RyR-gated intracellular Ca^{2+} stores, which may in turn inactivate L-type channels and allow for repolarization. We propose that APs in HCs (Murakami and Takahashi 1987; Shingai and Christensen 1983; Tachibana 1981) and spontaneous Ca^{2+} events (Kreitzer et al. 2012) represent the same phenomenon, by comparing event characteristics, Ca^{2+} dependence, and the involvement of L-type Ca^{2+} channels. This work will be instrumental in exploring the role that spontaneous activity in HCs may have in vision.

3 Retinal horizontal cells of goldfish (*Carassius auratus*) display subtype-specific differences in spontaneous action potentials *in situ*

This chapter includes material excerpted from an article submitted as:

Country, M. W., Htite, E. D., Samson, I., and Jonz, M. G. 2019. Retinal horizontal cells of goldfish (*Carassius auratus*) display subtype-specific differences in spontaneous action potentials in situ. *J. Comp. Neurol.* Submitted May 29 2020.

I performed all experiments presented in this chapter, except for contributions from two B.Sc. Honours students: Elly Dimya Htite recorded from 22 cells in slice preparations (Figs. 3.1A, B; 3.2, 3.3), and Isaiah Samson recorded from 56 cells for Fig. 3.5. I performed all analyses and wrote the manuscript. Special thanks to Santana Su and Dante Foschia whose early contributions were informative but were not used in this article.

3.1 Abstract

Horizontal cells (HCs) are neurons of the outer retina, which provide inhibitory feedback onto photoreceptors and contribute to image processing. HCs in teleosts may be classified into four subtypes (H1-H4) based on their morphology and location within the inner nuclear layer. HC subtypes have different roles: H1-H3 feed back onto different sets of cones, H4 feed back onto rods, and only H1 store and release the inhibitory neurotransmitter, γ-aminobutyric acid (GABA). Dissociated HCs exhibit spontaneous Ca^{2+}-based action potentials (APs), yet it is unclear if APs occur *in situ*, or if all subtypes exhibit APs. We measured intracellular Ca^{2+} with Fura-2 imaging and report APs in slice preparations of the goldfish retina. In HCs furthest from photoreceptors (i.e. H3/H4 subtypes), APs were less frequent, with greater duration and area under the curve (a measure of Ca^{2+} flux). Next, we classified HCs acutely dissociated from goldfish into subtypes using a quantitative method, integrating the ratio of the dendritic field size vs. soma size ($r_{d/s}$). H1 and H2 subtypes had low $r_{d/s}$ values (<8); H3/H4 had high values (>12). To verify this model, H1s were identified by immunoreactivity for GABA and 95% of these cells had an $r_{d/s}$ <4. In Ca^{2+} imaging experiments, APs were found across all subtypes. As $r_{d/s}$ increased, duration and area under the curve increased, while frequency decreased. Our results demonstrate the presence of Ca^{2+}-based APs in the goldfish retina *in situ* and show that HC subtypes H1 through H4 exhibit progressively longer and less frequent spontaneous APs.

3.2 Introduction

Horizontal cells (HCs) are interneurons in the outer retina, which provide inhibitory feedback onto photoreceptors, contributing to edge detection, visual contrast, and color opponency (Thoreson and Mangel 2012). In darkness, HCs are chronically stimulated with glutamate from photoreceptors, which leads to depolarization and constant Ca^{2+} influx through L-type Ca^{2+} channels and Ca^{2+}-permeable α-amino-3-hydroxy-5-methyl-4-isoxazolepropionic acid receptors (AMPARs) (Linn and Christensen 1992; Sun et al. 2010; Tachibana 1983; 1985). In fish, HCs produce slow (seconds- to minutes-long) Ca^{2+}-based action potentials (APs; Country et al. 2019; Johnston and Lam 1981; Lasater et al. 1984; Murakami and Takahashi 1987; Tachibana 1981), which are not well understood. These APs are dependent on Ca^{2+} entry through L-type Ca^{2+} channels and ryanodine receptors, and they occur in the absence of glutamate (Country et al. 2019). Depolarizing stimuli or K^+ channel blockers have been shown to trigger APs in a variety of preparations, including the intact retina (Murakami and Takahashi 1987), cultured cells (Lasater et al. 1984; Tachibana 1981), and acutely dissociated cells (Shingai and Christensen 1983). Even without depolarizing stimuli, APs have been shown to occur spontaneously in electrophysiological and intracellular Ca^{2+} imaging experiments (Country et al. 2019; Kreitzer et al. 2012; Tachibana 1981). While a role for APs in HCs has not yet been firmly established, it has been proposed that they may be important in the light-to-dark transition or in modulating feedback from HCs to photoreceptors (Country et al. 2019). There has been no information about which subtypes of HCs exhibit spontaneous APs, how Ca^{2+} dynamics might differ among subtypes, nor whether APs are present *in situ*. Such information may prove important to understanding both the function of APs in HCs, and the physiological differences among subtypes.

In teleost fish, HCs may be classified into four subtypes: H1, H2, H3, and H4 (Dowling et al. 1985; Lasater 1986; Song et al. 2008; Stell and Lightfoot 1975; Stell and Witkovsky 1973). These subtypes have different roles in vision: H1, H2, and H3 feed back onto different sets of cones, while H4 feed back onto rods. H1-H4 are numbered in order of increasing dendritic field size, decreasing soma size, and increasing distance from the photoreceptor layer (Stell and Lightfoot 1975). These differences in morphology are currently used to qualitatively distinguish HC subtypes, because for H2, H3, and H4, there are no subtype-specific biomarkers. H1 cells are the exception: they can be identified by their stores of the inhibitory neurotransmitter, γ-aminobutyric acid (GABA) (Marc et al. 1978; Paik et al. 2003). In addition to differences in morphology, many authors have found ion channel expression and membrane current to be subtype specific in HCs (Lasater 1986; Lohrke and Hofmann 1994; Malchow et al. 1990; Paik et al. 2003; Qian and Dowling 1993; Shen et al. 2006; Sullivan and Lasater 1992; 1990; Ueda et al. 1992), highlighting the need to report physiological data by subtype.

First, we recorded $[Ca^{2+}]_i$ over time in a goldfish retinal slice preparation. HCs *in situ* exhibited spontaneous Ca^{2+}-based APs. We report that APs were less frequent and had longer durations in HCs furthest from the outer nuclear layer. Next, given that previous studies (Song et al. 2008; Stell and Lightfoot 1975) analyzed HC morphometrics in fixed tissue, we asked whether a similar approach could distinguish subtypes of live HCs acutely dissociated from the goldfish retina. We modified the approach of Stell and Lightfoot (1975) and developed a novel method to identify HC subtype by measuring the ratio of dendritic field to soma size ($r_{d/s}$). We then set out to clarify whether spontaneous Ca^{2+} activity differed among HC subtypes. All subtypes of HCs presented spontaneous Ca^{2+}-based APs. HCs with a higher $r_{d/s}$ had fewer APs, with longer duration.

3.3 Methods

3.3.1 Ethical approval

Common goldfish were purchased from a commercial supplier (AQUAlity Tropical Fish Supply Inc., Mississauga, ON, Canada) and housed in the University of Ottawa aquatic facilities. Fish were maintained in a 170 l tank, with a flow-through system of fresh, aerated, and dechloraminated water at a stable temperature of 18°C. Fish were maintained on a constant light cycle of 12 h light:12 h dark. Animal care and handling procedures were approved by the University of Ottawa Animal Care and Veterinary Services (ACVS) protocol BL-1760, in accordance with Canadian Council on Animal Care (CCAC) regulations. Goldfish were dark adapted for at least 1 h, euthanized by rapid decapitation, and pithed.

3.3.2 Retinal slice preparation

Retinal "mini-slices" were prepared using a protocol modified from Sun et al. (2002) and Vessey et al. (2005). All reagents and chemicals were sourced from MilliporeSigma (Oakville, ON, Canada) unless otherwise stated. Eyes were enucleated and immediately placed in cold Ca^{2+}-free Ringer's solution (in mM: 120 NaCl, 2.6 KCl, 10 HEPES, 0.5 NaH_2PO_4, and 16 glucose, with pH adjusted to 7.8 with NaOH). The eye was punctured and cut around the ora serrata, and the iris, cornea, and lens were removed. The retina was removed from the eye cup and placed in hyaluronidase (100 U ml^{-1}, Cat. No. H-3506) in L-15 solution for 20 min at room temperature. L-15 solution was composed of 70% L-15 (Leibovitz's medium, Cat. No. L-1518) and 30% Ca^{2+}-free Ringer's. Isolated retinas were then washed 3 times with L-15 solution and transferred into a 60 mm plastic Petri dish (Corning Inc., Bedford, MA, USA, Cat. No. 430589) in extracellular solution (ECS). ECS consisted of (in mM): 120 NaCl, 5 KCl, 2.5 $CaCl_2$, 2 $MgCl_2$, 10 HEPES, and 10 glucose, with pH adjusted to 7.80 with NaOH. Retinas were then laid

vitreous side down and minced with a fine razor blade held in a haemostat. The resulting slices were transferred to 35 mm culture dishes (Corning Inc., Cat. No. 430165) for 15 min before dye loading. Culture dishes were pre-coated with 0.1% poly-L-lysine (Cat. No. A-005-C) for 10 min, rinsed three times with double-distilled water, and left to air-dry for at least 2 h before use.

In retinal slice experiments, HCs were identified based on their location in the distal region of the inner nuclear layer and by the characteristically horizontal layout of their dendritic fields.

3.3.3 Isolated cell preparation

Horizontal cells were isolated according to Jonz and Barnes (2007). Retinas were isolated and treated with hyaluronidase, as described above. Retinas were then washed 3 times for 3 min each in fresh L-15 solution and then placed in L-15 solution containing 7 U ml^{-1} papain (Worthington Biochemical Corporation, Lakewood, NJ, USA, Cat. No. 3126) for 40 min. Papain was previously activated with 2.5 mM L-cysteine (Cat. No. 168149). Retinas were again rinsed 3 times in fresh L-15 solution.

Small (~4 mm^2) sections of retina were removed and mechanically dissociated by repeated, gentle trituration in L-15 solution using a fire-polished Pasteur pipette (SATI International Scientific Inc., Dorval, QC, Canada, Cat. No. 123.203.01) in a 15 ml polypropylene centrifuge tube (FroggaBio Inc., Concord, ON, Canada, TB15-500). For immunohistochemistry experiments, the resulting cell suspension was immediately plated onto glass slides (Fisher Scientific Canada, Ottawa, ON, Canada, Cat. No. 12-550-343) for morphometric measurements. For Ca^{2+} imaging experiments, cell suspensions were plated onto 35 mm plastic Petri dishes (Corning Inc., Cat. No. 430165). Culture dishes were pre-coated for with 0.01% poly-L-lysine

(Cat. No. A-005-C) for 10 min, rinsed three times with double-distilled water, and air-dried for 2 h before use. Cells were allowed to settle for approximately 15 min before experiments.

3.3.4 Relative $[Ca^{2+}]_i$ measurements

Measurements of intracellular Ca^{2+} followed those of Country et al. (2019). Briefly, the membrane-permeable form of the Ca^{2+} indicator, Fura-2 (Fura-2-LeakRes-AM; Ion Biosciences, San Marcos, TX, USA, Cat. No. 1061), was used to assess relative changes in free $[Ca^{2+}]_i$. Isolated cell or slice preparations were protected from light and incubated in ECS prepared with 5 µM of Fura-2 and 0.1% v/v of a 10% w/v pluronic F-127 (Cat. No. P2443) solution for 30 min at room temperature to facilitate dye loading. Fura-2-loaded cells and slices were plated and maintained in dishes (Corning, Inc.) fitted with perfusion chambers (Warner Instruments Inc, Hamden, CT, USA, Cat. No. RC-33DL).

After loading, cells or slices were washed 3 times in ECS and imaged under low intensity brightfield illumination with a compound microscope (FN-1, Nikon, Tokyo, Japan). Fluorescence imaging was performed using a Lambda DG-5 wavelength changer (Sutter Instruments, Novato, CA, USA) to change excitation wavelength between 340 and 380 nm. Excitation and emission light were passed through a Nikon 40× water-immersion objective lens (numerical aperture 0.8) and emission light was filtered through a 510 nm band pass filter. Images were captured with a CCD camera (QImaging, Surrey, BC, Canada) by focusing on a region of interest encompassing an HC soma. Excitation wavelengths alternated between 340 and 380 nm, and emission intensity was recorded for both wavelengths every 2 s using NIS Elements (Nikon) software. Imaging data was logged in Excel (Microsoft Corp., Redmond, WA, USA).

The chamber was continuously perfused at ~1 ml min^{-1} by gravity-fed recording solutions at room temperature. Recording solution was removed from the chamber at the same rate using a variable-flow pump (Fisher). For kainate experiments, kainic acid (Tocris, Oakville, ON, Canada, Cat. No. 0222) was used at 50 μM to activate kainate-sensitive AMPARs.

3.3.5 Morphometry

Differential interference contrast and phase-contrast microscopy were performed on a Zeiss Axio Observer A1 microscope (Carl Zeiss, Oberkochen, Germany). Images were captured with QCapture (Quantative Imaging Corp., Surrey, BC, Canada) and measurements were performed with ImageJ software (Schneider et al. 2012). Images of cells analyzed with Ca^{2+} imaging were taken with an upright microscope (FN-1, Nikon), and were captured and measured with NIS Elements software (Nikon).

HCs were identified by their characteristic stellate morphology, flat bodies, and thick dendrites (Dowling et al. 1985; Tachibana 1981). Morphometry was performed using an adapted method from Stell and Lightfoot (1975), who approximated an ellipse representing the dendritic spread of each HC. In the present study, the longest distance between two dendritic points was defined as the major axis. On either side of this major axis, a perpendicular line was drawn from the major axis to the furthest dendritic tip. These two lines were summed together to make the minor axis. An ellipse representing the approximate dendritic spread of the HC was calculated using the formula for the area (A) of an ellipse:

$$A = \pi \cdot \frac{major\ axis}{2} \cdot \frac{minor\ axis}{2}$$

This process was repeated for the soma. The ratio ($r_{d/s}$) of the ellipse representing the dendritic field versus the ellipse representing the soma was measured in all cells.

3.3.6 Immunocytochemistry and fluorescence microscopy

Cells were plated and fixed for 30 min at room temperature with 4% paraformaldehyde in phosphate buffered solution (PBS) containing (in mM): 137 NaCl, 15.2 Na_2PO_4, 2.7 KCl, 1.5 KH_2PO_4, and pH adjusted to 7.8 with NaOH (Bradford et al. 1994). Cells were rinsed in PBS, permeabilized with 0.1% Triton X-100 in PBS for 10 min, and rinsed again. Cells were incubated overnight at 4°C in PBS containing 1:500 polyclonal rabbit anti-GABA (MilliporeSigma, Cat. No. A2052; Antibody Registry AB_477652). GABA is a widely conserved neurochemical, and this antibody has been used to label GABAergic neurons across a range of species including *Drosophila* (Levy and Larsen 2013), lamprey (Menard et al. 2007), chicken (Suarez et al. 2006), and rat (Talos et al. 2006). Finally, cells were rinsed and incubated in PBS with 1:50 goat anti-rabbit secondary antibodies conjugated to fluorescein isothiocyanate (FITC; Jackson Immunoresearch, West Grove, PA), rinsed, and coverslipped. As a negative control for the primary antibody, anti-GABA was pre-adsorbed with 1 mM GABA (Sigma-Aldrich, Cat. No. A2129) before incubation. To control for the secondary antibody, the primary antibody was omitted. For immunocytochemistry experiments, all fluorescence images were taken with a Zeiss Axio Observer A1 microscope with QCapture software. Excitation and emission light was passed through a Zeiss 09 filter set (450-490 nm bandpass filter for excitation, 515 nm long pass filter for emission) and a Zeiss 63× objective lens (numerical aperture 0.85).

3.3.7 Analysis

Raw traces from Ca^{2+} imaging experiments are presented as the ratio of fluorescence emission intensity after excitation with 340 nm and 380 nm (F_{340}/F_{380}). These values are proportional to $[Ca^{2+}]_i$. Parameters chosen to describe each spontaneous event included event frequency, duration, amplitude, area under the curve (AUC), and time to peak (TTP) from

baseline level. Baseline $[Ca^{2+}]_i$ levels were also analyzed for cell experiments, but were not measured in slices due to confounding fluorescence from out-of-focus cells. Events were analysed using a peak analysis algorithm in OriginPro 2016 (OriginLab Corp. Northampton, MA, USA). Frequency was measured as the number of events per sampled time period (5 min). Duration was measured as the time (s) between the start and end of each event using a local maximum function compared to baseline. Amplitude (F_{340}/F_{380}) was measured as the difference between the peak value and baseline directly before the event, as determined by the Origin peak analysis gadget using a second derivative algorithm for determining baseline values. AUC ($F_{340}/F_{380} \cdot s$) approximates Ca^{2+} influx into the cytosol and was calculated as the exact integral of amplitude over time of each event from $[Ca^{2+}]_i$ baseline:

$$\int_{event\ start}^{event\ end} f(amplitude)dt$$

TTP was the time (s) between the start of the event and the peak amplitude of that event. Baseline measurements were determined as the average of the last 30 s of resting baseline (F_{340}/F_{380}) of each sampled time period. Parameters of Ca^{2+} events were averaged from the last two spontaneous events of each cell. All parameters were tested for correlation with Pearson's r test in Prism 5 (GraphPad Software Inc., San Diego, CA, USA). For Fig. 3.1F and G, 30s of $[Ca^{2+}]_i$ baseline was averaged just before kainate application, and again after 5 min in kainate.

3.4 Results

3.4.1 HCs present spontaneous Ca^{2+} action potentials in situ

Spontaneous Ca^{2+} APs were observed in slices of the goldfish retina with the ratiometric dye, Fura-2 (Fig. 3.1). Representative brightfield and pseudocolor images are shown in Fig. 3.1A-D, and traces of $[Ca^{2+}]_i$-based fluorescence ratios over time are shown in Fig. 3.1E. During

each AP, ratios increased sharply to a peak, decayed slowly at first, and then quickly returned to baseline.

Teleost HCs are known to have functional kainate-sensitive AMPARs (Ishida and Neyton 1985), and kainate has been used to positively identify HCs in slices (Babai and Thoreson 2009; Vessey et al. 2005). Application of 50 μM kainate abolished APs and increased fluorescence ratios in HCs by 25% (n = 18, $p < 0.0001$) (Fig. 3.1F,G). HCs were the most distal cells to show an increase in $[Ca^{2+}]_i$; kainate did not increase $[Ca^{2+}]_i$ in the outer nuclear layer.

To assess the characteristics of *in situ* spontaneous Ca^{2+}-based APs, we measured the frequency, duration, amplitude, AUC, and TTP of APs from 30 HCs from slices of 10 goldfish. Frequency distributions of these data are graphed in Fig. 3.2. Within a five-minute sampling period, we observed a median of 1 event with an interquartile range (IQR) of 0 (Fig. 3.2A). APs were slow: they lasted for a median duration of 120 s (IQR 68 s; Fig. 3.2B). Amplitude (Fig. 3.2C) and AUC (Fig. 3.2D) were calculated from changes in Fura-2 emission ratios, and increased commensurately with $[Ca^{2+}]_i$. The median amplitude was 0.097 (units of F_{340}/F_{380}; IQR 0.11) and the median AUC was 5.8 (IQR 7.4). The median TTP was 34 s (IQR 34 s; Fig. 3.2E).

3.4.2 AP characteristics vary with distance from photoreceptors

Parameters of APs *in situ* (frequency, duration, amplitude, AUC, and TTP) from Fig. 3.2 were plotted against distance from the HC soma to the outer nuclear layer (ONL; Fig. 3.3). Frequency is reported for 30 cells. 25 of these (83.3%) presented APs within the 5-min sampling period, and were analyzed for duration, amplitude, AUC, and TTP. AP frequency was negatively correlated with the distance from the ONL ($r^2 = 0.20$, $p < 0.05$), whereas AUC ($r^2 = 0.17$, $p < 0.05$) and duration ($r^2 = 0.26$, $p<0.01$) were positively correlated. Amplitude and TTP were not significantly correlated with distance from the ONL.

3.4.3 Mapping a frequency distribution of morphology of dissociated HCs

In separate experiments, HCs were isolated and imaged. Variations in typical HC morphology are displayed in Fig. 3.4. Some smaller cells had large, flat somata with several short dendrites (Fig. 3.4A,B), similar to reports of H1 and H2 subtypes in goldfish (Stell and Lightfoot 1975), carp, zebrafish (Song et al. 2008), and perch (Dowling et al. 1985; Lasater 1986). Others had smaller, rounder somata with fewer, longer dendrites, similar to reports of H3 or H4 in teleosts (Fig. 3.4C,D). These were observed less frequently in our preparation.

We imaged and measured $r_{d/s}$ for 143 HCs isolated from the retinas of 11 fish (Fig. 3.5). Figs. 3.5A and 3.5B demonstrates measurement of dendritic field area and soma area, respectively. The number of observations of each $r_{d/s}$ value is displayed as a frequency distribution in Fig. 3.5C. Mapping of images of HCs to the spectrum of $r_{d/s}$ values revealed that cells with low $r_{d/s}$ (<8) corresponded to H1 and H2 subtypes, and cells with high $r_{d/s}$ (>12) resembled H3 and H4 subtypes. In addition, the distribution in Fig. 3.5C was bimodal, suggesting that H1 and H2 were most dominant, with a smaller proportion of H3 and H4.

GABA-positive cells had low $r_{d/s}$ *values*

In separate experiments, all four subtypes of HCs were fixed and prepared for GABA immunocytochemistry (Fig. 3.6A-F). Only H1 cells displayed GABA-immunoreactivity (IR) (Fig. 3.6A-C). Fig. 3.6G displays the distribution of $r_{d/s}$ of all 136 cells (*circles*) from 3 fish, including 56 of those cells with GABA-IR (*squares*). All HCs with GABA-IR had an $r_{d/s}$ lower than 8, and 95% (53/56) had an $r_{d/s}$ lower than 4. Thus, a low $r_{d/s}$ was predictive of GABA-IR.

No labelling was observed with omission of the primary antibody, or when the primary antibody was pre-adsorbed with 1 mM GABA.

3.4.4 All HC subtypes exhibit spontaneous Ca^{2+}-based action potentials

Spontaneous Ca^{2+}-based APs were analyzed in 156 cells from 51 fish using Fura-2, and $r_{d/s}$ was measured for each cell. Representative pseudocolor images of APs are shown in Fig. 3.7, and changes in $[Ca^{2+}]_i$ with time for each subtype are shown in Fig. 3.8. Transients were typically of long duration and ranged from 10 – 40 s. $[Ca^{2+}]_i$ peaked early and slowly returned to baseline. Spontaneous activity was found in cells regardless of $r_{d/s}$.

Parameters of Ca^{2+}-based APs, such as amplitude, AUC, duration, time to peak, frequency, and baseline $[Ca^{2+}]_i$, were analyzed and plotted against $r_{d/s}$ values for each cell (Fig. 3.9). Frequency and baseline are reported for all 156 cells. Of these, 124 (79.5%) presented spontaneous APs within the 5-min sampling period, and were analyzed for duration, amplitude, AUC, and TTP. AUC and duration were positively correlated with $r_{d/s}$ (AUC $r^2 = 0.059$, $p < 0.01$; duration $r^2 = 0.043$, $p < 0.05$), whereas frequency was negatively correlated with $r_{d/s}$ ($r^2 = 0.047$, $p < 0.01$). No significant correlations were found for TTP, amplitude, or baseline $[Ca^{2+}]_i$.

In Fura-2 Ca^{2+}-imaging experiments, we applied kainate to HCs across the gamut of $r_{d/s}$. Kainate elicited an increase in $[Ca^{2+}]_i$ in all 19 cells tested (Fig. 3.10). $[Ca^{2+}]_i$ peaked quickly, followed by a brief trough, and then a slow rise in $[Ca^{2+}]_i$ until kainate was washed out. In many cases, before kainate was superfused, cells exhibited spontaneous Ca^{2+}-based APs (Fig. 3.10A,B,D). In these cells, spontaneous Ca^{2+} transients ceased during the kainate-elicited response.

Figure 3.1. Horizontal cells present spontaneous Ca^{2+}-based action potentials *in situ*.
Goldfish retinal slices were imaged in brightfield (*A*) before Fura-2-based Ca^{2+} imaging. *B-D.* Pseudocolor fluorescence images indicate $[Ca^{2+}]_i$ during Ca^{2+}-based action potentials, as measured by the fluorescence ratio of Fura-2 emission. Higher ratios (green/yellow/red) indicate high $[Ca^{2+}]_i$; low ratios (blue/violet) indicate low $[Ca^{2+}]_i$. *B, C,* and *D* show $[Ca^{2+}]_i$ before, during, and after spontaneous action potentials, respectively. Two horizontal cells are labelled with white arrowheads, and recordings of their $[Ca^{2+}]_i$ over time are displayed in *E.* The black trace represents the bottom-most cell labelled in *A-D*; the red trace was recorded from the top cell. Dotted lines indicate the timepoints for images *B, C,* and *D*. *F.* In response to 50 μM kainate, $[Ca^{2+}]_i$ increased in horizontal cells but not in photoreceptor somata of the outer nuclear layer. *G*. Kainate increased $[Ca^{2+}]_i$ in 18/18 horizontal cells *in situ* ($p < 0.0001$). Scale bar: 25 μm. Scales in *E* and *F* indicate the Fura-2 fluorescence emission ratio (F_{340}/F_{380}) and time in seconds. OS, outer segments of photoreceptors; ONL, outer nuclear layer; INL, inner nuclear layer; IPL, inner plexiform layer.

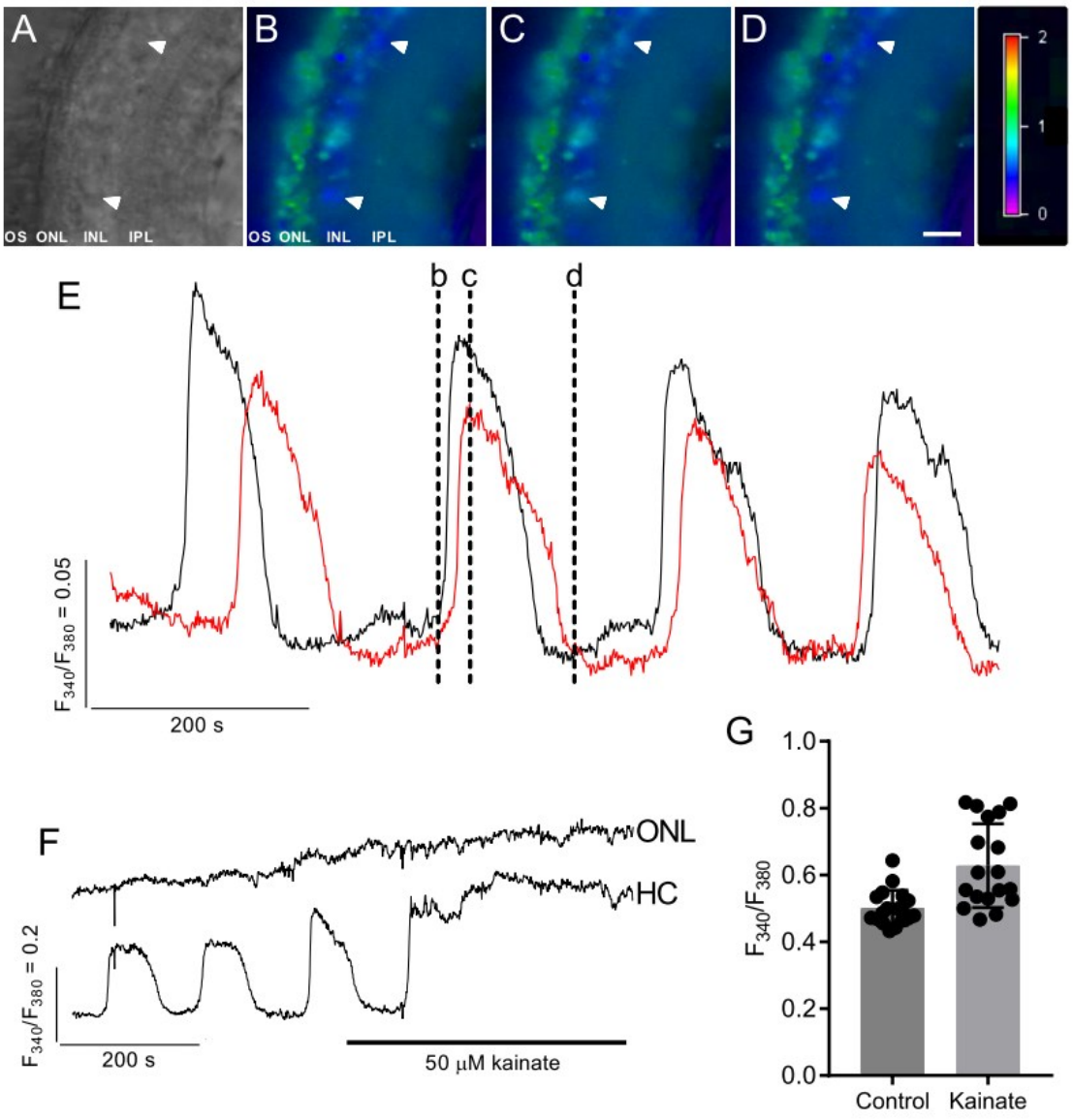
A
B
C
D
OS ONL INL IPL
OS ONL INL IPL
2
1
0
E
b c d
F340/F380 = 0.05
200 s
F
ONL
HC
F340/F380 = 0.2
200 s
50 μM kainate
G
1.0
0.8
0.6
0.4
0.2
0.0
F340/F380
Control
Kainate

Figure 3.1

Figure 3.2. Frequency distributions of action potential parameters of horizontal cells *in situ.*

Spontaneous Ca^{2+} action potentials were measured in 30 cells, and the frequency distribution for the following parameters were plotted: frequency of spontaneous action potentials within a 5-min sampling period (*A*), duration (*B*), amplitude (*C*), area under the curve (*D*), and the time for an action potential to reach its peak (*E*).

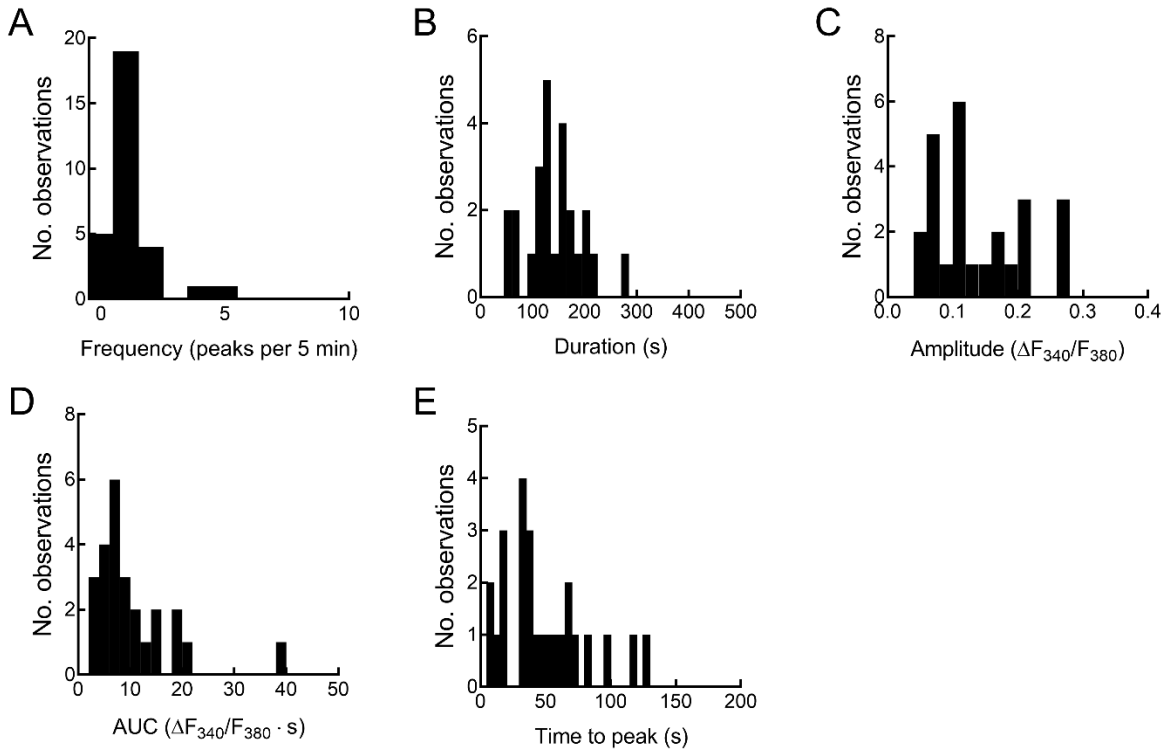
A
No. observations
Frequency (peaks per 5 min)
B
No. observations
Duration (s)
C
No. observations
Amplitude (ΔF340/F380)
D
No. observations
AUC (ΔF340/F380 · s)
E
No. observations
Time to peak (s)

Figure 3.2

Figure 3.3. Ca^{2+} action potential parameters vs. distance from the outer nuclear layer. *A.* Number of transients within 5 min. *B*. Duration. *C.* Amplitude of Ca^{2+} action potentials. *D*. Area under the curve (AUC). *E.* Time to peak. 30 cells were analyzed for frequency in *A*. 25 of these presented APs and were analyzed in *B-D.* Significant positive correlations were found for AUC ($r^2 = 0.169$, $p < 0.05$) and duration ($r^2 = 0.259$, $p < 0.01$); frequency was negatively correlated with $r_{d/s}$ ($r^2 = 0.199$, $p < 0.05$). No significant correlations were found for amplitude or TTP.

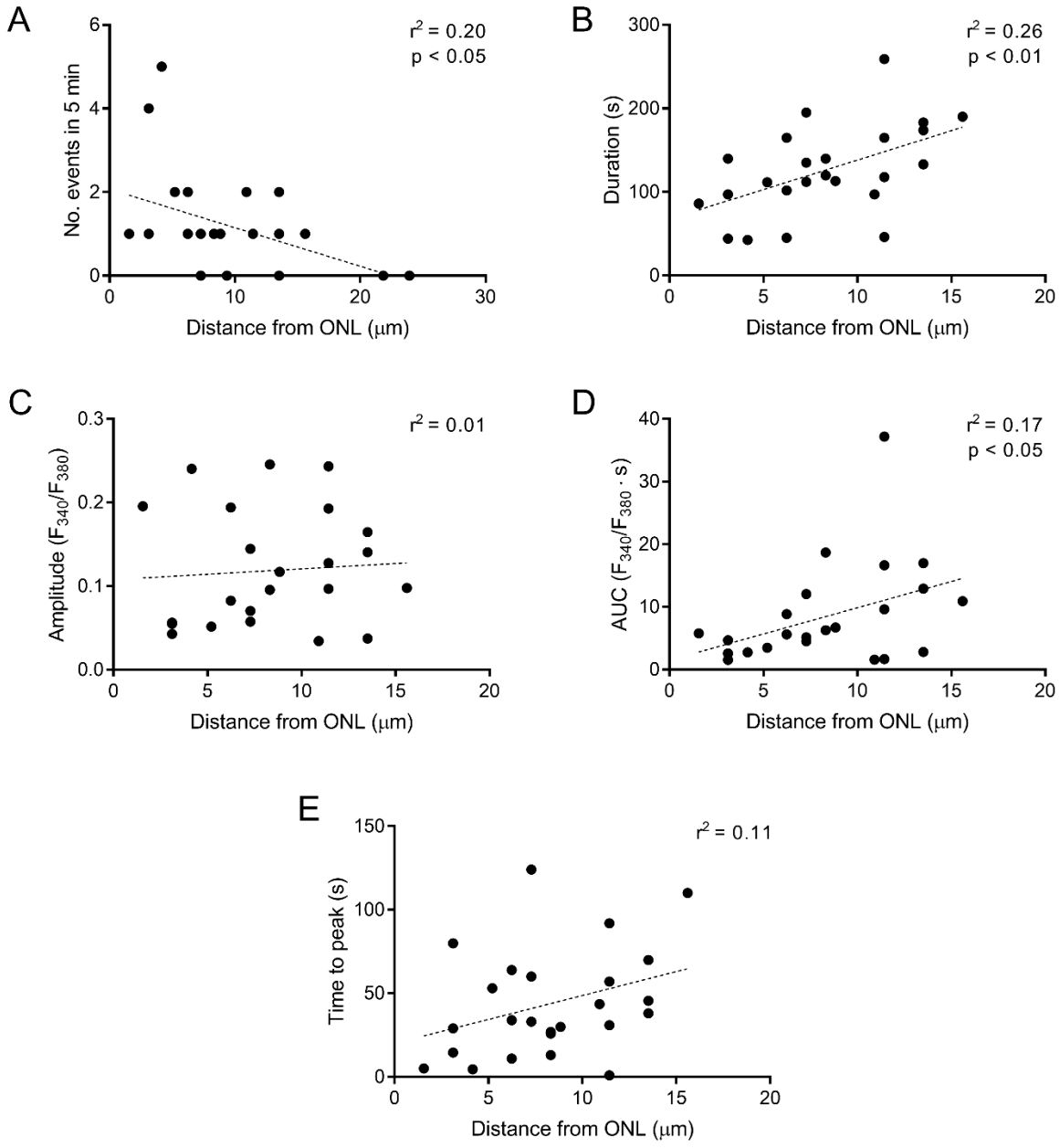
A
No. events in 5 min
r^2 = 0.20
p < 0.05
Distance from ONL (μm)
B
Duration (s)
r^2 = 0.26
p < 0.01
Distance from ONL (μm)
C
Amplitude (F_{340}/F_{380})
r^2 = 0.01
Distance from ONL (μm)
D
AUC (F_{340}/F_{380} · s)
r^2 = 0.17
p < 0.05
Distance from ONL (μm)
E
Time to peak (s)
r^2 = 0.11
Distance from ONL (μm)

Figure 3.3

Figure 3.4. Horizontal cell subtypes have unique morphology.

Representative morphologies of horizontal cell subtypes H1 (*A*), H2 (*B*), H3 (*C*), and H4 (*D*). Images were acquired using differential interference contrast microscopy. Scale bar: 10 μm.

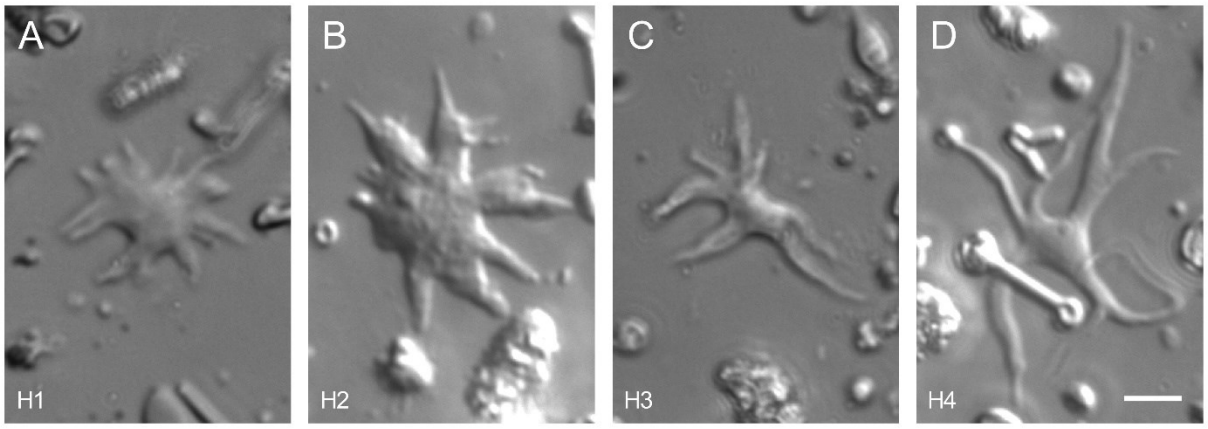

Figure 3.4

Figure 3.5. Measurement and frequency of horizontal cell subtype morphology.

A ratio ($r_{d/s}$) was obtained of the approximate area of the dendritic field (*A*) and the approximate area of the soma (*B*). *Major* represents the major axis, while $minor_1$ and $minor_2$ represent the two arms of the minor axis. See Methods for further details. *C.* The frequency distribution of $r_{d/s}$ of 143 cells was bimodal, with peaks at 8 and 12. Traces of H1, H2, H3 and H4 cells from Fig. 3.4 are displayed above the x-axis according to their respective $r_{d/s}$.

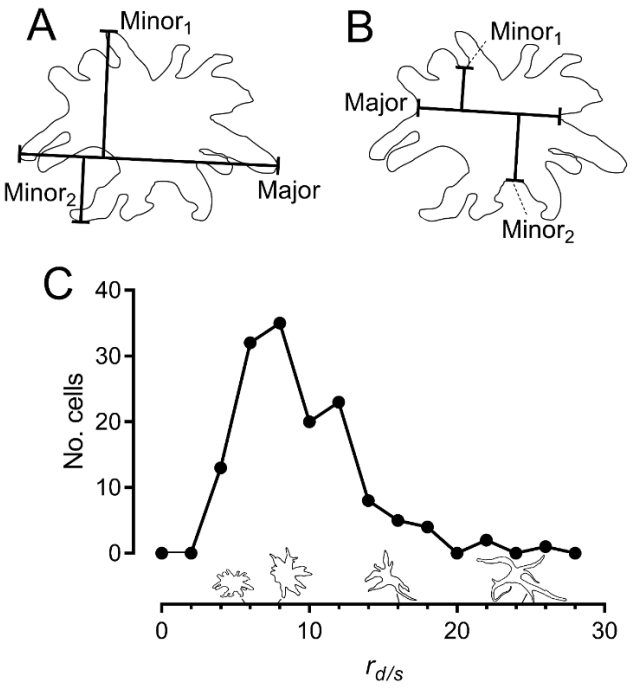
A
Minor1
Minor2
Major
B
Minor1
Major
Minor2
C
No. cells
40
30
20
10
0
0
10
20
30
rd/s

Figure 3.5

Figure 3.6. GABA-immunoreactive H1 horizontal cells have low $r_{d/s}$.

Horizontal cells were incubated with antibodies against GABA and imaged with phase-contrast and wide-field fluorescence microscopy. A representative phase-contrast image of an H1 cell is shown in *A*, followed by GABA-immunoreactivity (IR) in *B* and an overlay of both images in *C*. H1 cells showed strong, diffuse GABA-IR. *D-F.* Merged phase-contrast and fluorescence images for H2, H3, and H4 (respectively) showed no GABA-IR. Scale bar: 10 μm. *G.* Frequency distribution of the $r_{d/s}$ of all 136 cells (*circles*), 56 of which presented GABA-IR (*squares* and shaded area).

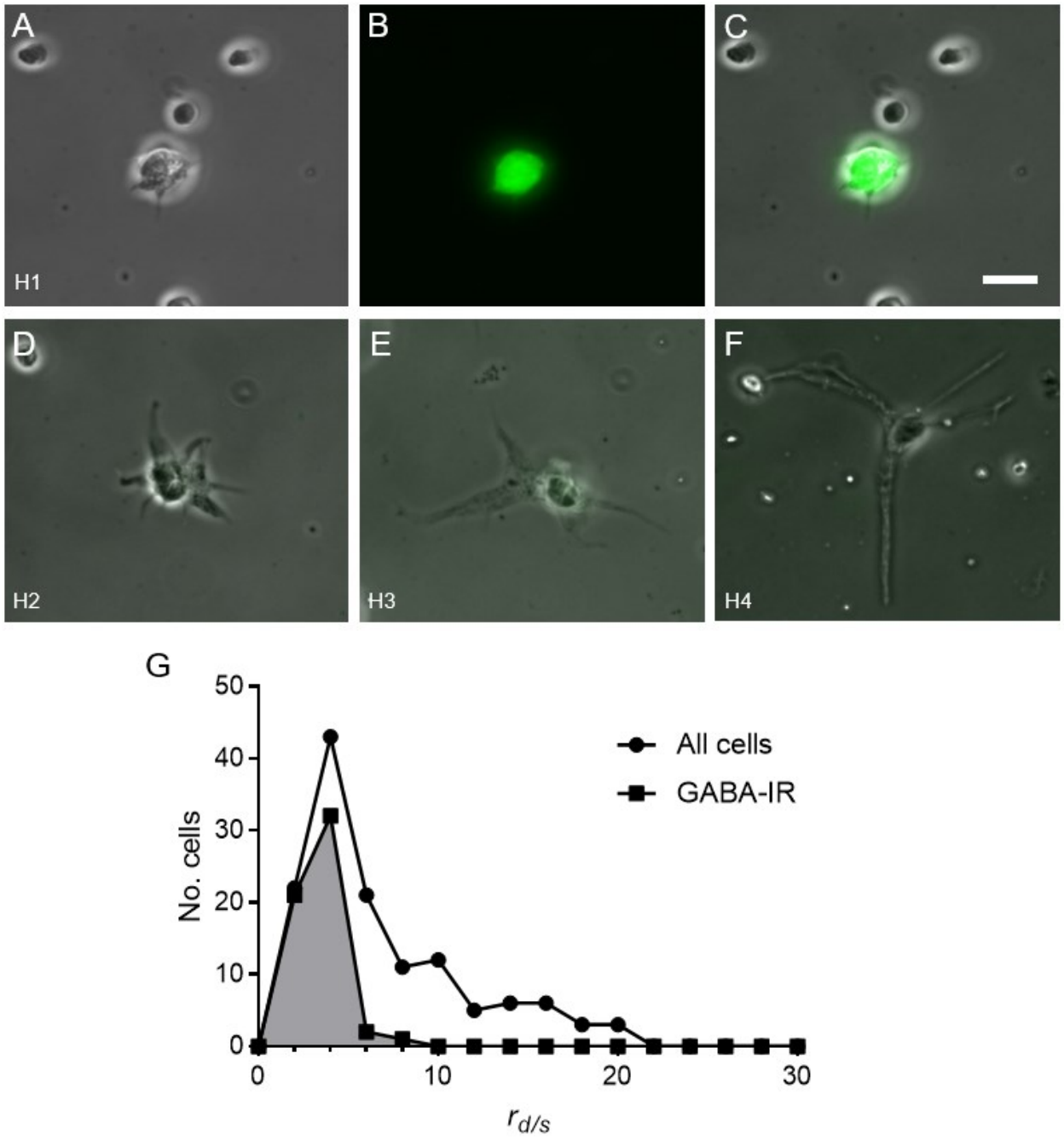
A
B
C
H1
D
E
F
H2
H3
H4
G
50
40
30
20
10
0
No. cells
All cells
GABA-IR
0
10
20
30
$r_{d/s}$

Figure 3.6

Figure 3.7. Fura-2-based Ca^{2+} imaging of action potentials in isolated horizontal cell subtypes.

A-*C*. H1, H2, and H3/H4-like cells (respectively) are shown in brightfield (left). On the right, pseudocolor fluorescence images indicate $[Ca^{2+}]_i$ during Ca^{2+}-based action potentials, as measured by the fluorescence ratio of Fura-2 emission. Higher ratios (green/yellow/red) indicate high $[Ca^{2+}]_i$; low ratios (blue/violet) indicate low $[Ca^{2+}]_i$. The three fluorescence images for each cell show $[Ca^{2+}]_i$ immediately before an action potential, at peak $[Ca^{2+}]_i$, and immediately afterwards. Scale bars: *A*, 10 μm. *B*, 10 μm. *C*, 25 μm.

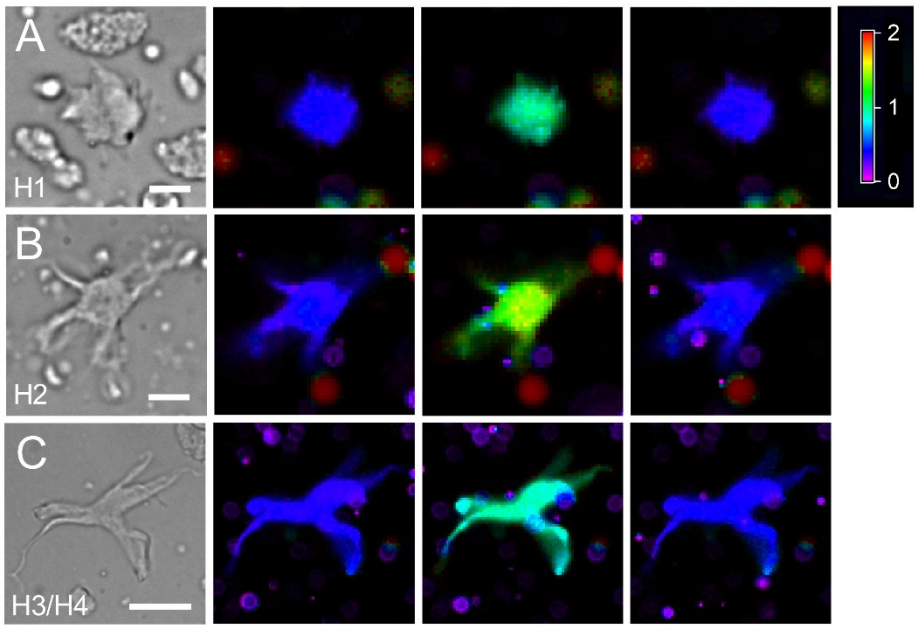

Figure 3.7

Figure 3.8. Spontaneous Ca^{2+} action potentials exist in all subtypes.

A-D. Representative recordings from cells with $r_{d/s}$ values of approximately 4, 8, 12, and 25 and corresponding to the morphology of H1, H2, H3/H4, respectively. All cells showed spontaneous transients of ~10–40 s, followed by a return to a stable baseline $[Ca^{2+}]_i$. Scale bars indicate the Fura-2 fluorescence emission ratio (F_{340}/F_{380}) and time in seconds.

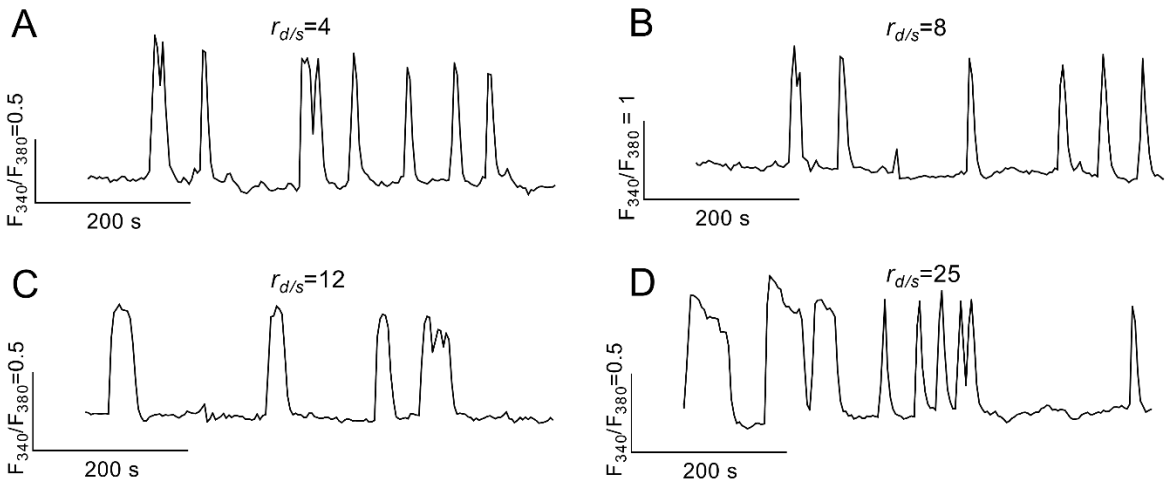
A
$r_{d/s}$=4
F_{340}/F_{380}=0.5
200 s
B
$r_{d/s}$=8
F_{340}/F_{380} = 1
200 s
C
$r_{d/s}$=12
F_{340}/F_{380}=0.5
200 s
D
$r_{d/s}$=25
F_{340}/F_{380}=0.5
200 s

Figure 3.8

Figure 3.9. Ca^{2+} transient parameters vs. $r_{d/s}$.

A. Number of transients within 5 min. *B*. Duration of Ca^{2+} transients. *C.* Amplitude. *D*. Area under the curve (AUC). *E.* Time to peak (TTP). *F.* $[Ca^{2+}]_i$ baseline. Frequency and baseline were measured in 156 cells. Within the 5-min sampling period, 124 of these presented APs which were analyzed in *B*-*E*. Significant positive correlations were found for AUC ($r^2 = 0.059$, $p < 0.01$) and duration ($r^2 = 0.043$, $p < 0.05$); frequency was negatively correlated with $r_{d/s}$ ($r^2 = 0.047$, $p < 0.01$). No significant correlations were found for amplitude, TTP, or baseline.

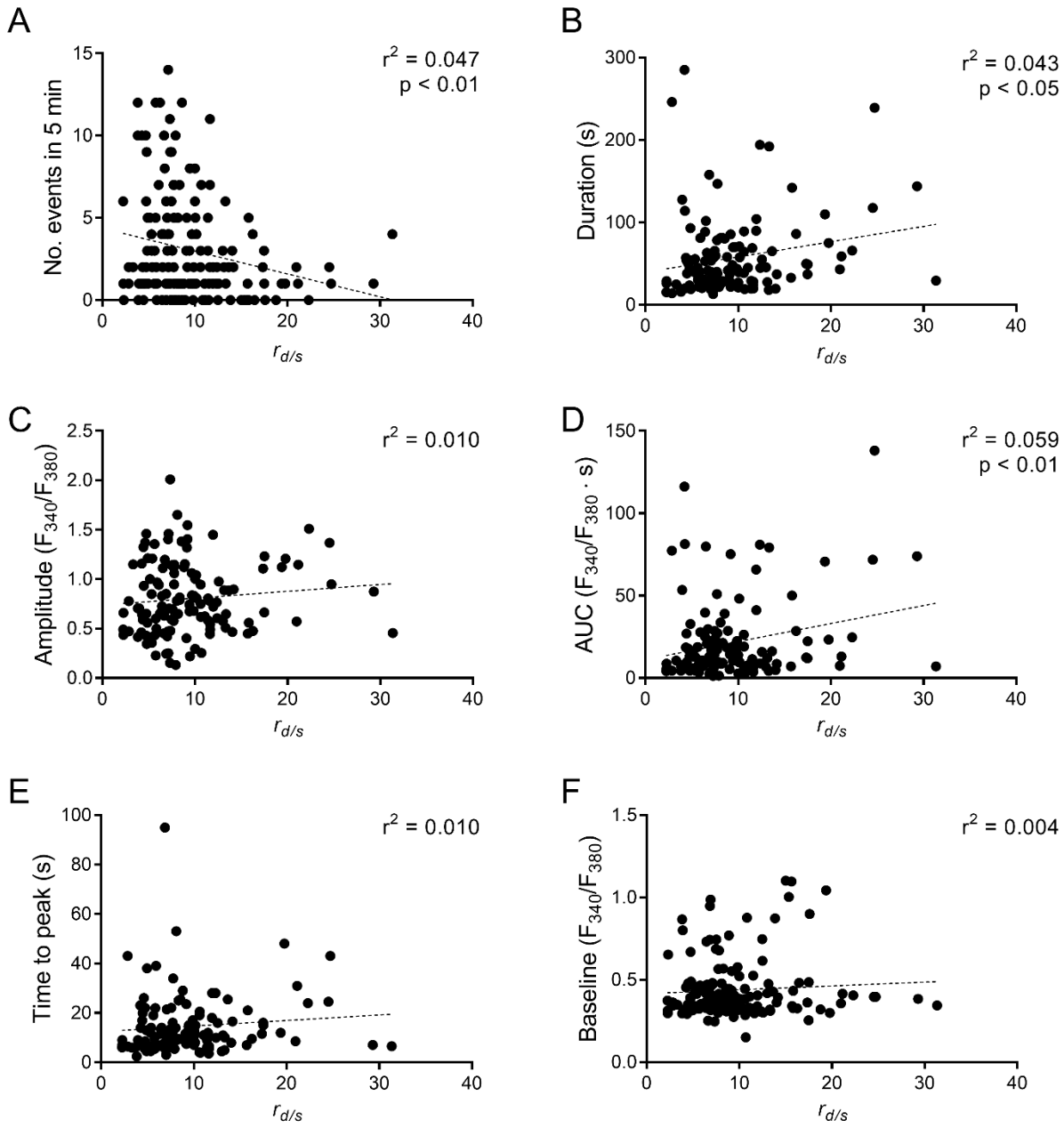
A
No. events in 5 min
r² = 0.047
p < 0.01
r_d/s
B
Duration (s)
r² = 0.043
p < 0.05
r_d/s
C
Amplitude (F340/F380)
r² = 0.010
r_d/s
D
AUC (F340/F380 · s)
r² = 0.059
p < 0.01
r_d/s
E
Time to peak (s)
r² = 0.010
r_d/s
F
Baseline (F340/F380)
r² = 0.004
r_d/s

Figure 3.9

Figure 3.10. Kainate increased $[Ca^{2+}]_i$ in all horizontal cells.

A-D. Representative Ca^{2+} imaging traces from horizontal cells with $r_{d/s}$ values of 4, 8, 11 and 16 and corresponding to the morphology of H1, H2, H3/H4, respectively. 50 μM kainate elicited an increase in $[Ca^{2+}]_i$ in 19/19 cells from across the gamut of $r_{d/s}$. In all subtypes, $[Ca^{2+}]_i$ peaked quickly, diminished partially, and rose slowly and steadily until kainate was washed out. Scale bars indicate the Fura-2 fluorescence emission ratio (F_{340}/F_{380}) and time in seconds.

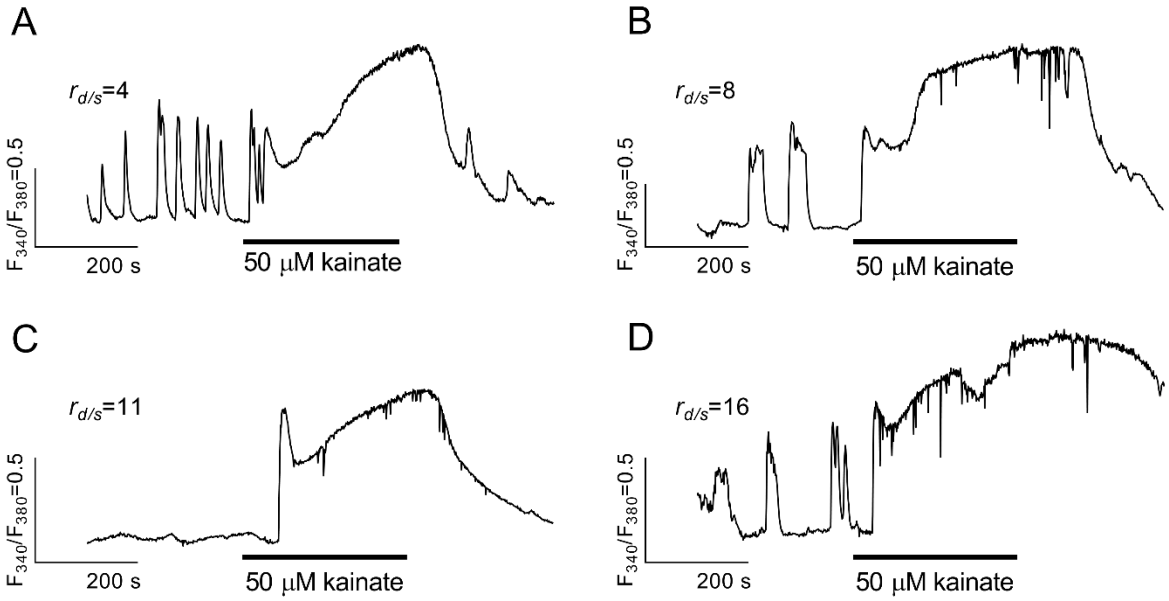
A
$r_{d/s}$=4
F_{340}/F_{380}=0.5
200 s
50 μM kainate
B
$r_{d/s}$=8
F_{340}/F_{380}=0.5
200 s
50 μM kainate
C
$r_{d/s}$=11
F_{340}/F_{380}=0.5
200 s
50 μM kainate
D
$r_{d/s}$=16
F_{340}/F_{380}=0.5
200 s
50 μM kainate

Figure 3.10

3.5 Discussion

In this report, we describe spontaneous Ca^{2+}-based APs in HCs *in situ*. We provide two lines of evidence that APs vary among subtypes. First, we compared APs among HCs based on their distance from photoreceptors. In the inner nuclear layer, subtypes of HCs are organized into sublaminae, such that H1 cells are closest to photoreceptors and H4 are furthest (Stell and Lightfoot 1975). We found that the furthest HCs had fewer APs, but of a greater duration and AUC (a measure of Ca^{2+} influx). Secondly, we isolated cells *in vitro* to more accurately identify subtypes by morphology and compared APs among subtypes. As there are no biomarkers to distinguish HC subtypes, we developed a quantitative method to classify isolated HC subtypes by taking a ratio of dendritic field area to soma area ($r_{d/s}$). We show that dissociated H1 cells (labelled with antibodies for GABA) had the lowest $r_{d/s}$ of all subtypes, which supports $r_{d/s}$ as a classification system. All subtypes of HC displayed spontaneous APs. AP parameters correlated with $r_{d/s}$ just as they correlated with the distance from photoreceptors: HCs with a larger $r_{d/s}$ had fewer APs, but of longer duration and greater AUC. These trends suggest that as subtype number increases from H1 to H4, APs become longer, less frequent, and involve more Ca^{2+} influx.

APs *in situ* involved a sharp rise in $[Ca^{2+}]_i$, a slow decay, and then a precipitous return to baseline $[Ca^{2+}]_i$, similar to APs of isolated cells in this study and in previous reports (Country et al. 2019; Kreitzer et al. 2012). However, APs *in situ* were less frequent (median of 1 event per 5 min compared to 7 events per 5 min in Country et al., 2019), took longer to attain peak (34 s vs. 6 s) and lasted longer (120 s vs. 18 s). After incubation in Fura-2-AM, excess extracellular Fura-2-AM may be incompletely washed out of thick retinal slices, which would prolong Fura-2 uptake and increase Ca^{2+} buffering in HCs. Increased exogenous Ca^{2+} buffer has been shown to

prolong Ca^{2+} transients in other cell types (Capel and Terrar 2015; Tse et al. 1994). This may account for the differences we observed *in situ*. Alternatively, input from photoreceptors and interplexiform cells (Mangel and Dowling 1987) may modulate APs *in situ*, prolonging them.

In previous reports using fixed retina, HC subtypes were assessed morphometrically by graphing minor vs. major axis length of dendritic fields (Song et al., 2008) or by approximating an ellipse over the dendritic field of the cells and comparing it to perikaryal (soma) width (Song et al. 2008; Stell and Lightfoot 1975). These *in situ* approaches could not distinguish H1 and H2 cells from each other, but could identify H1/H2 from H3 or H4. The present study categorized freshly-dissociated HCs by taking a ratio of the surface area of the dendritic field vs. the soma ($r_{d/s}$), expanding on the method of Stell and Lightfoot (1975). $r_{d/s}$ showed a bimodal distribution, in which cells with $r_{d/s} < 8$ resembled H1 and H2 as described in previous reports (e.g. Lasater 1986), whereas cells with $r_{d/s} > 12$ resembled H3 and H4 subtypes (e.g. Lasater 1986). We therefore propose that the first peak of the bimodal frequency distribution consists mainly of H1 and H2 cells, whereas the second peak consists of H3 and H4.

To confirm the presence of H1 cells within the $r_{d/s}$ distribution, we measured the $r_{d/s}$ values of HCs labeled with a marker for the H1-specific neurotransmitter, GABA (Marc et al. 1978; Paik et al. 2003). GABA-positive cells had the lowest $r_{d/s}$ values and were found entirely within the first peak of the $r_{d/s}$ distribution. Additionally, GABA-positive cells comprised 41.1% (56/136) of all fixed cells observed, which is in line with reports that H1 is the most common subtype in fish (e.g., Ariel et al. 1984; Young and Dowling 1984). Verification of other HC subtypes within the $r_{d/s}$ distribution will await the development of subtype-specific markers. Notably, $r_{d/s}$ peaked at a slightly lower value in immunocytochemistry experiments ($r_{d/s}$ of 4),

compared to live cells ($r_{d/s}$ of 8). The decrease in $r_{d/s}$ may have been caused by the effects of fixation on cell morphology.

HCs of teleosts (e.g. goldfish, carp, catfish) and skates are known to exhibit Ca^{2+}-dependent APs (Country et al. 2019; Johnston and Lam 1981; Lasater et al. 1984; Murakami and Takahashi 1987; Tachibana 1981). In many reports, the APs occurred spontaneously (Country et al. 2019), especially in the presence of Ba^{2+} or K^{+} channel blockers (Tachibana, 1981; Murakami and Takahashi, 1987). More recently, spontaneous, all-or-nothing Ca^{2+} transients were found in goldfish in Ca^{2+} imaging experiments (Country et al. 2019; Kreitzer et al. 2012). These transients represent APs, and involve Ca^{2+} influx into the cytosol via L-type Ca^{2+} channels and ryanodine receptors (Country et al. 2019).

The current study is the first to demonstrate that APs exist in tissue, and in each HC subtype. These insights are important in understanding the possible physiological function of spontaneous APs. APs may affect vision in one of two ways: in the transition from light to darkness APs may rapidly depolarize HC membrane potential, and/or APs may affect feedback to photoreceptors, since changes to cytosolic and cleft [Ca^{2+}] are known to affect several receptors on HCs and photoreceptors (Ayoub and Lam 1985; Country et al. 2019; Huang et al. 2006; Jackman et al. 2011). The implications of the present study are that the effects of spontaneous APs may impact rods and all types of cones in a manner that is attributable to subtype-specific AP characteristics.

A major finding in the present study was that two indicators of HC subtype (distance from the photoreceptors and $r_{d/s}$) were negatively correlated with AP frequency, and positively correlated with duration and AUC. These trends in frequency, duration, and AUC are likely related. As AP duration increases, there would be more time for AUC to increase, and less time

for subsequent events to occur. Notably, rod HCs (H4) would have fewer, longer APs than other subtypes, which raises the question of whether rods are affected differently than cones. The significance of these differences is unclear without a better understanding of AP function in HCs. There were no significant correlations with either metric ($r_{d/s}$ and distance from photoreceptors) and amplitude, TTP, or [Ca^{2+}] baseline.

In Ca^{2+} imaging experiments, all cells tested responded to kainate with an increase in Ca^{2+}, as in previous reports (Ishida and Neyton 1985; Vessey et al. 2005). Similarly, kainate abolished APs in cells and slices. These data suggest that kainate-sensitive AMPA receptors exist on all HC subtypes, and confirm that the functionality of these receptors is preserved *in vitro* after enzymatic and mechanical dissociation. Notably, spontaneous APs in all subtypes ceased during kainate treatment, even in cells which exhibited spontaneous APs before and afterwards. As noted previously (Country et al. 2019), the present findings suggest that AP frequency would be reduced in prolonged darkness, when release of glutamate from photoreceptors is high.

3.6 Conclusion

Here we present the novel finding that HCs present APs *in situ*, which may suggest a role for APs in retinal physiology and vision. This study has developed a quantitative method of identifying HC subtypes using the ratio of the surface area of the dendritic field to that of the soma ($r_{d/s}$). Used in conjunction with characteristics such as cell size and dendritic morphology, $r_{d/s}$ serves as a tool for identifying HC subtype *in vitro*. We present evidence that all HC subtypes present Ca^{2+}-based APs, but that parameters, such as duration, AUC, and frequency are

subtype-specific. These findings may be important to clarify the function of spontaneous APs in HCs.

4 mK_{ATP} channels mediate hypoxia tolerance in retinal horizontal cells of goldfish (*Carassius auratus*) and may confer hypoxia tolerance in rainbow trout (*Oncorhynchus mykiss*)

I performed all experiments and analyses for this chapter, and prepared this manuscript.

4.1 Introduction

The retina is part of the central nervous system, and therefore shares the high ATP demand of the brain (Country 2017; Wong-Riley 2010). Normally, over 50% of ATP supply is used to pump ions across neuronal membranes, both to maintain membrane potentials and to extrude Ca^{2+} from the cytosol (Ames 1992; Nilsson and Lutz 2004). When neurons receive insufficient O_2 (hypoxia) or blood supply (ischemia), ATP supply is reduced, neurons depolarize, and intracellular Ca^{2+} concentrations ($[Ca^{2+}]_i$) reach toxic levels (Bickler and Buck 1998). Several other phenomena increase $[Ca^{2+}]_i$ even further, as depolarization opens voltage-gated Ca^{2+} channels and releases excitatory neurotransmitters such as glutamate (Szydlowska and Tymianski 2010). High $[Ca^{2+}]_i$ is toxic to cells, and is recognized as a common final step among many pathways which trigger cell death (Bickler 1992; Orrenius and Nicotera 1994). This pathway from hypoxia to Ca^{2+}-mediated cell death is called excitotoxicity, and is central in strokes and several types of blindness (Bickler and Kelleher 1992; Choi 1992; Osborne et al. 2004).

Some species have adapted strategies to survive extended periods of hypoxia. Some turtles (e.g. *Trachemys* spp. and *Chrysemys* spp.) can survive months in hypoxic, ice-covered ponds by reducing their neuronal activity to a "pilot light" level (Jackson and Heisler 1982; Lutz and Nilsson 2004). The Crucian carp (*Carassius carassius*) can survive months of hypoxia at ~4ºC (Holopainen and Pitkänen 1985; Nilsson and Lutz 2004), and the congeneric goldfish (*C. auratus*) can withstand hypoxia for days at 4ºC, and for hours at room temperature (Walker and Johansen 1977; Wilkie et al. 2008). Instead of becoming comatose during hypoxia like turtles, *Carassius* spp. maintain a reduced level of neural activity and locomotion in hypoxia, possibly to search out waters with greater partial pressures of O_2 (P_{O2}) (Nilsson 2001; Nilsson et al. 1993b;

Vornanen et al. 2009; Wilkie et al. 2008). These strategies limit ATP turnover, preserve low $[Ca^{2+}]_i$, and prevent excitotoxicity (Bickler 1992; Bickler and Buck 1998; Jackson 2002; Nilsson and Lutz 2004). The retina is also resistant to hypoxia in these species. Electroretinogram responses to light are greatly diminished during anoxia in turtle (Stenslokken et al. 2008) and carp (Johansson et al. 1997) retinas, but recover completely upon reperfusion. These studies suggest vision withstands hypoxic insult in hypoxia-tolerant species, but the cellular mechanisms of hypoxia tolerance are poorly understood and are completely unexplored in the retina.

Mitochondria are the major consumers of O_2 and producers of ATP, and therefore they are well positioned to sense changes in metabolite supply (Pamenter 2014). In the turtle brain, hypoxia is sensed by mitochondrial K^+ ATP-dependent (mK_{ATP}) channels; the resulting mitochondrial depolarization triggers a second messenger pathway which downregulates plasma membrane ion channels and limits Ca^{2+} influx (Hawrysh and Buck 2013; Pamenter et al. 2016; Zivkovic and Buck 2010). mK_{ATP} channels are also required for ischemic preconditioning (IPC) in the mammalian retina, in which brief, sublethal bouts of ischemia protect against subsequent ischemic insult (Dreixler et al. 2008; Roth et al. 2006). Mitochondrial responses to hypoxia are unknown in the ectotherm retina.

Horizontal cells (HCs) are interneurons of the inner nuclear layer of the retina, which receive glutamatergic input from photoreceptors in the dark. In return, they provide inhibitory feedback to photoreceptors to improve visual contrast and colour opponency (Twig *et al.*, 2003; Thoreson & Mangel, 2012). The Ca^{2+}-permeable ion channels, Ca^{2+} buffering mechanisms, and Ca^{2+} pathways in HCs are well known, especially in teleost fish (reviewed in Country and Jonz 2017). Teleost HCs present spontaneous Ca^{2+}-based action potentials (APs) both *in vitro* and *in situ*, whose function is unknown (Chapters 2 and 3). These APs have been observed in Ca^{2+}

imaging experiments (Country et al. 2019; Kreitzer et al. 2012). Changes in APs may provide insight into how Ca^{2+} homeostasis is being maintained or threatened.

In the present study, we examined how hypoxia affects $[Ca^{2+}]_i$ in HCs. We compared responses of isolated HCs from the hypoxia-tolerant goldfish and the hypoxia-sensitive rainbow trout (*Oncorhynchus mykiss*). We showed that goldfish HCs maintain stable baseline $[Ca^{2+}]_i$ even after 1 h of hypoxia, while $[Ca^{2+}]_i$ increased in response to only 20 min of hypoxia in trout. We showed that hypoxia tolerance depends upon mK_{ATP} channels: blocking mK_{ATP} channels increased $[Ca^{2+}]_i$ in hypoxic goldfish HCs, while opening mK_{ATP} rescued $[Ca^{2+}]_i$ in hypoxic trout HCs. We present evidence that hypoxia stabilized $[Ca^{2+}]_i$ in an mK_{ATP}-dependent manner, preventing increases in $[Ca^{2+}]_i$ caused by blocking glycolysis. These results suggest that hypoxia is not just tolerated by goldfish HCs, but instead, hypoxia actively triggers a neuroprotective pathway to maintain $[Ca^{2+}]_i$ homeostasis.

4.2 Methods

4.2.1 Ethical approval

All animal care procedures were approved by the University of Ottawa Animal Care and Veterinary Services (protocol BL-1760), in accordance with regulations of the Canadian Council on Animal Care. Adult common goldfish were obtained from Mirdo Importations Canada (Montreal, QC, Canada), and maintained in 170 l tanks at 18°C. Rainbow trout were obtained from Linwood Acres Trout Farm (Campbellcroft, ON, Canada), and maintained in 170 l tanks at 13°C. Tanks received fresh, aerated, and dechloraminated water from a constant flow-through system. Tanks were maintained on a 12 h light:12 h dark photoperiod. Fish were dark adapted for approximately 1 h, euthanized by rapid decapitation and pithed.

4.2.2 Isolated cell preparation

HCs were isolated according to Jonz and Barnes (2007). Unless otherwise stated, all reagents and chemicals were sourced from MilliporeSigma (Oakville, ON, Canada). Eyes were enucleated and quickly placed into ice-cold Ca^{2+}-free Ringer's solution (in mM: 120 NaCl, 2.6 KCl, 10 HEPES, 0.5 NaH_2PO_4, and 16 glucose, with pH adjusted to 7.8 with NaOH). The eye was punctured at the ora serrata, and the anterior chamber of the eye was removed. The retina was carefully dissected out from the eye cup and placed in hyaluronidase (100 U ml^{-1}, Cat. No. H-3506) in L-15 solution at room temperature. L-15 solution comprised of 70% L-15 (Leibovitz's medium with glutamine) and 30% Ca^{2+}-free Ringer's solution. Retinas were washed 3 times for 3 min in fresh L-15 solution, and moved to L-15 solution containing 7 U ml^{-1} papain (Cat. No. 3126, Worthington Biochemical Corporation, Lakewood, NJ, USA) and 2.5 mM cysteine for 40 min. Retinas were washed 3 more times in L-15 solution, and cut into small sections (~4 mm^2). These sections were triturated 3 times to remove excess photoreceptors (Dowling et al. 1985). Then, they were moved to 1 ml of fresh L-15 solution and gently triturated to mechanically dissociate cells. The resulting cell suspension was moved to 35 mm culture dishes (Corning Inc., Bedford, MA, USA) containing perfusion chambers (Warner Instruments Inc, Hamden, CT, USA, Cat. No. RC-33DL). Dishes were pre-coated with 0.01% poly-L-lysine (Cat. No. A-005-C) for 10 min, rinsed three times with double-distilled water, and air-dried before use. Cells were left to settle for 15 min, and rinsed three times with extracellular solution (in mM: 120 NaCl, 5 KCl, 2.5 $CaCl_2$, 2 $MgCl_2$, 10 HEPES, and 10 glucose, with pH adjusted to 7.80 with NaOH) before dye loading.

4.2.3 Relative $[Ca^{2+}]_i$ measurements

Ca^{2+} imaging was performed according to Country et al. (2019). Briefly, to measure relative changes in free $[Ca^{2+}]_i$, cells were loaded with a membrane-permeant form of the Ca^{2+} indicator dye, Fura-2 (Fura-2-LeakRes-AM; Ion Biosciences, San Marcos, TX, USA, Cat. No. 1061). Cells were incubated with 5 μM of Fura-2 and 0.1% v/v of a 10% w/v Pluronic F-127 (Cat. No. P2443) in ECS at room temperature in the dark. After 30 min, dishes were washed 3 times with fresh ECS.

Cells were first observed with brightfield imaging using a compound microscope (FN-1, Nikon, Tokyo, Japan) and a Nikon 40× water-immersion objective (numerical aperture 0.8). HCs were identified by their characteristically large somata and thick dendrites, as in previous reports (Country et al. 2019; Dowling et al. 1985; Tachibana 1981). For fluorescence imaging, a Lambda DG-5 wavelength changer (Sutter Instruments, Novato, CA, USA) was used to rapidly alternate between 340 and 380 nm excitation wavelengths once per second. Emission light was filtered through a 510 nm band pass filter. Images were captured with a CCD camera (QImaging, Surrey, BC, Canada). Fluorescence ratios were recorded with NIS Elements (Nikon) software, by setting circular regions of interest within HC somata.

4.2.4 Experimental procedures and solutions

Cells were continuously superfused at ~1 ml min^{-1} by a gravity-driven system. Solutions were drained from the recording chamber at the same rate using a peristaltic pump (Fisher Scientific, Ottawa, ON, Canada). In all experiments, cells were observed for 10 min in ECS before superfusion with treatment solution. After treatment, the bath was washed with ECS for a 10 min recovery period. To create hypoxic solutions, solution reservoirs were bubbled with 100% N_2 for at least 30 min. This procedure produced recording solution with a P_{O2} of

approximately 25 mmHg (Jonz et al. 2004). Control solutions were bubbled with air for the same duration. Glibenclamide (80 μM; Cat. No. G0639), 5-hydroxydecanoic acid (5-HD; 100 μM; Cat. No. H135), and diazoxide (100 μM; Cat. No. D9035) were dissolved in dimethyl sulfoxide (DMSO), which never surpassed a final concentration of 0.25% v/v. To block glycolysis in experiments shown in Fig. 4.6, glucose was replaced with equimolar 2-deoxyglucose (2-DG; Cat. No. D8375).

4.2.5 Analysis

For Fura-2 recordings, ratios were calculated by dividing the fluorescence emission from 340 nm and 380 nm excitation (F_{340}/F_{380}). These values are proportional to $[Ca^{2+}]_i$. Ratios were exported to Excel (Microsoft Corp., Redmond, WA, USA) and analyzed in OriginPro 2016 (OriginLab Corp. Northampton, MA, USA). OriginPro's peak analysis gadget was used to approximate baseline using a second-derivative algorithm. The peak analysis gadget was then used to detect peaks using a local maximum function compared to baseline. For analysis, baseline was calculated as the last 30 s of baseline F_{340}/F_{380} for a given time period. AP amplitude was measured as the difference between peak F_{340}/F_{380} and baseline before the AP. Values of the last two APs of a given time period were averaged. For statistics, the values at the end of a treatment or recovery period were compared to the last 5 min before the treatment, and the fold-change was reported.

All statistical tests for Ca^{2+} imaging were performed in Prism 8 (GraphPad Software Inc., San Diego, CA, USA). Data are presented as mean ± standard deviation. In Fig. 4.6, a Kruskal-Wallis test was used with Dunn's post-hoc test. All columns were compared with all other columns, with a family-wise significance level of 0.05. One-tailed Mann-Whitney tests were used in all other analyses except where otherwise listed.

4.3 Results

4.3.1 Hypoxia does not increase $[Ca^{2+}]_i$ in HCs of goldfish

HCs were isolated from goldfish and rainbow trout, and baseline $[Ca^{2+}]_i$ was monitored over time with the ratiometric Ca^{2+} imaging dye, Fura-2. HCs of both species presented spontaneous Ca^{2+}-based APs for the duration of normoxic recordings as controls. APs were similar in both species, and matched previous reports of spontaneous, seconds- to minutes-long Ca^{2+} transients in goldfish HCs (Country et al. 2019; Kreitzer et al. 2012): APs began with a steep rise in $[Ca^{2+}]_i$ followed by a prolonged plateau and a sharp return to baseline. To our knowledge, these trout experiments are the first to show spontaneous APs in HCs of any salmonid.

To test the hypothesis that goldfish HCs (but not trout) would maintain $[Ca^{2+}]_i$ baseline throughout hypoxia, we treated HCs of both species with normoxic or hypoxic solutions and monitored $[Ca^{2+}]_i$ over time. Representative brightfield images are shown in Fig. 4.1, along with pseudocolour representations of $[Ca^{2+}]_i$ in APs after treatment with normoxia or hypoxia. Traces of $[Ca^{2+}]_i$ over time are shown in Fig. 4.2A for goldfish, and Fig 4.2B for trout. In goldfish HCs, $[Ca^{2+}]_i$ baseline did not change in response to 20 min normoxia (n = 13) or 20 min hypoxia (n = 6). Similarly, $[Ca^{2+}]_i$ held stable throughout 1 h normoxia (n = 9) and 1 h hypoxia (n = 5; Figs. 4.1A-D, 4.2A,C).

Restoring $[Ca^{2+}]_i$ after an AP would likely require ATP for extrusion or sequestration; APs during hypoxia may therefore strain ATP supply. We tested the hypothesis that AP amplitude would be reduced during hypoxic treatment, possibly to reduce ATP demand. Even in 1 h exposures, APs persisted throughout treatment. However, in goldfish HCs, AP amplitude decreased during hypoxia but not normoxia (Fig. 4.2D). Amplitude returned to pre-treatment

values upon reperfusion with normoxic solution, and there was no difference in AP amplitude between hypoxia- and normoxia-treated cells in the recovery period (Fig. 4.2D).

In trout HCs, $[Ca^{2+}]_i$ baseline held stable in normoxia (1.18 ± 0.25-fold change, n = 13) but increased irreversibly in response to 20 min hypoxia (1.68 ± 0.81-fold change, n = 11; Fig. 4.1E-H, Fig. 4.2B,C). This represents a 50% increase in $[Ca^{2+}]_i$ ($p < 0.05$). Unlike the case in goldfish HCs, AP amplitude was not significantly diminished during hypoxic treatment (Fig. 4.2E). These data support the hypothesis that HCs of the hypoxia-tolerant goldfish, but not hypoxia-sensitive trout, maintain a stable $[Ca^{2+}]_i$ baseline during hypoxia.

4.3.2 mK_{ATP} channels are necessary to stabilize $[Ca^{2+}]_i$ in goldfish HCs during hypoxia

Next, we tested the hypothesis that mK_{ATP} channels were involved in neuroprotection against hypoxia, as has been reported in turtle cortical neurons (Hogg et al. 2014; Pamenter et al. 2008b) and in IPC in the mammalian retina (Dreixler et al. 2008; Roth et al. 2006). First, we exposed isolated goldfish HCs to the mK_{ATP} antagonists, glibenclamide (Fig. 4.3) and 5-HD (Fig. 4.4) along with either normoxia or hypoxia for 20 min. In normoxia, glibenclamide (80 μM; Pamenter et al. 2008b) had no effect on post-treatment $[Ca^{2+}]_i$ baseline (Fig. 4.3A). When co-applied with hypoxia, mK_{ATP} inhibition with glibenclamide led to an increase in $[Ca^{2+}]_i$ (1.26 ± 0.23-fold change, n = 12; Fig. 4.3B), a 22% increase over glibenclamide alone ($p < 0.05$; Fig. 4.3C). Consistent with the effects of hypoxia in Figure 4.2D, AP amplitude decreased during treatment with glibenclamide and hypoxia, but not with glibenclamide alone (Fig. 4.3D). AP amplitude was partially restored when glibenclamide and hypoxia were washed out, and there was no difference in AP amplitude during recovery (Fig. 4.3D).

Likewise, 20 min of 5-HD (100 μM; Pamenter et al. 2008b) alone had no effect on post-treatment $[Ca^{2+}]_i$ baseline (1.00 ± 0.07-fold change, n = 8; Fig. 4.4A). Co-application with

hypoxia increased baseline 1.06-fold (± 0.08, n = 10; Fig. 4.4B). This difference was subtle (6%) but significant ($p < 0.05$; Fig. 4.4C). AP amplitude decreased slightly during application of 5-HD alone (0.81 ± 0.23-fold change) as well as during co-application of 5-HD and hypoxia (0.84 ± 0.15-fold change; Fig. 4.4D). Upon recovery, amplitude was restored and there were no differences among treatments (Fig. 4.4D).

4.3.3 mK_{ATP} activation is sufficient to stabilize $[Ca^{2+}]_i$ in HCs of the hypoxia-sensitive trout

To test the hypothesis that an mK_{ATP}-dependent pathway could stabilize $[Ca^{2+}]_i$ in trout HCs, we applied the mK_{ATP} agonist, diazoxide (100 μM; Dukoff et al. 2014; Pamenter et al. 2008b), to isolated trout HCs in the presence and absence of hypoxia. $[Ca^{2+}]_i$ baseline did not change with diazoxide alone (n = 6; Fig. 4.5A), or when diazoxide was co-applied with hypoxia (n = 10; Fig. 4.5B,C). AP amplitude decreased during both conditions (diazoxide and normoxia, 0.66 ± 0.19-fold change; diazoxide and hypoxia, 0.48 ± 0.14-fold change; Fig. 4.5D). The decrease in hypoxia was greater, but was not significant ($p = 0.053$). Amplitude increased upon reperfusion, with no differences between treatment groups.

4.3.4 Hypoxia prevents increases in $[Ca^{2+}]_i$ baseline caused by inhibiting glycolysis

The previous experiments suggest a role for an mK_{ATP}-dependent pathway in neuroprotection during hypoxia. To test whether this pathway was also active in another low-energy condition, we replaced glucose with equimolar 2-DG to block glycolysis (Dvoriantchikova et al. 2012) in isolated goldfish HCs. Exposure to 1 h 2-DG increased post-treatment $[Ca^{2+}]_i$, compared to 1 h normoxic controls (normoxia, 1.16 ± 0.33-fold change, n = 9; 2-DG, 2.36 ± 1.57, n = 9; $p < 0.05$; Fig. 4.6A,D). However, co-application of 2-DG and hypoxia prevented this increase almost completely (1.23 ± 0.10-fold change, n = 4). This protection was

abolished in the presence of 5-HD (2.19 ± 1.03-fold change, $n = 9$; $p < 0.05$ *versus* normoxic control). These data further suggest a role for mK_{ATP} channels in hypoxic neuroprotection in goldfish HCs.

Next, we tested whether blocking glycolysis would reduce AP amplitude, as we observed during hypoxia in previous experiments. Amplitude decreased during all treatments, when compared to normoxic controls. This decrease was significant for 2-DG and for 2-DG + hypoxia ($p < 0.05$) but was not significant for 2-DG + hypoxia + 5-HD. Amplitude was partially restored in all three groups upon normoxic reperfusion.

Figure 4.1. Ca^{2+} imaging of action potentials in goldfish and rainbow trout HCs exposed to normoxia or hypoxia.

For each cell, brightfield images are shown on the left. On the right, pseudocolour fluorescence images depict fluorescence ratios of Fura-2 emission. Higher Fura-2 ratios (green/yellow/red) indicate higher $[Ca^{2+}]_i$; lower ratios (blue/violet) indicate lower $[Ca^{2+}]_i$. Each triplet of fluorescent images represents one action potential sampled within the last five min of the recovery period for each treatment. In each triplet, fluorescent images depict $[Ca^{2+}]_i$ before, during, and after an action potential, respectively. *A, B.* Goldfish HCs maintain low $[Ca^{2+}]_i$ baseline and present action potentials after superfusion with normoxic solution for 1 h. *C, D.* Low $[Ca^{2+}]_i$ baseline and action potentials are maintained in goldfish HCs despite 1 h of hypoxia. *E, F.* HCs of rainbow trout maintain $[Ca^{2+}]_i$ baseline and action potentials after 20 min superfusion with normoxic solution. *G, H.* 20 min of hypoxia increased $[Ca^{2+}]_i$ baseline in trout HCs. Scale bars represent 20 μM for *A*-*D*, and 10 μM for *E*-*H*.

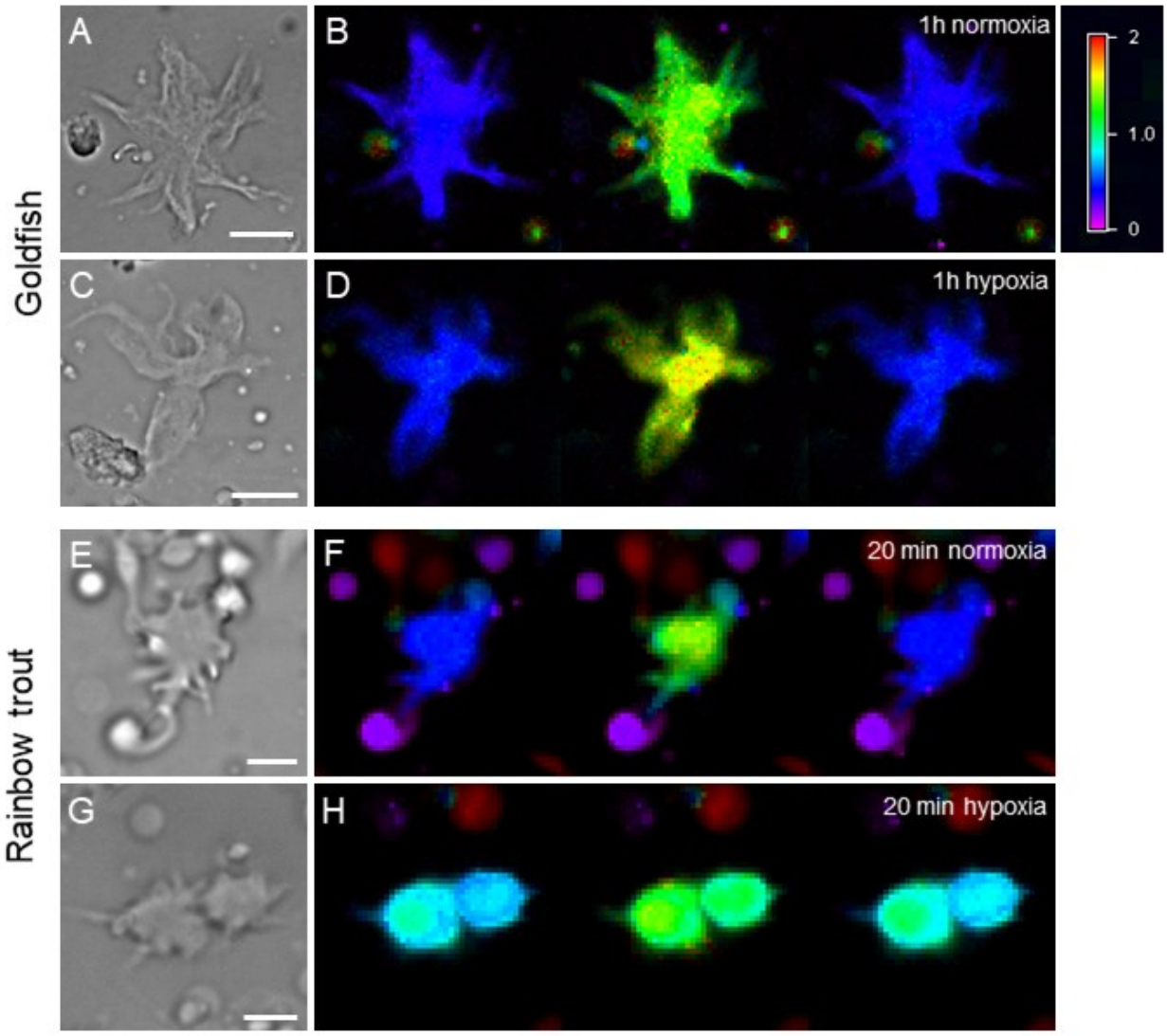
A
B
1h normoxia
2
1.0
0
Goldfish
C
D
1h hypoxia
E
F
20 min normoxia
Rainbow trout
G
H
20 min hypoxia

Figure 4.1

Figure 4.2. Hypoxia increases $[Ca^{2+}]_i$ baseline in HCs of rainbow trout, but not goldfish. *A.* Representative Fura-2-based $[Ca^{2+}]_i$ traces from goldfish HCs exposed to a normoxic solution (*top*) or to hypoxia (*bottom*) for 1 h. Ca^{2+}-based action potentials (represented here as transient increases in $[Ca^{2+}]_i$ throughout the traces) persisted in both conditions. *B.* Rainbow trout HCs maintained $[Ca^{2+}]_i$ baseline and presented Ca^{2+}-based action potentials throughout normoxia (*top*). $[Ca^{2+}]_i$ baseline increased in response to 20 min hypoxia (*bottom)*. *C.* Summary statistics of the fold-change in $[Ca^{2+}]_i$ baseline from pre-treatment values to 10 min post-treatment. $[Ca^{2+}]_i$ baseline did not increase in goldfish HCs in response to either 20 min or 1 h hypoxia. Rainbow trout HCs increased $[Ca^{2+}]_i$ after 20 min of hypoxic insult. *D.* Fold-change in action potential amplitude in goldfish HCs, during and after treatment with normoxia or hypoxia. *E.* Fold-change in amplitude in trout HCs. Scale bars in *A* and *B* indicate the Fura-2 fluorescence emission ratio (F_{340}/F_{380}) and time in seconds.

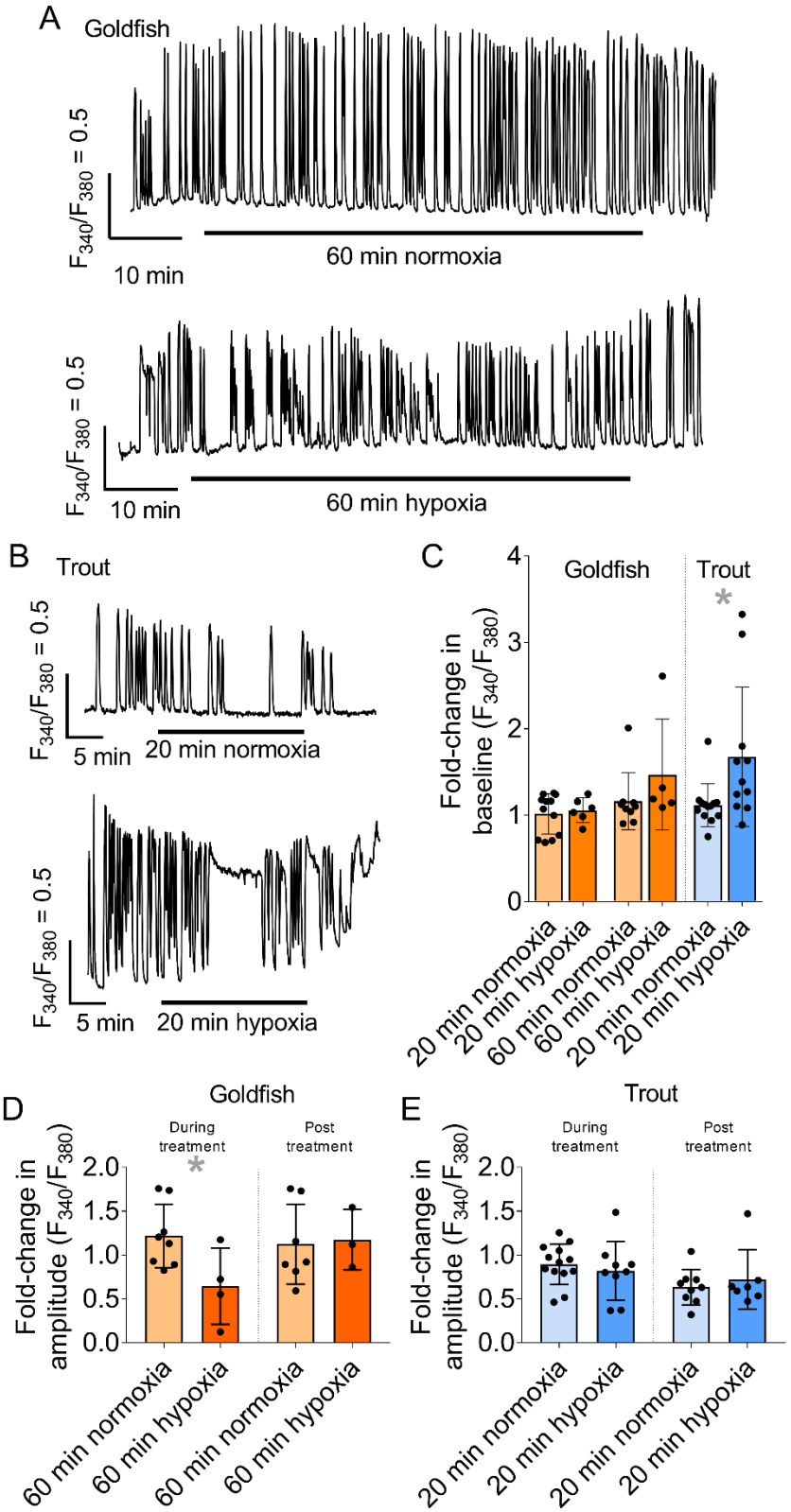
A
Goldfish
F_{340}/F_{380} = 0.5
10 min
60 min normoxia
F_{340}/F_{380} = 0.5
10 min
60 min hypoxia
B
Trout
F_{340}/F_{380} = 0.5
5 min
20 min normoxia
F_{340}/F_{380} = 0.5
5 min
20 min hypoxia
C
Goldfish
Trout
*
Fold-change in baseline (F_{340}/F_{380})
0
1
2
3
4
20 min normoxia
20 min hypoxia
60 min normoxia
60 min hypoxia
20 min normoxia
20 min hypoxia
D
Goldfish
During treatment
Post treatment
*
Fold-change in amplitude (F_{340}/F_{380})
0.0
0.5
1.0
1.5
2.0
60 min normoxia
60 min hypoxia
60 min normoxia
60 min hypoxia
E
Trout
During treatment
Post treatment
Fold-change in amplitude (F_{340}/F_{380})
0.0
0.5
1.0
1.5
2.0
20 min normoxia
20 min hypoxia
20 min normoxia
20 min hypoxia

Figure 4.2

Figure 4.3. Goldfish HCs do not maintain $[Ca^{2+}]_i$ in hypoxia when exposed to the mK_{ATP} antagonist, glibenclamide.

A. Representative recording of a goldfish HC exposed to 80 μM glibenclamide. The dotted horizontal line is shown to illustrate that $[Ca^{2+}]_i$ baseline does not deviate throughout the 20 min exposure or during washout. *B*. When co-applied with glibenclamide, hypoxia leads to a subtle increase in baseline $[Ca^{2+}]_i$, as shown by the deviation from the dotted line. *C*. Summary statistics show an increase in $[Ca^{2+}]_i$ baseline. *D.* Summary statistics of the fold-change in amplitude during and after treatment. Scale bars in *A* and *B* indicate the Fura-2 fluorescence emission ratio (F_{340}/F_{380}) and time in seconds.

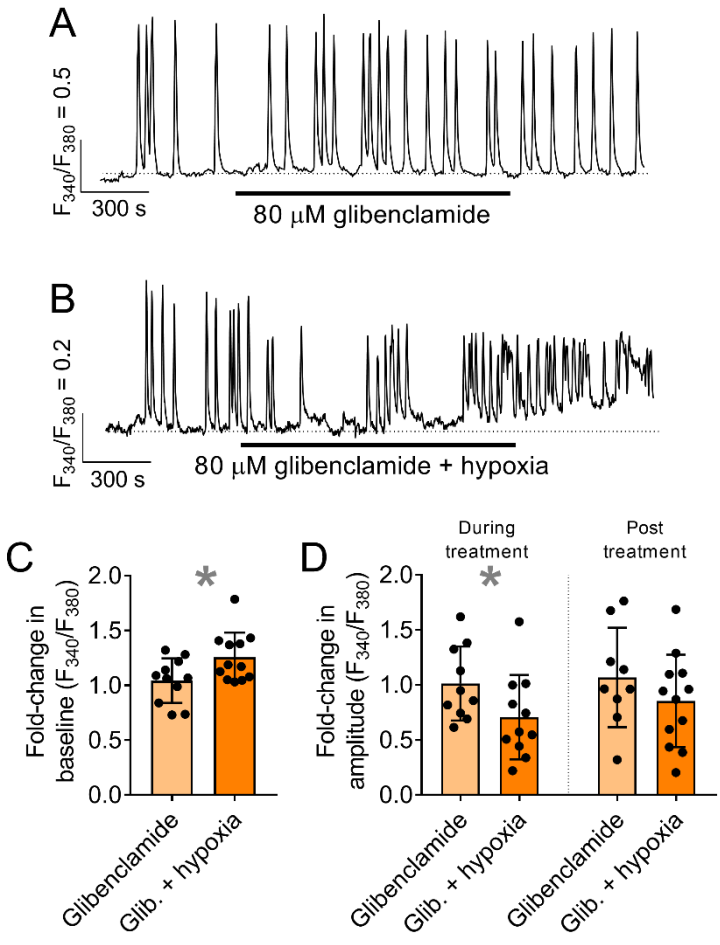
A
F340/F380 = 0.5
300 s
80 μM glibenclamide
B
F340/F380 = 0.2
300 s
80 μM glibenclamide + hypoxia
C
Fold-change in baseline (F340/F380)
2.0
1.5
1.0
0.5
0.0
*
Glibenclamide
Glib. + hypoxia
D
During treatment
Post treatment
Fold-change in amplitude (F340/F380)
2.0
1.5
1.0
0.5
0.0
*
Glibenclamide
Glib. + hypoxia
Glibenclamide
Glib. + hypoxia

Figure 4.3

Figure 4.4. Goldfish HCs do not maintain $[Ca^{2+}]_i$ in hypoxia when exposed to the mK_{ATP} antagonist, 5-hydroxydecanoic acid (5-HD).

A. A representative trace of a goldfish HC exposed to 100 μM 5-HD shows no change in $[Ca^{2+}]_i$ baseline. The dotted horizontal line is shown for clarity; baseline does not deviate from this line. *B*. When co-applied with 5-HD, hypoxia leads to a subtle (~6%) increase in baseline $[Ca^{2+}]_i$, as shown by the deviation from the dotted line. *C*. Summary statistics show an increase in $[Ca^{2+}]_i$ baseline ($p<0.05$, one-tailed Mann Whitney). *D.* Summary statistics of the fold-change in amplitude during and after treatment. Scale bars in *A* and *B* indicate the Fura-2 fluorescence emission ratio (F_{340}/F_{380}) and time in seconds.

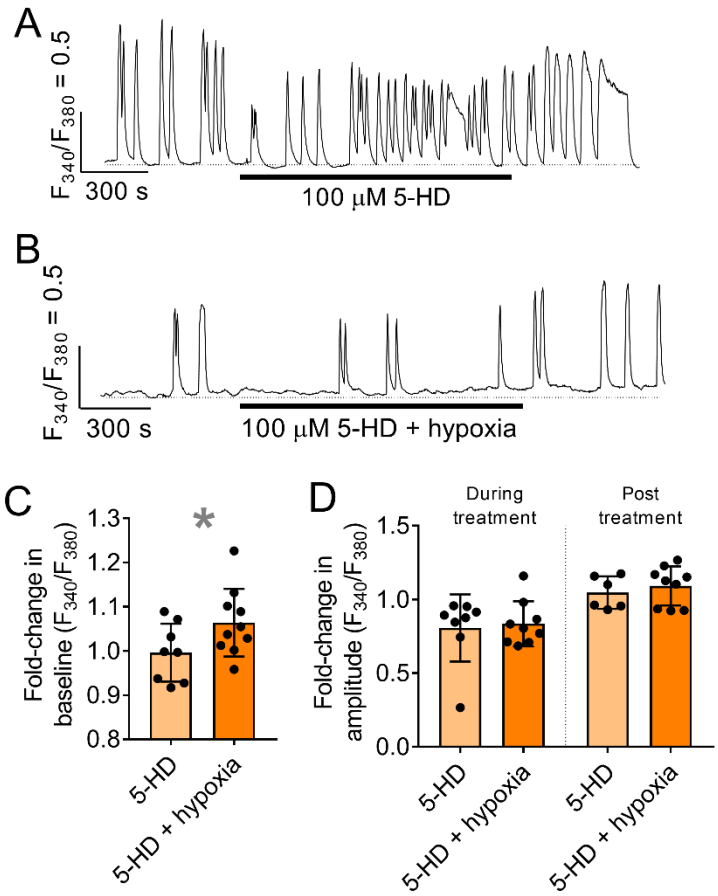
A
F_{340}/F_{380} = 0.5
300 s
100 μM 5-HD
B
F_{340}/F_{380} = 0.5
300 s
100 μM 5-HD + hypoxia
C
Fold-change in baseline (F_{340}/F_{380})
1.3
1.2
1.1
1.0
0.9
0.8
*
5-HD
5-HD + hypoxia
D
During treatment
Post treatment
Fold-change in amplitude (F_{340}/F_{380})
1.5
1.0
0.5
0.0
5-HD
5-HD + hypoxia
5-HD
5-HD + hypoxia

Figure 4.4

Figure 4.5. Diazoxide prevents $[Ca^{2+}]_i$ from increasing in trout HCs in response to hypoxia. *A.* $[Ca^{2+}]_i$ baseline is unchanged in a trout HC exposed to 100 μM diazoxide. The dotted horizontal line is shown for clarity. *B.* When co-applied with diazoxide, hypoxia did not increase $[Ca^{2+}]_i$. Amplitude decreased during the treatment and returned afterwards. *C.* Summary statistics show no increase in $[Ca^{2+}]_i$ baseline. *D.* Summary statistics of the fold-change in amplitude during and after treatment. Scale bars in *A* and *B* indicate the Fura-2 fluorescence emission ratio (F_{340}/F_{380}) and time in seconds.

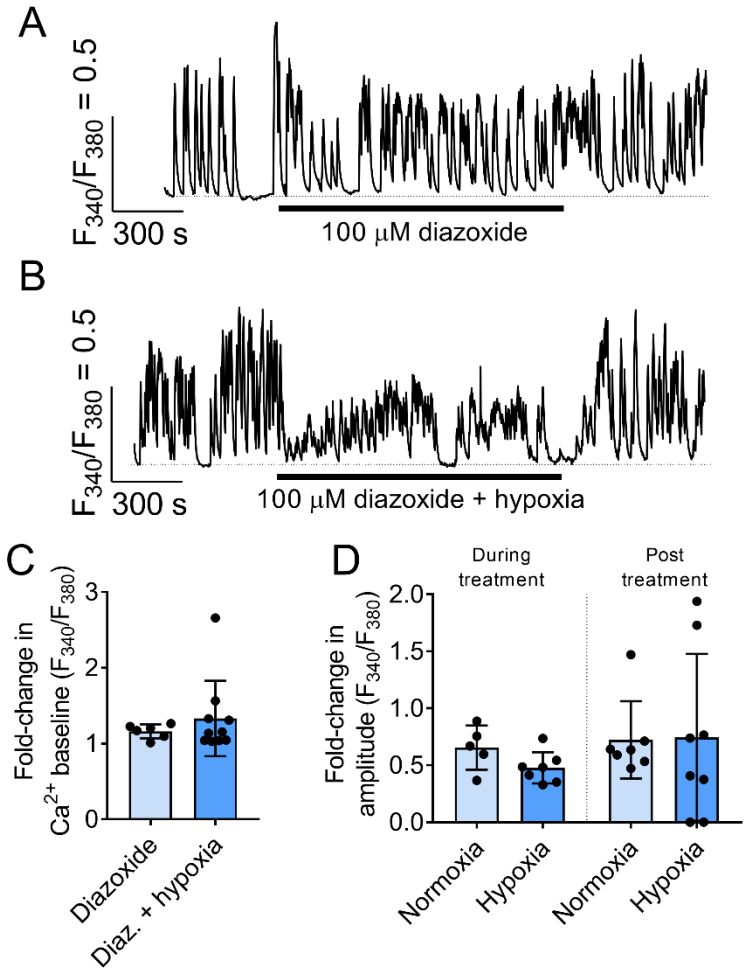
A
F_{340}/F_{380} = 0.5
300 s
100 μM diazoxide
B
F_{340}/F_{380} = 0.5
300 s
100 μM diazoxide + hypoxia
C
Fold-change in Ca^{2+} baseline (F_{340}/F_{380})
0
1
2
3
Diazoxide
Diaz. + hypoxia
D
During treatment
Post treatment
Fold-change in amplitude (F_{340}/F_{380})
0.0
0.5
1.0
1.5
2.0
Normoxia
Hypoxia
Normoxia
Hypoxia

Figure 4.5

Figure 4.6. Hypoxia prevents 2-deoxyglucose-triggered increases in $[Ca^{2+}]_i$ *via* an mK_{ATP}-dependent pathway.

A. Glycolysis was blocked by substituting glucose with equimolar (10 mM) 2-deoxyglucose (2-DG), which led to an increase in $[Ca^{2+}]_i$. *B.* Co-application of hypoxia prevented 2-DG from increasing $[Ca^{2+}]_i$. *C.* Applying the mK_{ATP} antagonist, 5-HD, along with 2-DG and hypoxia, prevented hypoxia from maintain $[Ca^{2+}]_i$ during 2-DG. *D.* Summary statistics show that 2-DG increased $[Ca^{2+}]_i$ compared to control, as did 2-DG when co-applied with hypoxia and 5-HD. ($p<0.05$, one-tailed Kruskal-Wallis with Dunn's post-test). *E.* Action potential amplitude reduced in all conditions during treatment, and reversed partially upon washout. Scale bars in *A-D* indicate the Fura-2 fluorescence emission ratio (F_{340}/F_{380}) and time in seconds.

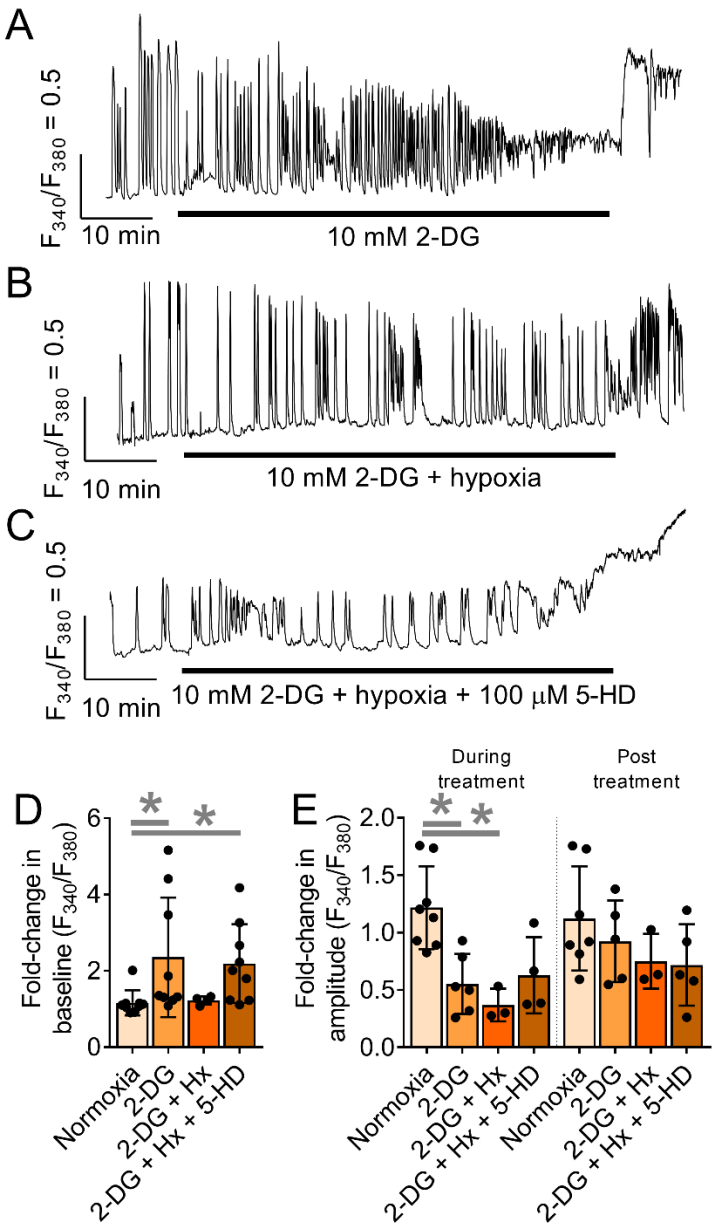
A
F_{340}/F_{380} = 0.5
10 min
10 mM 2-DG
B
F_{340}/F_{380} = 0.5
10 min
10 mM 2-DG + hypoxia
C
F_{340}/F_{380} = 0.5
10 min
10 mM 2-DG + hypoxia + 100 μM 5-HD
D
Fold-change in baseline (F_{340}/F_{380})
0
2
4
6
*
*
Normoxia
2-DG
2-DG + Hx
2-DG + Hx + 5-HD
E
During treatment
Post treatment
Fold-change in amplitude (F_{340}/F_{380})
0.0
0.5
1.0
1.5
2.0
*
*
Normoxia
2-DG
2-DG + Hx
2-DG + Hx + 5-HD
Normoxia
2-DG
2-DG + Hx
2-DG + Hx + 5-HD

Figure 4.6

4.4 Discussion

The present study establishes a novel neuroprotective pathway, which maintains $[Ca^{2+}]_i$ throughout hypoxia in HCs of the hypoxia-tolerant goldfish retina. We showed that goldfish HCs require functional mK_{ATP} channels to maintain $[Ca^{2+}]_i$. We demonstrated that hypoxia was not merely tolerated by goldfish HCs, but actively protected them: hypoxia prevented $[Ca^{2+}]_i$ from increasing in response to glycolytic inhibition with 2-deoxyglucose. This protective effect was negated by the mK_{ATP} antagonist 5-HD, further suggesting that mK_{ATP} channels are necessary for hypoxia tolerance.

Previous reports have shown hypoxia tolerance in the *Carassius* retina. In the Crucian carp, electroretinogram activity decreased during anoxia and was completely restored upon reperfusion, suggesting neuronal function and vision are not lost by anoxic insult (Johansson et al. 1997). In the goldfish retina, metabotropic glutamate receptors protected against apoptosis caused by 3 h of hypoxia and reperfusion at room temperature (Beraudi et al. 2007). In the present study, we showed that neurons of the goldfish retina resisted hypoxic increases in $[Ca^{2+}]_i$, which have been established as a precursor to excitotoxic cell death (Choi 1992; Szydlowska and Tymianski 2010).

The present study demonstrated that an mK_{ATP}-dependent pathway is required to stabilize $[Ca^{2+}]_i$ baseline in goldfish HCs. This work agrees with a growing body of evidence which shows a central role for mK_{ATP} and mitochondria in protection against hypoxia across a wide array of tissues and species. mK_{ATP} protection has been shown in diverse organs in mammals including the heart (O'Rourke 2004; Obal et al. 2005; Sheng et al. 2001), brain (Heurteaux et al. 1995), kidney (O'Sullivan et al. 2008; Rahgozar et al. 2003), liver (O'Sullivan et al. 2008), and

retina (Dreixler et al. 2008; Ettaiche et al. 2001; Roth et al. 2006). Likewise, mK_{ATP} protects against hypoxia in hypoxia-tolerant species, including in the turtle brain (Dukoff et al. 2014; Pamenter et al. 2008b) and in cardiomyocytes of hypoxia-tolerant fish such as the goldfish (Chen et al. 2005), the yellowtail flounder (*Limanda ferruginea*) (MacCormack and Driedzic 2002) and the armored catfish (*Liposarcus pardalis*) (MacCormack et al. 2003).

Among hypoxia-tolerant species, the neuronal mechanisms of hypoxia tolerance have been best studied in cortical neurons of the red-eared slider turtle (*Trachemys scripta*). These neurons maintained $[Ca^{2+}]_i$ for hours in hypoxia, but not when glycolysis was inhibited with iodoacetate (Bickler 1992). Pre-treating brain slices with anoxia protected against iodoacetate insult (Bickler 1992), similar to how hypoxia prevented increases in $[Ca^{2+}]_i$ during glycolytic inhibition in the present study. Furthermore, mK_{ATP} channels were necessary for neuroprotection in painted turtle (*Chrysemys picta*) cortical neurons (Pamenter et al. 2008b; Zivkovic and Buck 2010) as well as for neuroprotection in HCs in the present report.

Although the exact mechanisms of mK_{ATP}-dependent neuroprotection in turtles have yet to be established, there is evidence that hypoxia opens mK_{ATP}, which depolarizes mitochondria, triggering a subtle release of Ca^{2+} *via* the mitochondrial permeability transition pore (mPTP; Hawrysh and Buck 2013; Pamenter et al. 2008b; Zivkovic and Buck 2010). This slight increase in $[Ca^{2+}]_i$ activates second messenger pathways and ultimately downregulates AMPARs (Pamenter et al. 2008a; Zivkovic and Buck 2010), NMDARs (Pamenter et al. 2008b; Shin et al. 2005), and Ca^{2+}-dependent K^+ (K_{Ca}) channels (Rodgers-Garlick et al. 2013). This downregulation of membrane currents, or "channel arrest" (Hochachka 1986), would limit Ca^{2+} influx and reduce the ATP required to maintain transmembrane ion gradients, so as to conserve

energy during hypoxia. Channel arrest has been demonstrated in the goldfish brain (Wilkie et al. 2008), but not yet in the goldfish retina.

The mK_{ATP} protection we observed likely involves a different pathway than that of the turtle brain. In contrast with the turtle model, we did not observe an immediate increase in $[Ca^{2+}]_i$ after applying hypoxia to goldfish HCs, suggesting neuroprotection in goldfish HCs is Ca^{2+}-independent. Instead, we report that mK_{ATP} blockade increased $[Ca^{2+}]_i$ in hypoxia, whereas in the turtle, mK_{ATP} activation increased $[Ca^{2+}]_i$ (Hawrysh and Buck 2013; Pamenter et al. 2008b). Mitochondrial $[Ca^{2+}]_i$ release may not be a feasible strategy in HCs because they may have few mitochondria. Mitochondria are scarce in electron micrographs (Dowling and Boycott 1966; Yamada and Ishikawa 1965) and cytochrome c oxidase labelling is weak in HC somata (Kageyama and Meyer 1988).

Our results may align more closely with IPC in the mammalian retina, which is also Ca^{2+} independent. In the rat retina, mK_{ATP} channels are both necessary and sufficient for IPC (Dreixler et al. 2008; Roth et al. 2006; Stokfisz et al. 2017). Once open, mK_{ATP} activates two Ca^{2+}-independent isoforms of protein kinase C (PKC): PKC-δ and PKC-ε (Dreixler et al. 2008). HCs likely benefit because IPC prevents thinning of the inner nuclear and outer plexiform layers (Roth et al. 1998; Toprak et al. 2002; Zhu et al. 2007), and the δ isoform localizes to mammalian HCs (Dreixler et al. 2008). It is possible that neuroprotection is Ca^{2+}-independent in both mammalian and goldfish HCs, because $[Ca^{2+}]_i$ is already elevated throughout darkness due to constant glutamatergic input from photoreceptors. Future experiments could compare this HC pathway with neuroprotection in the inner retina (e.g. ganglion cells), since inner retinal neurons are not expected to undergo prolonged increases in $[Ca^{2+}]_i$ during the dark, as HCs are.

These models may offer insight into how mK_{ATP} open in the goldfish retina. Local decreases in [ATP] have been proposed to increase mK_{ATP} open probability in the turtle (Hogg et al. 2014), yet this is unlikely in goldfish HCs because blocking glycolysis dysregulated $[Ca^{2+}]_i$ in the current study. Adenosine and A1/A2a receptors are necessary for neuroprotection in the turtle (Buck and Bickler 1995; Pérez-Pinzón et al. 1993) and they open mK_{ATP} channels during IPC in the mammalian retina (Li and Roth 1999; Li et al. 2000). Adenosine may be a likely candidate as adenylates are released by goldfish HCs, where they may buffer the synaptic cleft and modulate feedback to cones (Vroman et al. 2014). Other candidate mK_{ATP} openers include nitric oxide and mitochondria-specific isoforms of PKC (Korge et al. 2002; Sasaki et al. 2000). PKC is present in HCs of the catfish (Pfeiffer-Linn and Lasater 1998) and nitric oxide synthase is present in goldfish H1 cells (Daniels and Baldridge 2011).

The specificity of mK_{ATP} agonists and antagonists has been called into question, as has the presence of a mK_{ATP}-specific channel (reviewed in Garlid and Halestrap 2012; Roth et al. 2006). Glibenclamide may inhibit plasmalemmal K_{ATP} channels, and 5-HD is a fatty acid which can interfere with lipid oxidation in mitochondria (Hanley and Daut 2005). Although diazoxide is over 1000× more specific for mK_{ATP} than for plasmalemmal K_{ATP} channels (Garlid et al. 1996), it has been shown to inhibit complex II of the electron transport chain and to lead to mitochondrial uncoupling (Kowaltowski et al. 2001). These concerns may raise the question of whether plasmalemmal ATP-dependent K^+ (K_{ATP}) channels could describe the results seen in our experiments. However, these off-target effects may require higher concentrations than those used in mK_{ATP} experiments (Garlid and Halestrap 2012; Kowaltowski et al. 2001), and are not themselves sufficient to explain the drugs' neuroprotective impacts in hypoxia (reviewed in O'Rourke 2004; Roth et al. 2006). Perhaps most convincingly, mK_{ATP} channel proteins were

recently reconstituted and shown to confer protection both *via* IPC and activation by diazoxide (Paggio et al. 2019), supporting the existence and protective role of mK_{ATP} channels. They are expressed and mediate hypoxic protection in a wide range of species including *Caenorhabditis elegans* nematodes (Wojtovich et al. 2012), turtles (Dukoff et al. 2014; Pamenter et al. 2008b), rats (Piriou et al. 2000; Roth et al. 2006), and humans (Jiang et al. 2006). In fish, mK_{ATP} channels have been found in the goldfish heart (Chen et al. 2005) and trout liver (Onukwufor et al. 2016).

In the present study, AP amplitude was reduced as ATP supply was challenged with hypoxia or with inhibition of glycolysis. Reductions in AP amplitude may be a neuroprotective response to hypoxia, so as to limit Ca^{2+} influx and reduce the ATP demand for extrusion or sequestration *via* Ca^{2+} ATPases. In support of this theory, mK_{ATP} activation in trout reduced AP amplitude and stabilized $[Ca^{2+}]_i$ baseline. However, reductions in AP amplitude were not sufficient to maintain $[Ca^{2+}]_i$, since $[Ca^{2+}]_i$ was dysregulated in multiple conditions despite amplitude reductions (i.e. glibenclamide and hypoxia; 2-DG; 2-DG, hypoxia, and 5-HD). This may be an example of channel arrest, either of L-type Ca^{2+} channels or of ryanodine receptors (RyRs) (Country et al. 2019), to limit increases in $[Ca^{2+}]_i$ during APs. Channel arrest is known to protect neurons of the goldfish telencephalon (Wilkie et al. 2008) and the turtle cortex (Pamenter et al. 2008a; Pamenter et al. 2008b; Rodgers-Garlick et al. 2013); however, to our knowledge it has yet to be shown in the retina.

Rainbow trout have been shown to be sensitive to hypoxia in previous reports (e.g., Hylland et al. 1995; Iftikar et al. 2010; Nilsson et al. 1993a), and a-, b-, and c-waves of the trout electroretinogram were all negatively affected by hypoxia (Ubels 1979). Our results confirmed the hypoxia sensitivity of trout retinal neurons. Furthermore, activating mK_{ATP} channels in trout

HCs prevented hypoxia from increasing $[Ca^{2+}]_i$ baseline, suggesting the mechanisms of hypoxia tolerance downstream of mK_{ATP} channel activation are conserved among fish. An additional takeaway from these studies relates to the hypoxia sensitivity of HCs, more generally. In mammals, HCs were resistant to excitotoxic cell death (Kim et al. 2010), possibly because they have adapted to long periods of high $[Ca^{2+}]_i$ in the dark. By showing that $[Ca^{2+}]_i$ is dysregulated in trout but not goldfish, our results suggest that neuroprotection is specific to goldfish, and not to HCs more generally.

Turtles are often considered the champions of hypoxia tolerance, partly because they greatly reduce electrical activity in their brains during anoxia, compared to modest reductions in goldfish and Crucian carp (Nilsson and Lutz 2004). But in the retina, this paradigm may be reversed: electroretinogram recordings suggest electrical activity in the turtle retina is reduced modestly (50%) in hypoxia (Stenslokken et al. 2008), and turtles respond to visual stimuli during their hibernation (Madsen et al. 2013). Carp shows upwards of a 90% reduction in electroretinogram activity in hypoxia (Johansson et al. 1997). Given this difference, we propose that the *Carassius* retina is the champion of *retinal* hypoxia tolerance, and merits consideration as a novel model of neuroprotection against hypoxia. This model may be important because strokes, and the majority of retinal diseases of the eye, involve ischemic cell death (Hayreh and Zimmerman 2005; Osborne et al. 2004). Blood flow is negatively affected in the eye in branch and central retinal artery occlusions, retinal vein occlusions, and glaucoma (Hayreh and Zimmerman 2005; Osborne et al. 2004; Osborne et al. 1999). Other diseases such as age-related macular degeneration and diabetic retinopathy can leave affected areas of the retina hypoxic, leading to cell death and vision loss (Blasiak et al. 2014; Sim et al. 2014). By clarifying the

cellular mechanisms by which goldfish retinal neurons survive hypoxia, we may learn of new strategies to mitigate or prevent retinal disease and protect vision.

4.5 Conclusion

The present study has shown a novel mK_{ATP}-dependent mechanism of neuroprotection in the vertebrate retina. We showed that $[Ca^{2+}]_i$ was dysregulated in hypoxia in HCs of the hypoxia-sensitive trout; in contrast, HCs of the hypoxia-tolerant goldfish maintained $[Ca^{2+}]_i$ even after 1 h of hypoxia. mK_{ATP} channels were necessary for neuroprotection in goldfish HCs and sufficient for neuroprotection in trout HCs. Finally, we showed that hypoxia stabilized $[Ca^{2+}]_i$ even as glycolysis was inhibited. Our results illustrate that hypoxia is not merely tolerated by goldfish, but that it actively protects neurons in the retina. This novel *in vitro* model is the first to explore intrinsic hypoxia tolerance in retinal neurons, and may lead to novel insights to protect against ischemic diseases of the eye.

5 General Discussion

This thesis used *in vitro* and *in situ* experiments to better understand the Ca^{2+} dynamics of retinal horizontal cells (HCs) of teleost fish. Experiments in Chapter 2 characterized spontaneous Ca^{2+}-based action potentials (APs) in goldfish HCs using Fura-2 Ca^{2+} imaging, voltage-sensitive dye imaging, and whole-cell current-clamp electrophysiology. In addition, Chapter 2 showed that APs depend on extracellular Ca^{2+}, L-type channel Ca^{2+} current, and Ca^{2+}-induced Ca^{2+} release (CICR) from ryanodine receptors (RyRs). This chapter is the first report devoted primarily to spontaneous APs, so as to create a foundation for functional studies to determine a possible role of this electrical activity in vision or retinal physiology. In Chapter 3, APs were reported in tissue slices for the first time, showing that HCs present APs even as their connections to other retinal neurons remained intact. Building on *in situ* methods, a novel method was presented to categorize HCs by subtype based on morphometry ($r_{d/s}$). Using this method, we showed that all subtypes of HC present spontaneous Ca^{2+}-based APs. *In situ* and *in vitro* data both showed that APs differed among subtypes: from subtype H1 through to H4, AP frequency decreased, while AP duration and area-under-the-curve (a proxy for Ca^{2+} influx) increased. Finally, Chapter 4 established a novel *in vitro* model of hypoxic neuroprotection in the goldfish retina. Goldfish HCs were shown to maintain $[Ca^{2+}]_i$ throughout hypoxia, whereas HCs of the hypoxia-sensitive trout lost Ca^{2+} homeostasis under similar conditions. Mitochondrial K^+ ATP-dependent (mK_{ATP}) channels were shown to be necessary for protection in goldfish, and sufficient to stabilize $[Ca^{2+}]_i$ in trout. Chapter 4 ended by showing that hypoxia could protect against $[Ca^{2+}]_i$ dysregulation caused by glycolytic inhibition; this neuroprotection was not previously known in *Carassius* spp. The following sections of the current chapter contextualize these studies and discuss future directions.

5.1 What role do APs serve in HCs?

The first intracellular recordings in any retinal neuron were recorded from goldfish HCs (Perlman et al. 2011; Svaetichin 1953). These recordings were graded potentials, meaning that they were changes in membrane potential commensurate with the stimulus applied to the cell. From that point onwards, a paradigm has dominated in which HCs respond to pre-synaptic input with graded potentials, and do not present all-or-nothing APs. Since then, APs have been induced in HCs with depolarizing stimuli or K^+ channel blockers in diverse preparations, including eyecups (Akopian et al. 1991), retinal slices (Murakami and Takahashi 1987), cell culture (Tachibana 1981), and freshly dissociated HCs (Johnston and Lam 1981; Shingai and Christensen 1986; 1983). Despite this, HC APs are not mentioned in models of spiking activity in the retina (Baden et al. 2013; Dowling 2012), possibly because they were poorly understood and their function in the retina or vision (if any) is unknown. Experiments in Chapters 2 and 3 showed that APs occur spontaneously and consistently in HCs. Perhaps the most important experiments to this end are the *in situ* experiments in Chapter 3, which are the first to show that APs occur spontaneously in retinal slices. Therefore, HCs present APs spontaneously, even when their synaptic connections are intact.

APs have been shown in a variety of fish including the skate (*Raja* spp.) (Lasater et al. 1984), catfish (*Ictalurus punctatus*) (Shingai and Christensen 1986; 1983), the common carp (*Cyprinus carpio*) (Murakami and Takahashi 1987), goldfish (Country et al. 2019; Tachibana 1981), and now, the rainbow trout (Chapter 4). Such a wide distribution – from elasmobranchs to cyprinids and salmonids – suggests that APs are ubiquitous among fish. Isolated reports also exist of Ca^{2+}-dependent, spike-like activity in HCs of *Xenopus* frogs (Akopian et al. 1997), the red-eared slider turtle (Akopian et al. 1991), and the cat (Ueda et al. 1992). In these three last species, APs were

elicited by depolarization or changes in light, and were not spontaneous. Regardless, these studies may suggest APs are conserved, increasing the likelihood that they serve a purpose in vision or retinal physiology.

With the foundation set in Chapters 2 and 3, the next logical step is to test for possible functions of Ca^{2+}-based APs in vision or retinal physiology. In the retina, HCs receive glutamatergic input from photoreceptors and provide inhibitory feedback. Three mechanisms have been proposed for this feedback (i.e. GABA, pH, and ephaptic hypotheses, as discussed in Chapter 1) and changes in HC $[Ca^{2+}]_i$ would likely affect all three mechanisms (discussed in section 2.5.2). Feedback of any type would result in changes in photoreceptor membrane potential. Therefore, to test the hypothesis that APs in HCs affect the membrane potential of rods or cones, voltage-sensitive dye experiments could be used in retinal slices. The membrane potential of both HCs and nearby photoreceptors could be monitored, to determine if the membrane potential of photoreceptor synaptic terminals changes during or after APs.

Several other possible roles for Ca^{2+} APs remain to be tested. One possible role was mentioned in section 2.5.2: APs may assist in the light-to-dark transition. In the turtle, in response to decreases in light, spike-like activity quickly depolarized HCs to their "dark membrane potential" (Akopian et al. 1991). This could be tested in fish eyecups; however, a caveat should be given that this would describe a role for elicited, and not spontaneous, APs. Another possible role relates to spinules formed in the HC-photoreceptor synapse in fish (Wagner 1980; Wagner and Djamgoz 1993; Weiler et al. 1996). These actin-based spinules increased the surface area of HC dendritic terminals in only minutes of exposure to light, but retracted in the dark in a Ca^{2+}-, calmodulin-, and protein kinase C-dependent manner (Schmitz et al. 1995; Wagner and Djamgoz 1993; Weiler et al. 1995) to modulate synaptic gain (Kirsch et al.

1990; Weiler and Wagner 1984). Spinule retraction did not require L-type Ca^{2+} channels, but instead required increases in $[Ca^{2+}]_i$ from Ca^{2+}-permeable AMPA receptors (Okada et al. 1999). However, once L-type channels open during an AP, CICR would elevate $[Ca^{2+}]_i$ to sufficient concentrations to retract spinules, and CICR is necessary for light-dependent synaptic plasticity in goldfish HCs (Hu et al. 2000; Huang et al. 2006). This would suggest spontaneous APs reduce synaptic gain at the HC-photoreceptor synapse.

5.2 Subtype-specific differences highlight a need for specific biomarkers

One of the goals of this thesis was to clarify the physiological differences among HC subtypes. Chapter 1 and Table 1.1 review what is known about ion channels in HCs, and highlight the paucity of information about ion channel expression among HC subtypes. Experiments in Chapter 3 showed that there are subtype-specific differences in AP frequency, duration, and Ca^{2+} influx. More generally, this work suggests subtypes may present important differences in physiology which may impact Ca^{2+} handling and vision. To address these differences, Chapter 3 presented a novel method to categorize APs by morphology, based on the ratio of dendritic field to the soma ($r_{d/s}$). This method was validated with antibodies for GABA (an H1-specific biomarker), showing that H1 have the lowest $r_{d/s}$ of all HCs. Because the $r_{d/s}$ approach for identifying HCs *in vitro* is quantitative, it offers improved and more reliable cell identification over the standard practice of identifying cells by eye.

The identity of H2, H3, and H4 cells using $r_{d/s}$ could not be validated because there are presently no known biomarkers for these subtypes. In fact, there is no biomarker for fish HCs in general: the biomarkers used to distinguish HCs from other cells in mammals, such as calbindin (Kim et al. 2010; Pasteels et al. 1990; Weruaga et al. 2000), have rarely stained fish HCs

(Hamano et al. 1990; Weruaga et al. 2000; Yazulla and Studholme 2002). The solution is to create novel, subtype-specific biomarkers. This is feasible, since monoclonal antibodies have been created for subtype-specific epitopes of carp HCs (Young and Dowling 1984) but the identities of the epitopes were never uncovered and the antibodies no longer exist (John Dowling, personal communication). Such antibodies would allow for further validation and optimization of $r_{d/s}$ for use in non-invasive experiments. Moreover, the presence of subtype-specific epitopes strongly suggests that there are subtype-specific proteins to be identified in these cells. Young and Dowling (1984) reported that H1 cells have the most specific epitopes. In fish, machinery to synthesize GABA (Marc et al. 1978; Paik et al. 2003) and nitric oxide (Daniels and Baldridge 2011; Djamgoz et al. 2000; Furukawa et al. 1997) may exist in H1 cells alone. Fish H1 have $GABA_C$ receptors while H2 and H3 have $GABA_A$ receptors (Paik et al. 2003). NMDA receptors may only be present on H1 (Jiang et al. 2008; Shen et al. 2006; Wang et al. 2008). Differences in protein expression may be related to differences in the types and magnitudes of K^+ currents (Lasater 1986; Malchow et al. 1990; Sullivan and Lasater 1990) and Ca^{2+} channel currents (Sullivan and Lasater 1992), as well as differences in connexin expression (Liu et al. 2009). Once developed, subtype-specific antibodies could be used to report physiological data by subtype in future experiments, to better understand the role of each subtype in vision.

5.3 Goldfish HCs as model neurons of hypoxia tolerance

A major finding of this thesis is that HCs of the goldfish retina displayed hypoxia tolerance (Chapter 4). Goldfish HCs maintained low $[Ca^{2+}]_i$ throughout hypoxic insult, as did neurons of the anoxia-tolerant turtle (Bickler 1992). This work expands on previous reports of hypoxia

tolerance of the *Carassius* retina (Beraudi et al. 2007; Johansson et al. 1997) and of neurons in the goldfish telencephalon (Wilkie et al. 2008). This opens the door for future experiments to clarify the cellular mechanisms of hypoxia tolerance in the ectotherm retina.

In experiments in goldfish HCs in Chapter 4, we observed a decrease in AP amplitude in hypoxia. Electrical activity also decreased in the Crucian carp retina and optic tectum in hypoxia (Johansson et al. 1997), suggesting vision is lost or greatly diminished without O_2. These downregulations presumably save considerable energy, which is important because the retina has a higher resting metabolism than nearly any other tissue (Ames et al. 1992; Country 2017; Wong-Riley 2010). Moreover, the retina uses a high proportion of glycogen even when O_2 is available (Ames 1992; Country 2017; Puchowicz et al. 2004), and so reducing retinal activity may spare glycogen, which has been shown to be the limiting factor in the hypoxic survival time of Crucian carp (Nilsson 1990). Vision is not likely crucial while over-wintering in ice-covered ponds because the fish are expected to eat less, if at all, due to reductions in locomotion (Nilsson 1990; Nilsson et al. 1993b), and the ice cover may offer some protection from predation.

Chapter 4 demonstrated that hypoxia tolerance in goldfish HCs required a mK_{ATP}-dependent pathway. This finding is in agreement with other reports of mK_{ATP}-dependent responses to hypoxia, including hypoxia tolerance in turtles (Pamenter et al. 2016) and ischemic preconditioning (IPC; Dirnagl and Meisel 2008; Liu et al. 1999). Downstream of mitochondria and mK_{ATP}, hypoxia responses differ among models (see section 4.4). In IPC in the mammalian retina, ROS increased during hypoxia or when mK_{ATP} channels were opened with diazoxide, and they may have been neuroprotective (Oldenburg et al. 2003; Roth et al. 2006). In contrast, ROS decreased in hypoxia in the turtle brain; moreover, this decrease would have increased NMDA receptor (NMDAR) current and Ca^{2+} influx, if not for NMDAR downregulation *via* mK_{ATP}

neuroprotection (Dukoff et al. 2014). Another difference is that mK_{ATP} activation in turtle led to a subtle increase in $[Ca^{2+}]_i$ (from the mitochondrial permeability transition pore; mPTP) which may have triggered neuroprotective, Ca^{2+}-dependent second messenger pathways (Hawrysh and Buck 2013; Pamenter et al. 2008b). In contrast, protection in the mammalian retina involved Ca^{2+}-independent isoforms of protein kinase C (PKC) downstream of mK_{ATP}, suggesting protection may have been Ca^{2+}-independent (Dreixler et al. 2008; Roth et al. 2006). Future experiments to clarify downstream targets of mK_{ATP} could determine whether protection in goldfish HCs is more similar to either of these pathways, or whether it involves unique mechanisms which are not observed in other species.

Previous reports postulated that fish of the genus *Carassius* have a different pathway of hypoxia tolerance than anoxia-tolerant turtles. Turtles minimize electrical activity in their brain and neurons throughout hypoxia, whereas carp and goldfish maintain locomotor and neural activity, albeit at a lower set point. Since this comparison was made in early reviews and turtles were dubbed the champions of hypoxia tolerance (e.g., Bickler and Buck 2007; Lutz and Nilsson 1997; Nilsson and Lutz 2004), many reports have clarified the cellular mechanisms of tolerance in the anoxia-tolerant turtle model (e.g., Dukoff et al. 2014; Hawrysh and Buck 2013; Hogg et al. 2014; Pamenter et al. 2011; Pamenter et al. 2008a; Pamenter et al. 2008b; Rodgers-Garlick et al. 2013; Zivkovic and Buck 2010) while a paucity of information has been released about these mechanisms in *Carassius* (Beraudi et al. 2007; Poli et al. 2003; Wilkie et al. 2008). Chapter 4 (section 4.5) argued that although turtles display greater electrical suppression in the brain, *Carassius* may be the champions of *retinal* hypoxia tolerance since they reduced their electroretinogram activity more completely (Johansson et al. 1997; Stenslokken et al. 2008). Moreover, turtles can reduce visual stimuli with eyelids, whereas *Carassius* likely have to rely

on cellular mechanisms to suppress electrical activity in the retina. The *in vitro* model of *Carassius* retinal neurons presented in Chapter 4 may clarify those mechanisms and offer unique insights into how cells can withstand hypoxia.

HCs are especially interesting models for hypoxia tolerance because their regular function in the retina requires that they be chronically depolarized by glutamate from photoreceptors. This constant exposure to glutamate might be expected to kill most neurons, because excitotoxic cell death is often triggered by prolonged exposure to ionotropic glutamate receptor agonists (Ferreira et al. 1996; Villani et al. 1997). Instead, HCs are reputedly resistant to excitotoxicity (McMahon and Ponomareva 1996; Mizuno et al. 2010), and therefore presumably have adaptations to withstand chronic depolarization, Ca^{2+} influx, elevated $[Ca^{2+}]_i$, and high ATP demand even in normoxia. One example is that HCs have an extraordinarily high capacity to buffer Ca^{2+}, and teleost fish HCs may have among the highest Ca^{2+} buffering capacities of any cell (Country and Jonz 2017; Solessio and Lasater 2002). The type of Ca^{2+} binding protein in HCs may also confer protection. Calbindin was strongly expressed in HCs of a wide variety of mammals (Cuenca et al. 2002; Haverkamp and Wässle 2000; Kantor et al. 2016; Massey and Mills 1996; Pasteels et al. 1990). Compared to other parvalbumin- and calretinin-positive retinal neurons, calbindin-positive HCs were relatively resistant to ischemia and reperfusion (Kim et al. 2010). Likewise, calbindin-positive cells in the ganglion cell layer resisted ischemic insult better than parvalbumin- and calretinin-positive cells (Kwon et al. 2005), and overexpression of calbindin reduced excitotoxic cell death in neurons elsewhere in the central nervous system (Fan et al. 2007; Yenari et al. 2001). These studies highlight that the unique physiology required of HCs may provide novel insights to avoid excitotoxic increases in $[Ca^{2+}]_i$.

5.4 Conclusion

This thesis has provided the first comprehensive characterization of spontaneous Ca^{2+}-based APs in HCs of the vertebrate retina using cellular imaging and electrophysiological techniques in *in vitro* and *in situ* preparations. The evidence presented expands our understanding of Ca^{2+} dynamics in HCs and challenges the long-held belief that neurons of the outer retina communicate solely *via* graded changes in membrane potential. As a *bona fide* phenomenon in HCs *in situ*, spontaneous APs may play a critical role in formation of the visual image in the retina. The present thesis sets a foundation for future studies to further investigate the function of APs, and identify their potential role in HCs and in inhibitory feedback to photoreceptors. Moreover, the present work has demonstrated that HCs of the goldfish (a hypoxia-tolerant organism) maintain $[Ca^{2+}]_i$ homeostasis throughout exposure to hypoxia, and has identified a novel mechanism involving mK_{ATP} channels through which hypoxia protects APs. Understanding how the retina can survive hypoxia is especially important to other conditions where neurons die from low O_2 or blood flow, including stroke, diabetic retinopathy, and macular degeneration. Lessons from hypoxia-tolerant species like goldfish promise to improve our understanding of ischemic disease, and might lead to novel strategies to prevent retinal damage, vision loss, and blindness.

REFERENCES

Akopian A, Krizaj D, and Witkovsky P. Both high-and low voltage-activated calcium currents contribute to the light-evoked responses of luminosity horizontal cells in the *Xenopus* retina. *Brain research* 762: 121-130, 1997.

Akopian A, McReynolds J, and Weiler R. Short-term potentiation of off-responses in turtle horizontal cells. *Brain research* 546: 132-138, 1991.

Ames A. Energy requirements of CNS cells as related to their function and to their vulnerability to ischemia: a commentary based on studies on retina. *Canadian Journal of Physiology and Pharmacology* 70: S158-S164, 1992.

Ames A, Li Y-Y, Heher E, and Kimble CR. Energy metabolism of rabbit retina as related to function: high cost of Na^+ transport. *Journal of Neuroscience* 12: 840-853, 1992.

Ariel M, Lasater EM, Mangel SC, and Dowling JE. On the sensitivity of H1 horizontal cells of the carp retina to glutamate, aspartate and their agonists. *Brain Res* 295: 179-183, 1984.

Ariel M, Mangel SC, and Dowling JE. *N*-methyl D-aspartate acts as an antagonist of the photoreceptor transmitter in the carp retina. *Brain Res* 372: 143-148, 1986.

Arundine M, Aarts M, Lau A, and Tymianski M. Vulnerability of central neurons to secondary insults after in vitro mechanical stretch. *J Neurosci* 24: 8106-8123, 2004.

Ayoub GS, and Lam DM. Accumulation of gamma-aminobutyric acid by horizontal cells isolated from the goldfish retina. *Vision Res* 27: 2027-2034, 1987.

Ayoub GS, and Lam DM. The content and release of endogenous GABA in isolated horizontal cells of the goldfish retina. *Vision Res* 25: 1187-1193, 1985.

Babai N, and Thoreson WB. Horizontal cell feedback regulates calcium currents and intracellular calcium levels in rod photoreceptors of salamander and mouse retina. *J Physiol* 587: 2353-2364, 2009.

Baden T, Euler T, Weckstrom M, and Lagnado L. Spikes and ribbon synapses in early vision. *Trends in neurosciences* 36: 480-488, 2013.

Barnes S. Center-surround antagonism mediated by proton signaling at the cone photoreceptor synapse. *J Gen Physiol* 122: 653-656, 2003.

Baylor DA, Fuortes MG, and O'Bryan PM. Receptive fields of cones in the retina of the turtle. *J Physiol* 214: 265-294, 1971.

Beraudi A, Bruno V, Battaglia G, Biagioni F, Rampello L, Nicoletti F, and Poli A. Pharmacological activation of mGlu2/3 metabotropic glutamate receptors protects retinal

neurons against anoxic damage in the goldfish *Carassius auratus*. *Experimental eye research* 84: 544-552, 2007.

Bickler PE. Cerebral anoxia tolerance in turtles: regulation of intracellular calcium and pH. *Am J Physiol* 263: R1298-1302, 1992.

Bickler PE, and Buck LT. Adaptations of vertebrate neurons to hypoxia and anoxia: maintaining critical Ca^{2+} concentrations. *J Exp Biol* 201: 12, 1998.

Bickler PE, and Buck LT. Hypoxia tolerance in reptiles, amphibians, and fishes: life with variable oxygen availability. *Annu Rev Physiol* 69: 145-170, 2007.

Bickler PE, Donohoe PH, and Buck LT. Hypoxia-induced silencing of NMDA receptors in turtle neurons. *J Neurosci* 20: 7, 2000.

Bickler PE, and Kelleher JA. Fructose-1,6-bisphosphate stabilizes brain intracellular calcium during hypoxia in rats. *Stroke* 23: 1617-1622, 1992.

Blasiak J, Petrovski G, Vereb Z, Facsko A, and Kaarniranta K. Oxidative stress, hypoxia, and autophagy in the neovascular processes of age-related macular degeneration. *Biomed Res Int* 2014: 768026, 2014.

Bradford CS, Sun L, Collodi P, and Barnes DW. Cell cultures from zebrafish embryos and adult tissues. *Journal of Tissue Culture Methods* 16: 99-107, 1994.

Bradford HF, Young AMJ, and Crowder JM. Continuous glutamate leakage from brain cells is balanced by compensatory high-affinity reuptake transport. *Neuroscience Letters* 81: 296-302, 1987.

Brandon C. Retinal GABA neurons: localization in vertebrate species using an antiserum to rabbit brain glutamate decarboxylase. *Brain research* 344: 286-295, 1985.

Buck LT, and Bickler PE. Adenosine and anoxia reduce *N*-methyl-D-aspartate receptor open probability in turtle cerebrocortex. *J Exp Biol* 201: 9, 1998.

Buck LT, and Bickler PE. Role of adenosine in NMDA receptor modulation in the cerebral cortex of an anoxia-tolerant turtle (*Chrysemys picta belli*). *J Exp Biol* 198: 8, 1995.

Buck LT, and Hochachka P. Anoxic suppression of Na^+-K^+-ATPase and constant membrane potential in hepatocytes: support for channel arrest. *Am J Physiol* 6, 1993.

Budde T, Meuth S, and Pape H-C. Calcium-dependent inactivation of neuronal calcium channels. *Nat Rev Neurosci* 3: 873-883, 2002.

Byzov AL, and Shura-Bura TM. Electrical feedback mechanism in the processing of signals in the outer plexiform layer of the retina. *Vision research* 26: 33-44, 1986.

Capel RA, and Terrar DA. Cytosolic calcium ions exert a major influence on the firing rate and maintenance of pacemaker activity in guinea-pig sinus node. *Front Physiol* 6: 23, 2015.

Chen J, Zhu JX, Wilson I, and Cameron JS. Cardioprotective effects of K_{ATP} channel activation during hypoxia in goldfish Carassius auratus. *J Exp Biol* 208: 2765-2772, 2005.

Choi DW. Excitotoxic cell death. *J Neurobiol* 23: 1261-1276, 1992.

Choi DW, and Rothman SM. The role of glutamate neurotoxicity in hypoxic-ischemic neuronal death. *Annu Rev Neurosci* 13: 171-182, 1990.

Clapham DE. Calcium signaling. *Cell* 131: 1047-1058, 2007.

Contreras JE, Sanchez HA, Veliz LP, Bukauskas FF, Bennett MV, and Saez JC. Role of connexin-based gap junction channels and hemichannels in ischemia-induced cell death in nervous tissue. *Brain Res Brain Res Rev* 47: 290-303, 2004.

Country MW. Retinal metabolism: A comparative look at energetics in the retina. *Brain Research* 1672: 50-57, 2017.

Country MW, Campbell BFN, and Jonz MG. Spontaneous action potentials in retinal horizontal cells of goldfish (*Carassius auratus*) are dependent upon L-type Ca^{2+} channels and ryanodine receptors. *J Neurophysiol* 122: 2284-2293, 2019.

Country MW, and Jonz MG. Calcium dynamics and regulation in horizontal cells of the vertebrate retina: lessons from teleosts. *J Neurophysiol* 117: 523-536, 2017.

Cuenca N, Deng P, Linberg KA, Lewis GP, Fisher SK, and Kolb H. The neurons of the ground squirrel retina as revealed by immunostains for calcium binding proteins and neurotransmitters. *Journal of neurocytology* 31: 649-666, 2002.

Cueva JG, Haverkamp S, Reimer RJ, Edwards R, Wässle H, and Brecha NC. Vesicular γ-aminobutyric acid transporter expression in amacrine and horizontal cells. *Journal of Comparative Neurology* 445: 227-237, 2002.

Cunningham JR, and Neal MJ. Effect of excitatory amino acids on gamma- aminobutyric acid release from frog horizontal cells. *The Journal of physiology* 362: 51-67, 1985.

D'Andrea P, and Vittur F. Gap junctions mediate intercellular calcium signalling in cultured articular chondrocytes. *Cell Calcium* 20: 389-397, 1996.

Daniels BA, and Baldridge WH. The light-induced reduction of horizontal cell receptive field size in the goldfish retina involves nitric oxide. *Vis Neurosci* 28: 137-144, 2011.

Dermietzel R, Kremer M, Paputsoglu G, Stang A, Skerrett IM, Gomes D, Srinivas M, Janssen-Bienhold U, Weiler R, Nicholson BJ, Bruzzone R, and Spray DC. Molecular and functional diversity of neural connexins in the retina. *J Neurosci* 20: 8331-8343, 2000.

DeVries S, and Schwartz E. Modulation of an electrical synapse between solitary pairs of catfish horizontal cells by dopamine and second messengers. *J Physiol* 414: 351-375, 1989.

DeVries SH, and Schwartz EA. Hemi-gap-junction channels in solitary horizontal cells of the catfish retina. *The Journal of Physiology* 445: 201-230, 1992.

Dirnagl U, and Meisel A. Endogenous neuroprotection: Mitochondria as gateways to cerebral preconditioning? *Neuropharmacology* 55: 334-344, 2008.

Dixon DB, Takahashi K, Bieda M, and Copenhagen DR. Quinine, intracellular pH and modulation of hemi-gap junctions in catfish horizontal cells. *Vision Res* 36: 3925-3931, 1996.

Dixon DB, Takahashi K, and Copenhagen DR. L-glutamate suppresses HVA calcium current in catfish horizontal cells by raising intracellular proton concentration. *Neuron* 11: 267-277, 1993.

Djamgoz MB, Sekaran S, Angotzi AR, Haamedi S, Vallerga S, Hirano J, and Yamada M. Light-adaptive role of nitric oxide in the outer retina of lower vertebrates: a brief review. *Philos Trans R Soc Lond B Biol Sci* 355: 1199-1203, 2000.

Dougoud M, Vinckenbosch L, Mazza C, Schwaller B, and Pecze L. The Effect of Gap Junctional Coupling on the Spatiotemporal Patterns of Ca^{2+} Signals and the Harmonization of Ca^{2+}-Related Cellular Responses. *PLoS Computational Biology* 12: 2016.

Dowling JE. *The retina: an approachable part of the brain*. Harvard University Press, 1987.

Dowling JE. *The retina: an approachable part of the brain*. Harvard University Press, 2012.

Dowling JE, and Boycott BB. Organization of the primate retina: electron microscopy. *Proceedings of the Royal Society of London Series B Biological Sciences* 166: 80-111, 1966.

Dowling JE, Pak MW, and Lasater E. White perch horizontal cells in culture: methods, morphology and process growth. *Brain Res* 360: 8, 1985.

Dowling JE, and Ripps H. Effect of magnesium on horizontal cell activity in the skate retina. *Nature* 242: 3, 1973.

Dreixler JC, Shaikh AR, Shenoy SK, Shen Y, and Roth S. Protein kinase C subtypes and retinal ischemic preconditioning. *Exp Eye Res* 87: 300-311, 2008.

Dukoff DJ, Hogg DW, Hawrysh PJ, and Buck LT. Scavenging ROS dramatically increase NMDA receptor whole-cell currents in painted turtle cortical neurons. *The Journal of Experimental Biology* 217: 3346-3355, 2014.

Dvoriantchikova G, Ivanov D, Barakat D, Grinberg A, Wen R, Slepak VZ, and Shestopalov VI. Genetic ablation of Pannexin1 protects retinal neurons from ischemic injury. *PLoS One* 7: e31991, 2012.

Endeman D, Fahrenfort I, Sjoerdsma T, Steijaert M, ten Eikelder H, and Kamermans M. Chloride currents in cones modify feedback from horizontal cells to cones in goldfish retina: Chloride currents in cones. *The Journal of physiology* 590: 5581-5595, 2012.

Erecińska M, and Silver IA. Ions and energy in mammalian brain. *Progress in Neurobiology* 43: 37-71, 1994.

Ettaiche M, Heurteaux C, Blondeau N, Borsotto M, Tinel N, and Lazdunski M. ATP-sensitive potassium channels (K_{ATP}) in retina: a key role for delayed ischemic tolerance. *Brain Res* 890: 118-129, 2001.

Fahrenfort I, Steijaert M, Sjoerdsma T, Vickers E, Ripps H, van Asselt J, Endeman D, Klooster J, Numan R, ten Eikelder H, von Gersdorff H, and Kamermans M. Hemichannel-mediated and pH-based feedback from horizontal cells to cones in the vertebrate retina. *PLoS One* 4: e6090, 2009.

Fan Y, Shi L, Gu Y, Zhao Y, Xie J, Qiao J, Yang G-Y, Wang Y, and Lu C-Z. Pretreatment with PTD-calbindin D 28k alleviates rat brain injury induced by ischemia and reperfusion. *Journal of Cerebral Blood Flow & Metabolism* 27: 719-728, 2007.

Ferreira IL, Duarte CB, and Carvalho AP. Ca^{2+} influx through glutamate receptor-associated channels in retina cells correlates with neuronal cell death. *Eur J Pharmacol* 302: 153-162, 1996.

Furukawa T, Yamada M, Petruv R, Djamgoz MBA, and Yasui S. Nitric oxide, 2-amino-4-phosphonobutyric acid and light/dark adaptation modulate short-wavelength-sensitive synaptic transmission to retinal horizontal cells. *Neuroscience Research* 27: 65-74, 1997.

Gardner CL, Jones JR, Baer SM, and Crook SM. Drift-diffusion simulation of the ephaptic effect in the triad synapse of the retina. *Journal of computational neuroscience* 38: 129-142, 2015.

Garlid KD, and Halestrap AP. The mitochondrial K_{ATP} channel—Fact or fiction? *Journal of Molecular and Cellular Cardiology* 52: 578-583, 2012.

Garlid KD, Paucek P, Yarov-Yarovoy V, Sun X, and Schindler PA. The mitochondrial K_{ATP} channel as a receptor for potassium channel openers. *The Journal of biological chemistry* 271: 8796-8799, 1996.

Guo C, Hirano AA, Stella SL, Bitzer M, and Brecha NC. Guinea pig horizontal cells express GABA, the GABA- synthesizing enzyme GAD65, and the GABA vesicular transporter. *Journal of Comparative Neurology* 518: 1647-1669, 2010.

Halestrap AP. What is the mitochondrial permeability transition pore? *Journal of Molecular and Cellular Cardiology* 46: 821-831, 2009.

Halestrap AP, and Richardson AP. The mitochondrial permeability transition: A current perspective on its identity and role in ischaemia/reperfusion injury. *Journal of Molecular and Cellular Cardiology* 78: 129-141, 2015.

Hamano K, Kiyama H, Emson PC, Manabe R, and Nakuchi M. Localization of two calcium binding proteins, calbindin (28 kD) and parvalbumin (12 kD), in the vertebrate retina. *J Comp Neurol* 302: 8, 1990.

Hanley PJ, and Daut J. K_{ATP} channels and preconditioning: A re-examination of the role of mitochondrial K_{ATP} channels and an overview of alternative mechanisms. *Journal of Molecular and Cellular Cardiology* 39: 17-50, 2005.

Haverkamp S, Grunert U, and Wassle H. The cone pedicle, a complex synapse in the retina. *Neuron* 27: 85-95, 2000.

Haverkamp S, and Wässle H. Immunocytochemical analysis of the mouse retina. *Journal of Comparative Neurology* 424: 1-23, 2000.

Hawrysh PJ, and Buck LT. Anoxia-mediated calcium release through the mitochondrial permeability transition pore silences NMDA receptor currents in turtle neurons. *The Journal of experimental biology* 216: 4375-4387, 2013.

Hayashida Y, and Yagi T. On the interaction between voltage-gated conductances and Ca^{2+} regulation mechanisms in retinal horizontal cells. *J Neurophysiol* 87: 11, 2002.

Hayashida Y, Yagi T, and Yasui S. Ca^{2+} regulation by the Na^{+}-Ca^{2+} exchanger in retinal horizontal cells depolarized by L-glutamate. *Neurosci Res* 31: 11, 1998.

Hayreh SS, and Zimmerman MB. Central Retinal Artery Occlusion: Visual Outcome. *American Journal of Ophthalmology* 140: 376.e371-376.e, 2005.

Heurteaux C, Lauritzen I, Widmann C, and Lazdunski M. Essential role of adenosine, adenosine A1 receptors, and ATP-sensitive K^{+} channels in cerebral ischemic preconditioning. *Proc Natl Acad Sci U S A* 92: 4666-4670, 1995.

Hirano AA, Brandstatter JH, and Brecha NC. Cellular distribution and subcellular localization of molecular components of vesicular transmitter release in horizontal cells of rabbit retina. *J Comp Neurol* 488: 70-81, 2005.

Hirano AA, Liu X, Boulter J, Grove J, Pérez de Sevilla Müller L, Barnes S, and Brecha NC. Targeted deletion of vesicular GABA transporter from retinal horizontal cells eliminates feedback modulation of photoreceptor calcium channels. *eneuro* 3: 2016.

Hirasawa H, and Kaneko A. pH changes in the invaginating synaptic cleft mediate feedback from horizontal cells to cone photoreceptors by modulating Ca^{2+} channels. *J Gen Physiol* 122: 657-671, 2003.

Hirota S, Pertens E, and Janssen LJ. The reverse mode of the Na^{+}/Ca^{2+} exchanger provides a source of Ca^{2+} for store refilling following agonist-induced Ca^{2+} mobilization. *Am J Physiol Lung Cell Mol* 292: L438-L447, 2007.

Hochachka PW. Defense strategies against hypoxia and hypothermia. *Science* 231: 8, 1986.

Höfer T, Politi A, and Heinrich R. Intercellular Ca^{2+} wave propagation through gap-junctional Ca^{2+} diffusion: a theoretical study. *Biophysical Journal* 80: 75-87, 2001.

Hoffert JR, and Ubels JL. The intraocular pO_2 and electroretinogram of the trout as affected by temperature and ventilatory flow. *Comparative Biochemistry and Physiology Part A: Physiology* 62: 563-568, 1979.

Hogan PG, and Rao A. Dissecting I_{CRAC}, a store-operated calcium current. *Trends Biochem Sci* 32: 235-245, 2007.

Hogg DW, Hawrysh PJ, and Buck LT. Environmental remodelling of GABAergic and glutamatergic neurotransmission: rise of the anoxia-tolerant turtle brain. *J Therm Biol* 44: 85-92, 2014.

Hollmann M, and Heinemann S. Cloned glutamate receptors. *Annual review of neuroscience* 17: 31-108, 1994.

Holopainen IJ, and Pitkänen AK. Population size and structure of crucian carp (*Carassius carassius* (*L.*)) in two small, natural ponds in Eastern Finland. In: *Annales Zoologici Fennici*JSTOR, 1985, p. 397-406.

Hu J-F, Liu Y, and Liang P-J. Stimulus pattern related plasticity of synapses between cones and horizontal cells in carp retina. *Brain research* 857: 321-326, 2000.

Huang S, Hu J, Gong H, and Liang P. Postsynaptic calcium pathway contributes to synaptic plasticity between retinal cones and luminosity-type horizontal cells. *Acta Physiologica Sinica, Chinese Edition* 58: 407, 2006.

Huang SY, and Liang PJ. Ca^{2+}-permeable and Ca^{2+}-impermeable AMPA receptors coexist on horizontal cells. *Neuroreport* 16: 263-266, 2005.

Huang SY, Liu Y, and Liang PJ. Role of Ca^{2+} store in AMPA-triggered Ca^{2+} dynamics in retinal horizontal cells. *Neuroreport* 15: 2311-2315, 2004.

Hylland P, Milton S, Pek M, Nilsson GE, and Lutz PL. Brain Na^+/K^+-ATPase activity in two anoxia tolerant vertebrates: crucian carp and freshwater turtle. *Neuroscience letters* 235: 89-92, 1997.

Hylland P, Nilsson GE, and Johansson D. Anoxic brain failure in an ectothermic vertebrate: release of amino acids and K^+ in rainbow trout thalamus. *Am J Physiol* 269: R1077-1084, 1995.

Iftikar FI, Matey V, and Wood CM. The ionoregulatory responses to hypoxia in the freshwater rainbow trout *Oncorhynchus mykiss*. *Physiological and Biochemical Zoology* 83: 343-355, 2010.

Ishida AT, Kaneko A, and Tachibana M. Responses of solitary retinal horizontal cells from *Carassius auratus* to L-glutamate and related amino acids. *J Physiol* 348: 16, 1984.

Ishida AT, and Neyton J. Quisqualate and L-glutamate inhibit retinal horizontal-cell responses to kainate. *Proc Natl Acad Sci U S A* 82: 1837-1841, 1985.

Jackman SL, Babai N, Chambers JJ, Thoreson WB, and Kramer RH. A positive feedback synapse from retinal horizontal cells to cone photoreceptors. *PLoS Biol* 9: e1001057, 2011.

Jackson DC. Hibernating without oxygen: physiological adaptations of the painted turtle. *J Physiol* 543: 731-737, 2002.

Jackson DC, and Heisler N. Plasma ion balance of submerged anoxic turtles at 3°C: The role of calcium lactate formation. *Respiration physiology* 49: 159-174, 1982.

Jacoby J, Kreitzer MA, Alford S, Qian H, Tchernookova BK, Naylor ER, and Malchow RP. Extracellular pH dynamics of retinal horizontal cells examined using electrochemical and fluorometric methods. *Journal of neurophysiology* 107: 868-879, 2012.

Janssen-Bienhold U, Dermietzel R, and Weiler R. Distribution of connexin43 immunoreactivity in the retinas of different vertebrates. *J Comp Neurol* 396: 310-321, 1998.

Janssen-Bienhold U, Schultz K, Gellhaus A, Schmidt P, Ammermuller J, and Weiler R. Identification and localization of connexin26 within the photoreceptor-horizontal cell synaptic complex. *Visual neuroscience* 18: 169-178, 2001.

Jiang MT, Ljubkovic M, Nakae Y, Shi Y, Kwok WM, Stowe DF, and Bosnjak ZJ. Characterization of human cardiac mitochondrial ATP-sensitive potassium channel and its regulation by phorbol ester in vitro. *American journal of physiology Heart and circulatory physiology* 290: H1770-1776, 2006.

Jiang XD, Wang XL, Sun Y, Gong HQ, and Liang PJ. NMDA modulation of GABA transporter current in carp retinal horizontal cells. *Brain Res* 1240: 105-110, 2008.

Johansson D, and Nilsson GE. Roles of energy status, K_{ATP} channels and channel arrest in fish brain K^+ gradient dissipation during anoxia. *J Exp Biol* 198: 6, 1995.

Johansson D, Nilsson GE, and Doving KB. Anoxic depression of light-evoked potentials in retina and optic tectum of crucian carp. *Neurosci Lett* 237: 73-76, 1997.

Johnston D, and Lam DMK. Regenerative and passive membrane properties of isolated horizontal cells from a teleost retina. *Nature* 292: 4, 1981.

Jonz MG, and Barnes S. Proton modulation of ion channels in isolated horizontal cells of the goldfish retina. *J Physiol* 581: 529-541, 2007.

Jonz MG, Fearon IM, and Nurse CA. Neuroepithelial oxygen chemoreceptors of the zebrafish gill. *The Journal of physiology* 560: 737-752, 2004.

Kageyama GH, and Meyer RL. Histochemical localization of cytochrome oxidase in the retina and optic tectum of normal goldfish: a combined cytochrome oxidase-horseradish peroxidase study. *J Comp Neurol* 270: 354-371, 1988.

Kamermans M, Fahrenfort I, Schultz K, Janssen-Bienhold U, Sjoerdsma T, and Weiler R. Hemichannel-mediated inhibition in the outer retina. *Science* 292: 3, 2001.

Kaneko A, and Stuart AE. Coupling between horizontal cells in the carp retina revealed by diffusion of Lucifer yellow. *Neuroscience Letters* 47: 7, 1984.

Kantor O, Mezey S, Adeghate J, Naumann A, Nitschke R, Enzsoly A, Szabo A, Lukats A, Nemeth J, Somogyvari Z, and Volgyi B. Calcium buffer proteins are specific markers of human retinal neurons. *Cell Tissue Res* 365: 29-50, 2016.

Kim SA, Jeon JH, Son MJ, Cha J, Chun MH, and Kim IB. Changes in transcript and protein levels of calbindin D28k, calretinin and parvalbumin, and numbers of neuronal populations expressing these proteins in an ischemia model of rat retina. *Anat Cell Biol* 43: 218-229, 2010.

Kirsch M, Djamgoz MB, and Wagner H-J. Correlation of spinule dynamics and plasticity of the horizontal cell spectral response in cyprinid fish retina: quantitative analysis. *Cell and Tissue Research* 260: 123-130, 1990.

Klaassen LJ, Sun Z, Steijaert MN, Bolte P, Fahrenfort I, Sjoerdsma T, Klooster J, Claassen Y, Shields CR, Ten Eikelder HM, Janssen-Bienhold U, Zoidl G, McMahon DG, and Kamermans M. Synaptic transmission from horizontal cells to cones is impaired by loss of connexin hemichannels. *PLoS Biol* 9: e1001107, 2011.

Köhler M, Burnashev N, Sakmann B, and Seeburg PH. Determinants of Ca^{2+} permeability in both TM1 and TM2 of high affinity kainate receptor channels: Diversity by RNA editing. *Neuron* 10: 491-500, 1993.

Korge P, Honda HM, and Weiss JN. Protection of cardiac mitochondria by diazoxide and protein kinase C: Implications for ischemic preconditioning. *Proceedings of the National Academy of Sciences* 99: 3312-3317, 2002.

Kowaltowski A, Seetharaman S, Paucek P, and Garlid K. Bioenergetic consequences of opening the ATP-sensitive K^+ channel of heart mitochondria. *American Journal of Physiology* 49: H649-H657, 2001.

Kreitzer MA, Collis LP, Molina AJ, Smith PJ, and Malchow RP. Modulation of extracellular proton fluxes from retinal horizontal cells of the catfish by depolarization and glutamate. *J Gen Physiol* 130: 169-182, 2007.

Kreitzer MA, Jacoby J, Naylor E, Baker A, Grable T, Tran E, Booth SE, Qian H, and Malchow RP. Distinctive patterns of alterations in proton efflux from goldfish retinal horizontal cells monitored with self-referencing H^+-selective electrodes. *Eur J Neurosci* 36: 3040-3050, 2012.

Kwon O-J, Kim J-Y, Kim S-Y, and Jeon C-J. Alterations in the localization of calbindin D28K-, calretinin-, and parvalbumin-immunoreactive neurons of rabbit retinal ganglion cell layer from ischemia and reperfusion. *Molecules & Cells (Springer Science & Business Media BV)* 19: 2005.

Lam DM, and Ayoub GS. Biochemical and biophysical studies of isolated horizontal cells from the teleost retina. *Vision Res* 23: 433-444, 1983.

Lam DMK, Su YYT, Chin CA, Brandon C, Wu J-Y, Marc RE, and Lasater EM. GABA-ergic horizontal cells in the teleost retina. *Brain Research Bulletin* 5: 137-140, 1980.

Lasater E, and Dowling JE. Dopamine decreases conductance of the electrical junctions between cultured retinal horizontal cells. *Proc Natl Acad Sci U S A* 82: 5, 1985.

Lasater EM. Ionic currents of cultured horizontal cells isolated from white perch retina. *J Neurophysiol* 55: 499-513, 1986.

Lasater EM. Retinal horizontal cell gap junctional conductance is modulated by dopamine through a cyclic AMP-dependent protein kinase. *Proc Natl Acad Sci U S A* 84: 7319-7323, 1987.

Lasater EM, and Dowling JE. Carp horizontal cells in culture respond selectively to L-glutamate and its agonists. *Proc Natl Acad Sci U S A* 79: 936-940, 1982.

Lasater EM, Dowling JE, and Ripps H. Pharmacological properties of isolated horizontal and bipolar cells from the skate retina. *J Neurosci* 4: 1966-1975, 1984.

Lasater EM, and Lam DM. The identification and some functions of GABAergic neurons in the distal catfish retina. *Vision research* 24: 497-506, 1984.

Lee H, and Brecha NC. Immunocytochemical evidence for SNARE protein-dependent transmitter release from guinea pig horizontal cells. *The European journal of neuroscience* 31: 1388-1401, 2010.

Levy P, and Larsen C. Odd-skipped labels a group of distinct neurons associated with the mushroom body and optic lobe in the adult *Drosophila* brain. *J Comp Neurol* 521: 3716-3740, 2013.

Li B, and Roth S. Retinal ischemic preconditioning in the rat: requirement for adenosine and repetitive induction. *Invest Ophthalmol Vis Sci* 40: 1200-1216, 1999.

Li B, Yang C, Rosenbaum DM, and Roth S. Signal transduction mechanisms involved in ischemic preconditioning in the rat retina in vivo. *Exp Eye Res* 70: 755-765, 2000.

Linn CL, and Gafka AC. Modulation of a voltage-gated calcium channel linked to activation of glutamate receptors and calcium-induced calcium release in the catfish retina. *J Physiol* 535: 47-63, 2001.

Linn CP, and Christensen BN. Excitatory amino acid regulation of intracellular Ca^{2+} in isolated catfish cone horizontal cells measured under voltage- and concentration-clamp conditions. *J Neurosci* 12: 2156-2164, 1992.

Lipton P. Ischemic cell death in brain neurons. *Physiol Rev* 79: 139, 1999.

Liu CR, Xu L, Zhong YM, Li RX, and Yang XL. Expression of connexin 35/36 in retinal horizontal and bipolar cells of carp. *Neuroscience* 164: 1161-1169, 2009.

Liu X, Hirano AA, Sun X, Brecha NC, and Barnes S. Calcium channels in rat horizontal cells regulate feedback inhibition of photoreceptors through an unconventional GABA- and pH-sensitive mechanism. *J Physiol* 591: 3309-3324, 2013.

Liu Y, Sato T, O'Rourke B, and Marban E. Mitochondrial ATP-dependent potassium channels novel effectors of cardioprotection? *Circulation* 97: 2463-2469, 1998.

Liu Y, Sato T, Seharaseyon J, Szewczyk A, O'Rourke B, and Marban E. Mitochondrial ATP-dependent potassium channels. Viable candidate effectors of ischemic preconditioning. *Ann N Y Acad Sci* 874: 27-37, 1999.

Lohrke S, and Hofmann HD. Voltage-gated currents of rabbit A- and B-type horizontal cells in retinal monolayer cultures. *Vis Neurosci* 11: 369-378, 1994.

Lutz PL, and Nilsson GE. Contrast strategies for anoxic brain survival - glycolysis up or down. *J Exp Biol* 200: 9, 1997.

Lutz PL, and Nilsson GE. Vertebrate brains at the pilot light. *Respiratory Physiology & Neurobiology* 141: 285-296, 2004.

Lv T, Gong HQ, and Liang PJ. Caffeine-induced Ca^{2+} oscillations in type I horizontal cells of the carp retina and the contribution of the store-operated Ca^{2+} entry pathway. *PLoS One* 9: e100095, 2014.

Lyons MR, and West AE. Mechanisms of specificity in neuronal activity-regulated gene transcription. *Prog Neurobiol* 94: 259-295, 2011.

MacCormack TJ, and Driedzic WR. Mitochondrial ATP-sensitive K^+ channels influence force development and anoxic contractility in a flatfish, yellowtail flounder Limanda ferruginea, but not Atlantic cod Gadus morhua heart. *Journal of experimental biology* 205: 1411-1418, 2002.

MacCormack TJ, Treberg JR, Almeida-Val VM, Val AL, and Driedzic WR. Mitochondrial K_{ATP} channels and sarcoplasmic reticulum influence cardiac force development under anoxia in the Amazonian armored catfish Liposarcus pardalis. *Comparative Biochemistry and Physiology Part A: Molecular & Integrative Physiology* 134: 441-448, 2003.

Madsen JG, Wang T, Beedholm K, and Madsen PT. Detecting spring after a long winter: coma or slow vigilance in cold, hypoxic turtles? *Biology Letters* 9: 20130602, 2013.

Malchow RP, Qian HH, Ripps H, and Dowling JE. Structural and functional properties of two types of horizontal cell in the skate retina. *J Gen Physiol* 95: 177-198, 1990.

Mangel SC, and Dowling JE. The interplexiform-horizontal cell system of the fish retina: effects of dopamine, light stimulation and time in the dark. *Proc R Soc Lond B Biol Sci* 231: 91-121, 1987.

Marc RE, Stell WK, Bok D, and Lam DM. GABA-ergic pathways in the goldfish retina. *J Comp Neurol* 182: 221-244, 1978.

Massey SC, and Mills SL. A calbindin- immunoreactive cone bipolar cell type in the rabbit retina. *Journal of Comparative Neurology* 366: 15-33, 1996.

Masumiya H, Li P, Zhang L, and Chen SRW. Ryanodine sensitizes the Ca^{2+} release channel (ryanodine receptor) to Ca^{2+} activation. *Journal of Biological Chemistry* 276: 39727-39735, 2001.

Matthews EA, and Dietrich D. Buffer mobility and the regulation of neuronal calcium domains. *Front Cell Neurosci* 9: 48, 2015.

McMahon DG. Modulation of electrical synaptic transmission in zebrafish retinal horizontal cells. *J Neurosci* 14: 1722-1734, 1994.

McMahon DG, and Brown DR. Modulation of gap junction channel gating at zebrafish retinal electrical synapses. *Journal of Neurophysiology* 72: 2257-2268, 1994.

McMahon DG, and Mattson MP. Horizontal cell electrical coupling in the giant danio: synaptic modulation by dopamine and synaptic maintenance by calcium. *Brain Res* 718: 89-96, 1996.

McMahon DG, and Ponomareva LV. Nitric oxide and cGMP modulate retinal glutamate receptors. *J Neurophysiol* 76: 2307-2315, 1996.

McPheeters MT, Wang YT, Werdich AA, Jenkins MW, and Laurita KR. An infrared optical pacing system for screening cardiac electrophysiology in human cardiomyocytes. *PLoS One* 12: e0183761, 2017.

Menard A, Auclair F, Bourcier-Lucas C, Grillner S, and Dubuc R. Descending GABAergic projections to the mesencephalic locomotor region in the lamprey *Petromyzon marinus*. *J Comp Neurol* 501: 260-273, 2007.

Micci MA, and Christensen BN. Distribution of the inositol trisphosphate receptor in the catfish retina. *Brain Res* 720: 139-147, 1996.

Micci MA, and Christensen BN. Na^{+}/Ca^{2+} exchange in catfish retina horizontal cells: regulation of intracellular Ca^{2+} store function. *Am J Physiol* 274: C1625-1633, 1998.

Miller AM, and Schwartz EA. Evidence for the identification of synaptic transmitters released by photoreceptors of the toad retina. *J Physiol* 334: 325-349, 1983.

Milton SL, Thompson JW, and Lutz PL. Mechanisms for maintaining extracellular glutamate levels in the anoxic turtle striatum. *American Journal of Physiology - Regulatory, Integrative and Comparative Physiology* 282: R1317-R1323, 2002.

Mizuno F, Barabas P, Krizaj D, and Akopian A. Glutamate-induced internalization of $Ca_v1.3$ L-type Ca^{2+} channels protects retinal neurons against excitotoxicity. *J Physiol* 588: 953-966, 2010.

Molina AJ, Verzi MP, Birnbaum AD, Yamoah EN, Hammar K, Smith PJ, and Malchow RP. Neurotransmitter modulation of extracellular H^+ fluxes from isolated retinal horizontal cells of the skate. *The Journal of physiology* 560: 639-657, 2004.

Mosinger J, and Yazulla S. Double-label analysis of GAD-and GABA-like immunoreactivity in the rabbit retina. *Vision research* 27: 23-30, 1987.

Mosinger JL, Yazulla S, and Studholme KM. GABA-like immunoreactivity in the vertebrate retina: a species comparison. *Exp Eye Res* 42: 631-644, 1986.

Motulsky HJ, and Brown RE. Detecting outliers when fitting data with nonlinear regression–a new method based on robust nonlinear regression and the false discovery rate. *BMC bioinformatics* 7: 123, 2006.

Murakami M, and Takahashi KI. Calcium action potential and its use for measurement of reversal potentials of horizontal cell responses in carp retina. *J Physiol* 386: 16, 1987.

Murry CE, Richard VJ, Reimer KA, and Jennings RB. Ischemic preconditioning slows energy metabolism and delays ultrastructural damage during a sustained ischemic episode. *Circulation research* 66: 913-931, 1990.

Nielsen MS, Axelsen LN, Sorgen PL, Verma V, Delmar M, and Holstein-Rathlou NH. Gap junctions. *Compr Physiol* 2: 1981-2035, 2012.

Nilsson GE. Long-term anoxia in crucian carp: changes in the levels of amino acid and monoamine neurotransmitters in the brain, catecholamines in chromaffin tissue, and liver glycogen. *Journal of experimental biology* 150: 295, 1990.

Nilsson GE. Surviving anoxia with the brain turned on. *News Physiol Sci* 16: 5, 2001.

Nilsson GE, and Lutz PL. Anoxia tolerant brains. *J Cereb Blood Flow Metab* 24: 475-486, 2004.

Nilsson GE, Pérez-Pinzón M, Dimberg K, and Winberg S. Brain sensitivity to anoxia in fish as reflected by changes in extracellular K^+ activity. *American Journal of Physiology-Regulatory, Integrative and Comparative Physiology* 264: R250-R253, 1993a.

Nilsson GE, Rosen P, and Johansson D. Anoxic depression of spontaneous locomotor-activity in crucian carp quantified by a computerized imaging technique. *Journal of Experimental Biology* 180: 153-162, 1993b.

O'Dell T, and Christensen BN. *N*-methyl-D-aspartate receptors coexist with kainate and quisqualate receptors on single isolated catfish horizontal cells. *Brain Res* 381: 359-362, 1986.

O'Dell TJ, and Christensen BN. Horizontal cells isolated from catfish retina contain two types of excitatory amino acid receptors. *Journal of Neurophysiology* 61: 1097-1109, 1989.

O'Rourke B. Evidence for mitochondrial K^+ channels and their role in cardioprotection. *Circ Res* 94: 420-432, 2004.

O'Sullivan JC, Fu D, Alam HB, and McCabe JT. Diazoxide increases liver and kidney HSP25 and HSP70 after shock and stroke. *J Surg Res* 149: 120-130, 2008.

Obal D, Dettwiler S, Favoccia C, Scharbatke H, Preckel B, and Schlack W. The influence of mitochondrial K_{ATP}-channels in the cardioprotection of preconditioning and postconditioning by sevoflurane in the rat in vivo. *Anesthesia and analgesia* 101: 1252-1260, 2005.

Okada T, Schultz K, Geurtz W, Hatt H, and Weiler R. AMPA-preferring receptors with high Ca^{2+} permeability mediate dendritic plasticity of retinal horizontal cells. *Eur J Neurosci* 11: 1085-1095, 1999.

Oldenburg O, Cohen MV, and Downey JM. Mitochondrial K_{ATP} channels in preconditioning. *Journal of Molecular and Cellular Cardiology* 35: 569-575, 2003.

Onukwufor JO, Stevens D, and Kamunde C. Bioenergetic and volume regulatory effects of mitoK_{ATP} channel modulators protect against hypoxia-reoxygenation-induced mitochondrial dysfunction. *J Exp Biol* 219: 2743-2751, 2016.

Orrenius S, and Nicotera P. The calcium ion and cell death. *Journal of neural transmission Supplementum* 43: 1-11, 1994.

Osborne NN, Casson RJ, Wood JP, Chidlow G, Graham M, and Melena J. Retinal ischemia: mechanisms of damage and potential therapeutic strategies. *Prog Retin Eye Res* 23: 91-147, 2004.

Osborne NN, Ugarte M, Chao M, Chidlow G, Bae JH, Wood JP, and Nash MS. Neuroprotection in relation to retinal ischemia and relevance to glaucoma. *Surv Ophthalmol* 43 Suppl 1: S102-128, 1999.

Overgaard J, Gesser H, and Wang T. Tribute to P. L. Lutz: cardiac performance and cardiovascular regulation during anoxia/hypoxia in freshwater turtles. *J Exp Biol* 210: 1687-1699, 2007.

Paggio A, Checchetto V, Campo A, Menabò R, Di Marco G, Di Lisa F, Szabo I, Rizzuto R, and De Stefani D. Identification of an ATP-sensitive potassium channel in mitochondria. *Nature* 572: 609-603, 2019.

Paik SS, Park NG, Lee SJ, Han HK, Jung CS, Bai SH, and Chun MH. GABA receptors on horizontal cells in the goldfish retina. *Vision Res* 43: 2101-2106, 2003.

Pamenter M. *Comparative insights into mitochondrial adaptations to anoxia in brain*. 2016, p. 723-724.

Pamenter ME. Mitochondria: a multimodal hub of hypoxia tolerance. *Canadian Journal of Zoology* 92: 569-589, 2014.

Pamenter ME, Gomez CR, Richards JG, and Milsom WK. Mitochondrial responses to prolonged anoxia in brain of red-eared slider turtles. *Biology Letters* 12: 2016.

Pamenter ME, Hogg DW, Ormond J, Shin DS, Woodin MA, and Buck LT. Endogenous $GABA_A$ and $GABA_B$ receptor-mediated electrical suppression is critical to neuronal anoxia tolerance. *Proceedings of the National Academy of Sciences* 108: 11274-11279, 2011.

Pamenter ME, Shin DS, and Buck LT. AMPA receptors undergo channel arrest in the anoxic turtle cortex. *Am J Physiol Regul Integr Comp Physiol* 294: R606-613, 2008a.

Pamenter ME, Shin DS, Cooray M, and Buck LT. Mitochondrial ATP-sensitive K^+ channels regulate NMDAR activity in the cortex of the anoxic western painted turtle. *J Physiol* 586: 1043-1058, 2008b.

Pasteels B, Rogers J, Blachier F, and Pochet R. Calbindin and calretinin localization in retina from different species. *Visual neuroscience* 5: 1-16, 1990.

Peng PL, Zhong X, Tu W, Soundarapandian MM, Molner P, Zhu D, Lau L, Liu S, Liu F, and Lu Y. ADAR2-dependent RNA editing of AMPA receptor subunit GluR2 determines vulnerability of neurons in forebrain ischemia. *Neuron* 49: 719-733, 2006.

Perez-Pinzon M, Rosenthal M, Sick TJ, Lutz PL, Pablo J, and Mash D. Downregulation of sodium channels during anoxia: a putative survival strategy of turtle brain. *American Journal of Physiology-Regulatory, Integrative and Comparative Physiology* 262: R712-R715, 1992.

Pérez-Pinzón MA, Lutz PL, Sick TJ, and Rosenthal M. Adenosine, a "retaliatory" metabolite, promotes anoxia tolerance in turtle brain. *Journal of Cerebral Blood Flow & Metabolism* 13: 728-732, 1993.

Perlman I, Kolb H, and Nelson R. S-potentials and horizontal cells. *Webvision: the organization of the retina and visual system [Internet] Salt Lake City (UT): University of Utah Health Sciences Center* 2011.

Pfeiffer-Linn CL, and Lasater EM. Multiple second-messenger system modulation of voltage-activated calcium currents in teleost retinal horizontal cells. *J Neurophysiol* 80: 377-388, 1998.

Pfeiffer-Linn CL, and Lasater EM. Whole cell and single-channel properties of a unique voltage-activated sustained calcium current identified in teleost retinal horizontal cells. *J Neurophysiol* 75: 609-619, 1996.

Piriou V, Chiari P, Knezynski S, Bastien O, Loufoua J, Lehot JJ, Foëx P, Annat G, and Ovize M. Prevention of isoflurane-induced preconditioning by 5-hydroxydecanoate and gadolinium: possible involvement of mitochondrial adenosine triphosphate-sensitive potassium and stretch-activated channels. *Anesthesiology (Philadelphia)* 93: 756-764, 2000.

Plummer BN, Cutler MJ, Wan X, and Laurita KR. Spontaneous calcium oscillations during diastole in the whole heart: the influence of ryanodine reception function and gap junction coupling. *American journal of physiology Heart and circulatory physiology* 300: H1822-1828, 2011.

Poli A, Beraudi A, Villani L, Storto M, Battaglia G, Gerevini VDG, Cappucio I, Caricasole A, D'Onofrio M, and Nicoletti F. Group II metabotropic glutamate receptors regulate the vulnerability to hypoxic brain damage. *J Neurosci* 23: 7, 2003.

Prochnow N, Hoffmann S, Dermietzel R, and Zoidl G. Replacement of a single cysteine in the fourth transmembrane region of zebrafish pannexin 1 alters hemichannel gating behavior. *Exp Brain Res* 199: 255-264, 2009a.

Prochnow N, Hoffmann S, Vroman R, Klooster J, Bunse S, Kamermans M, Dermietzel R, and Zoidl G. Pannexin1 in the outer retina of the zebrafish, *Danio rerio*. *Neuroscience* 162: 1039-1054, 2009b.

Puchowicz MA, Xu K, Magness D, Miller C, Lust WD, Kern TS, and LaManna JC. Comparison of glucose influx and blood flow in retina and brain of diabetic rats. *J Cereb Blood Flow Metab* 24: 449-457, 2004.

Qian H, and Dowling JE. Novel GABA responses from rod-driven retinal horizontal cells. *Nature* 361: 162-164, 1993.

Rabl K, and Thoreson WB. Calcium-dependent inactivation and depletion of synaptic cleft calcium ions combine to regulate rod calcium currents under physiological conditions. *Eur J Neurosci* 16: 2070-2077, 2002.

Rahgozar M, Willgoss DA, Gobe GC, and Endre ZH. ATP-dependent K^+ channels in renal ischemia reperfusion injury. *Ren Fail* 25: 885-896, 2003.

Raviola E, and Gilula NB. Intramembrane organization of specialized contacts in the outer plexiform layer of the retina. A freeze-fracture study in monkeys and rabbits. *The Journal of cell biology* 65: 192-222, 1975.

Rodgers-Garlick C, Hogg D, and Buck L. Oxygen-sensitive reduction in Ca^{2+}-activated K^+ channel open probability in turtle cerebrocortex. *Neuroscience* 237: 243-254, 2013.

Roth S, Dreixler JC, Shaikh AR, Lee KH, and Bindokas V. Mitochondrial potassium ATP channels and retinal ischemic preconditioning. *Invest Ophthalmol Vis Sci* 47: 2114-2124, 2006.

Roth S, Li B, Rosenbaum PS, Gupta H, Goldstein IM, Maxwell KM, and Gidday JM. Preconditioning provides complete protection against retinal ischemic injury in rats. *Investigative ophthalmology & visual science* 39: 777, 1998.

Rowe JS, and Ruddock KH. Hyperpolarization of retinal horizontal cells by excitatory amino acid neurotransmitter antagonists. *Neurosci Lett* 30: 251-256, 1982.

Saez JC, Connor JA, Spray DC, and Bennett MV. Hepatocyte gap junctions are permeable to the second messenger, inositol 1,4,5-trisphosphate, and to calcium ions. *Proc Natl Acad Sci U S A* 86: 2708-2712, 1989.

Sakuranaga M, and Naka K. Signal transmission in the catfish retina. I. Transmission in the outer retina. *Journal of neurophysiology* 53: 373-389, 1985.

Sasaki N, Sato T, Ohler A, apos, Rourke B, and Marbán E. Activation of mitochondrial ATP-dependent potassium channels by nitric oxide. *Circulation (New York, NY)* 101: 439-445, 2000.

Schmidt KF. Properties of glutamate-gated ion channels in horizontal cells of the perch retina. *Vision Res* 37: 2023-2028, 1997.

Schmitz Y, Kohler K, and Zrenner E. Evidence for calcium/calmodulin dependence of spinule retraction in retinal horizontal cells. *Visual neuroscience* 12: 413-424, 1995.

Schmitz Y, and Wolburg H. Gap junction morphology of retinal horizontal cells is sensitive to pH alterations in vitro. *Cell and tissue research* 263: 303-310, 1991.

Schneider CA, Rasband WS, and Eliceiri KW. NIH Image to ImageJ: 25 years of image analysis. *Nat Methods* 9: 671-675, 2012.

Schwartz EA. Transport-mediated synapses in the retina. *Physiol Rev* 82: 875-891, 2002.

Shen Y, Lu T, and Yang X-L. Modulation of desensitization at glutamate receptors in isolated crucian carp horizontal cells by concanavalin A, cyclothiazide, aniracetam and PEPA. *Neuroscience* 89: 979-990, 1999.

Shen Y, Zhang AJ, and Yang XL. Uncoupling of horizontal cells alters the receptive fields of retinal bipolar cells. *Neuroreport* 14: 2159-2162, 2003.

Shen Y, Zhang M, Jin Y, and Yang XL. Functional *N*-methyl-D-aspartate receptors are expressed in cone-driven horizontal cells in carp retina. *Neurosignals* 15: 174-179, 2006.

Sheng W, James C, and Yongge L. Dual roles of mitochondrial K_{ATP} channels in diazoxide-mediated protection in isolated rabbit hearts. *American Journal of Physiology - Heart and Circulatory Physiology* 280: 246-255, 2001.

Shibata M, Hattori H, Sasaki T, Gotoh J, Hamada J, and Fukuuchi Y. Subcellular localization of a promoter and an inhibitor of apoptosis (Smac/DIABLO and XIAP) during brain ischemia/reperfusion. *Neuroreport* 13: 1985-1988, 2002.

Shields CR, Klooster J, Claassen Y, Ul-Hussain M, Zoidl G, Dermietzel R, and Kamermans M. Retinal horizontal cell-specific promoter activity and protein expression of zebrafish connexin 52.6 and connexin 55.5. *J Comp Neurol* 501: 765-779, 2007.

Shin DS, Wilkie MP, Pamenter ME, and Buck LT. Calcium and protein phosphatase 1/2A attenuate *N*-methyl-D-aspartate receptor activity in the anoxic turtle cortex. *Comparative biochemistry and physiology Part A, Molecular & integrative physiology* 142: 50-57, 2005.

Shingai R, and Christensen BN. Excitable properties and voltage-sensitive ion conductances of horizontal cells isolated from catfish (*Ictalurus punctatus*) retina. *J Neurophysiol* 56: 32-49, 1986.

Shingai R, and Christensen BN. Sodium and calcium currents measured in isolated catfish horizontal cells under voltage clamp. *Neuroscience* 10: 893-897, 1983.

Shoubridge EA, and Hochachka P. Ethanol: novel end product of vertebrate anaerobic metabolism. *Science* 209: 308-309, 1980.

Sim DA, Keane PA, Rajendram R, Karampelas M, Selvam S, Powner MB, Fruttiger M, Tufail A, and Egan CA. Patterns of peripheral retinal and central macula ischemia in diabetic retinopathy as evaluated by ultra-widefield fluorescein angiography. *Am J Ophthalmol* 158: 144-153, 2014.

Solessio E, and Lasater EM. Calcium-induced calcium release and calcium buffering in retinal horizontal cells. *Vis Neurosci* 19: 713-725, 2002.

Song PI, Matsui JI, and Dowling JE. Morphological types and connectivity of horizontal cells found in the adult zebrafish (*Danio rerio*) retina. *J Comp Neurol* 506: 328-338, 2008.

Stell WK, and Lightfoot DO. Color-specific interconnections of cones and horizontal cells in the retina of the goldfish. *J Comp Neurol* 159: 473-502, 1975.

Stell WK, and Witkovsky P. Retinal structure in the smooth dogfish, *Mustelus canis*: light microscopy of photoreceptor and horizontal cells. *J Comp Neurol* 148: 33-45, 1973.

Stenslokken KO, Milton SL, Lutz PL, Sundin L, Renshaw GM, Stecyk JA, and Nilsson GE. Effect of anoxia on the electroretinogram of three anoxia-tolerant vertebrates. *Comparative biochemistry and physiology Part A, Molecular & integrative physiology* 150: 395-403, 2008.

Stokfisz K, Ledakowicz-Polak A, Zagorski M, and Zielinska M. Ischaemic preconditioning - current knowledge and potential future applications after 30 years of experience. *Advances in medical sciences* 62: 307-316, 2017.

Stryer L. Visual excitation and recovery. *J Biol Chem* 266: 10711-10714, 1991.

Suarez J, Davila JC, Real MA, Guirado S, and Medina L. Calcium-binding proteins, neuronal nitric oxide synthase, and GABA help to distinguish different pallial areas in the developing and adult chicken. I. Hippocampal formation and hyperpallium. *J Comp Neurol* 497: 751-771, 2006.

Sullivan JM, and Lasater EM. Sustained and transient calcium currents in horizontal cells of the white bass retina. *J Gen Physiol* 99: 85-107, 1992.

Sullivan JM, and Lasater EM. Sustained and transient potassium currents of cultured horizontal cells isolated from white bass retina. *J Neurophysiol* 64: 1758-1766, 1990.

Sun X, Hirano AA, Brecha NC, and Barnes S. Calcium-activated BK_{Ca} channels govern dynamic membrane depolarizations of horizontal cells in rodent retina. *J Physiol* 595: 4449-4465, 2017.

Sun Y, Jiang XD, Liu X, Gong HQ, and Liang PJ. Synaptic contribution of Ca^{2+}-permeable and Ca^{2+}-impermeable AMPA receptors on isolated carp retinal horizontal cells and their modulation by Zn^{2+}. *Brain Res* 1317: 60-68, 2010.

Sun Z, Risner ML, van Asselt JB, Zhang DQ, Kamermans M, and McMahon DG. Physiological and molecular characterization of connexin hemichannels in zebrafish retinal horizontal cells. *J Neurophysiol* 107: 2624-2632, 2012.

Sun Z, Zhang DQ, and McMahon DG. Zinc modulation of hemi-gap-junction channel currents in retinal horizontal cells. *J Neurophysiol* 101: 1774-1780, 2009.

Suryanarayanan A, and Slaughter MM. Synaptic transmission mediated by internal calcium stores in rod photoreceptors. *J Neurosci* 26: 1759-1766, 2006.

Svaetichin G. The cone action potential. *Acta physiol scand* 29: 565-599, 1953.

Szabadfi K, Mester L, Reglodi D, Kiss P, Babai N, Racz B, Kovacs K, Szabo A, Tamas A, Gabriel R, and Atlasz T. Novel neuroprotective strategies in ischemic retinal lesions. *Int J Mol Sci* 11: 544-561, 2010.

Szydlowska K, and Tymianski M. Calcium, ischemia and excitotoxicity. *Cell Calcium* 47: 122-129, 2010.

Tachibana M. Ionic currents of solitary horizontal cells isolated from goldfish retina. *J Physiol* 345: 329-351, 1983.

Tachibana M. Membrane properties of solitary horizontal cells isolated from goldfish retina. *J Physiol* 321: 141-161, 1981.

Tachibana M. Permeability changes induced by L-glutamate in solitary retinal horizontal cells isolated from *Carassius auratus*. *J Physiol* 358: 153-167, 1985.

Takahashi K, Dixon DB, and Copenhagen DR. Modulation of a sustained calcium current by intracellular pH in horizontal cells of fish retina. *J Gen Physiol* 101: 695-714, 1993.

Talos DM, Fishman RE, Park H, Folkerth RD, Follett PL, Volpe JJ, and Jensen FE. Developmental regulation of alpha-amino-3-hydroxy-5-methyl-4-isoxazole-propionic acid receptor subunit expression in forebrain and relationship to regional susceptibility to hypoxic/ischemic injury. I. Rodent cerebral white matter and cortex. *J Comp Neurol* 497: 42-60, 2006.

Teranishi T, Negishi K, and Kato S. Dopamine modulates S-potential amplitude and dye-coupling between external horizontal cells in carp retina. *Nature* 301: 4, 1983.

Thoreson WB, and Burkhardt DA. Effects of synaptic blocking agents on the depolarizing responses of turtle cones evoked by surround illumination. *Visual neuroscience* 5: 571-583, 1990.

Thoreson WB, and Mangel SC. Lateral interactions in the outer retina. *Prog Retin Eye Res* 31: 407-441, 2012.

Toprak AB, Ozbilgin K, Toprak V, Tuglu I, and Guler C. A histological analysis of the protective effect of ischemic preconditioning in the rat retina. *Curr Eye Res* 24: 234-239, 2002.

Tse A, Tse FW, and Hille B. Calcium homeostasis in identified rat gonadotrophs. *J Physiol* 477 (Pt 3): 511-525, 1994.

Twig G, Levy H, and Perlman I. Color opponency in horizontal cells of the vertebrate retina. *Prog Retin Eye Res* 22: 31-68, 2003.

Ubels JL. Retinomotor activity and the c-wave of the hypoxic trout retina. *Investigative Ophthalmology & Visual Science* 18: 756, 1979.

Ueda Y, Kaneko A, and Kaneda M. Voltage-dependent ionic currents in solitary horizontal cells isolated from cat retina. *J Neurophysiol* 68: 1143-1150, 1992.

Van Dongen AM. *Biology of the NMDA receptor*. CRC Press, 2008.

Verweij J, Hornstein EP, and Schnapf JL. Surround antagonism in macaque cone photoreceptors. *J Neurosci* 23: 10249-10257, 2003.

Verweij J, Kamermans M, and Spekreijse H. Horizontal cells feed back to cones by shifting the cone calcium-current activation range. *Vision Research* 36: 11, 1996.

Vessey JP, Stratis AK, Daniels BA, Da Silva N, Jonz MG, Lalonde MR, Baldridge WH, and Barnes S. Proton-mediated feedback inhibition of presynaptic calcium channels at the cone photoreceptor synapse. *J Neurosci* 25: 4108-4117, 2005.

Villani L, Guarnieri T, and Dell'Erba G. Apoptosis is induced by excitotoxicity in goldfish retina. *Journal of Brain Research* 38: 481-486, 1997.

Vornanen M, Stecyk JAW, and Nilsson GE. The anoxia-tolerant Crucian carp (*Carassius carassius L.*). 27: 397-441, 2009.

Vroman R, Klaassen LJ, Howlett MH, Cenedese V, Klooster J, Sjoerdsma T, and Kamermans M. Extracellular ATP hydrolysis inhibits synaptic transmission by increasing ph buffering in the synaptic cleft. *PLoS Biol* 12: e1001864, 2014.

Wadel K, Neher E, and Sakaba T. The coupling between synaptic vesicles and Ca^{2+} channels determines fast neurotransmitter release. *Neuron* 53: 563-575, 2007.

Wagner H-J. Light-dependent plasticity of the morphology of horizontal cell terminals in cone pedicles of fish retinas. *Journal of Neurocytology* 9: 573-590, 1980.

Wagner H-J, and Djamgoz MB. Spinules: a case for retinal synaptic plasticity. *Trends in neurosciences* 16: 201-206, 1993.

Walker RM, and Johansen PH. Anaerobic metabolism in goldfish (*Carassius auratus*). *Canadian Journal of Zoology* 55: 1304-1311, 1977.

Wang XL, Jiang XD, and Liang PJ. Intracellular calcium concentration changes initiated by *N*-methyl-D-aspartic acid receptors in retinal horizontal cells. *NeuroReport* 19: 4, 2008.

Warren TJ, Hook MJ, Supuran CT, and Thoreson WB. Sources of protons and a role for bicarbonate in inhibitory feedback from horizontal cells to cones in *Ambystoma tigrinum* retina. *J Physiol* 2016.

Watson WD, Facchina SL, Grimaldi M, and Verma A. Sarco-endoplasmic reticulum Ca^{2+}-ATPase (SERCA) inhibitors identify a novel calcium pool in the central nervous system. *J Neurochem* 87: 30-43, 2003.

Wei-LaPierre L, and Dirksen RT. Isolating a reverse-mode ATP synthase–dependent mechanism of mitoflash activation. *Journal of General Physiology* 151: 708-713, 2019.

Weiler R, Schultz K, and Janssen-Bienhold U. Ca^{2+}-dependency of spinule plasticity at dendrites of retinal horizontal cells and its possible implication for the functional role of spinules. *Vision Res* 36: 3891-3900, 1996.

Weiler R, Schultz K, and Janssen-Bienhold U. Retraction of spinule-type neurites from carp retinal horizontal cell dendrites during dark adaptation involves the activation of Ca^{2+}/calmodulin-dependent protein kinase II. *Eur J Neurosci* 7: 1914-1919, 1995.

Weiler R, and Wagner H-J. Light-dependent change of cone-horizontal cell interactions in carp retina. *Brain research* 298: 1-9, 1984.

Weruaga E, Velasco A, Brinon J, Arevalo R, Aijon J, and Alonso J. Distribution of the calcium-binding proteins parvalbumin, calbindin D-28k and calretinin in the retina of two teleosts. *Journal of chemical neuroanatomy* 19: 1-15, 2000.

Wilkie MP, Pamenter ME, Alkabie S, Carapic D, Shin DS, and Buck LT. Evidence of anoxia-induced channel arrest in the brain of the goldfish (*Carassius auratus*). *Comp Biochem Physiol C Toxicol Pharmacol* 148: 355-362, 2008.

Wojtovich AP, DiStefano P, Sherman T, Brookes PS, and Nehrke K. Mitochondrial ATP-sensitive potassium channel activity and hypoxic preconditioning are independent of an inwardly rectifying potassium channel subunit in *Caenorhabditis elegans*. *FEBS letters* 586: 428-434, 2012.

Wong-Riley MT. Energy metabolism of the visual system. *Eye and Brain* 2: 99, 2010.

Wu SM, and Dowling JE. Effects of GABA and glycine on the distal cells of the cyprinid retina. *Brain research* 199: 401-414, 1980.

Yamada E, and Ishikawa T. The fine structure of the horizontal cells in some vertebrate retinae. In: *Cold Spring Harbor symposia on quantitative biology*Cold Spring Harbor Laboratory Press, 1965, p. 383-392.

Yamakura T, Sakimura K, Masayoshi M, and Shimoji K. The sensitivity of AMPA-selective glutamate receptor channels to pentobarbital is determined by a single amino acid residue of the α2 subunit. *FEBS letters* 374: 412-414, 1995.

Yang XL, Tornqvist K, and Dowling JE. Modulation of cone horizontal cell activity in the teleost fish retina. I. Effects of prolonged darkness and background illumination on light responsiveness. *J Neurosci* 8: 2259-2268, 1988.

Yasui S. Ca and Na homeostasis in horizontal cells of the cyprinid fish retina: evidence for Na-Ca exchanger and Na-K pump. *Neurosci Res Suppl* 6: S133-146, 1987.

Yau KW. Phototransduction mechanism in retinal rods and cones. The Friedenwald Lecture. *Invest Ophthalmol Vis Sci* 35: 9-32, 1994.

Yazulla S, and Studholme KM. Neurochemical anatomy of the zebrafish retina as determined by immunocytochemistry. In: *Chemical Anatomy of the Zebrafish Retina*Springer, 2002, p. 3-44.

Yenari MA, Minami M, Sun GH, Meier TJ, Kunis DM, McLaughlin JR, Ho DY, Sapolsky RM, and Steinberg GK. Calbindin d28k overexpression protects striatal neurons from transient focal cerebral ischemia. *Stroke* 32: 1028-1035, 2001.

Young LH, and Dowling JE. Monoclonal antibodies distinguish subtypes of retinal horizontal cells. *Proc Natl Acad Sci U S A* 81: 6255-6259, 1984.

Zhang DQ, and McMahon DG. Direct gating by retinoic acid of retinal electrical synapses. *Proc Natl Acad Sci U S A* 97: 14754-14759, 2000.

Zhu Y, Zhang Y, Ojwang BA, Brantley MA, Jr., and Gidday JM. Long-term tolerance to retinal ischemia by repetitive hypoxic preconditioning: role of HIF-1alpha and heme oxygenase-1. *Invest Ophthalmol Vis Sci* 48: 1735-1743, 2007.

Zivkovic G, and Buck LT. Regulation of AMPA receptor currents by mitochondrial ATP-sensitive K^+ channels in anoxic turtle neurons. *J Neurophysiol* 104: 1913-1922, 2010.

Zoidl G, Bruzzone R, Weickert S, Kremer M, Zoidl C, Mitropoulou G, Srinivas M, Spray DC, and Dermietzel R. Molecular cloning and functional expression of zfCx52.6: a novel connexin with hemichannel-forming properties expressed in horizontal cells of the zebrafish retina. *J Biol Chem* 279: 2913-2921, 2004.

Zoidl G, Kremer M, Zoidl C, Bunse S, and Dermietzel R. Molecular diversity of connexin and pannexin genes in the retina of the zebrafish *Danio rerio*. *Cell Commun Adhes* 15: 169-183, 2008.

Zorov DB, Filburn CR, Klotz L-O, Zweier JL, and Sollott SJ. Reactive oxygen species (ROS)-induced ROS release: A new phenomenon accompanying induction of the mitochondrial permeability transition in cardiac myocytes. *The Journal of experimental medicine* 192: 1001-1014, 2000.

Zorov DB, Juhaszova M, and Sollott SJ. Mitochondrial reactive oxygen species (ROS) and ROS-induced ROS release. *Physiol Rev* 94: 909-950, 2014.

Zucker RS. Calcium- and activity-dependent synaptic plasticity. *Curr Opin Neurobiol* 9: 305-313, 1999.